Reactivity Theory of Transition-Metal Surfaces: A Brønsted−Evans−Polanyi Linear Activation Energy−Free-Energy Analysis

Rutger A. van Santen,*,† Matthew Neurock,‡ and Sharan G. Shetty†

Schuit Institute of Catalysis, Laboratory of Inorganic Chemistry and Catalysis, Eindhoven University of Technology, Den Dolech 2, 5612 AZ Eindhoven, The Netherlands and Departments of Chemical Engineering and Chemistry, University of Virginia, 102 Engineers' Way, Charlottesville, Virginia 22904-4741

Received May 6, 2009

Contents

1. Introduction

The exponential increase in computational processor speed, the development of novel computational architectures, together with the tremendous advances in ab initio theoretical methods that have emerged over the past two decades have led to unprecedented advances in our ability to probe the fundamental chemistry that occurs on complex catalytic surfaces. In particular, advances in density functional theory (DFT) have made it possible to elucidate the elementary steps and mechanisms in surface-catalyzed processes that would be difficult to explore experimentally. The advanced state of plane wave DFT has made it possible to rapidly examine systematic changes to the metal or the reactant in order to establish structure−property relationships. As a result, extensive data based on the energetics for various different surface-catalyzed reactions has been generated. This invites a detailed theoretical analysis of the factors that control reaction paths and corresponding potential-energy surfaces of surface reactions. Such a theoretical analysis will not only provide interesting new insights into the intricate relationship between the chemical bonding features, structure, and energies of transition states but also serve as a basis for the development of analytical expressions that relate transition-state properties to more easily accessible thermodynamic properties. The Brønsted−Evans−Polanyi (BEP) relationship is one such example which has been widely applied in the analysis of surface elementary reaction steps.[1−8]

$$\delta E_{act} = \alpha \delta E_r \quad (1)$$

The BEP equation (eq 1) directly relates the change in activation energy of the reaction, δE_{act}, to the corresponding

Rutger Anthony van Santen received his Ph.D. degree in Theoretical Chemistry in 1971 from the University of Leiden, joining Shell, Amsterdam, as a research chemist the following year. In 1988 he became Professor of Catalysis at the Eindhoven University of Technology. In 1991 he became the director of The Netherlands Institute of Research in Catalysis, and in 2005 he was appointed the Royal Netherlands Academy of Science and Arts Professor. He is a member of the Royal Dutch Academy of Arts and Sciences, Dutch Academy of Engineering, Foreign Associate of the United States National Academy of Engineering (NAE), and Fellow of the Royal Society of Chemistry (RSC, GB). He has been active in many national and international catalysis research programs and organizations. He is the author or editor of 14 books, over 600 research papers, and 16 patents and has been awarded several national and international awards and visiting professorships. His main research interest is the molecular mechanistic understanding of catalytic reactions.

* To whom correspondence should be addressed. E-mail: r.a.v.santen@tue.nl.
† Eindhoven University of Technology.
‡ University of Virginia.

10.1021/cr9001808
Published on Web 12/30/2009

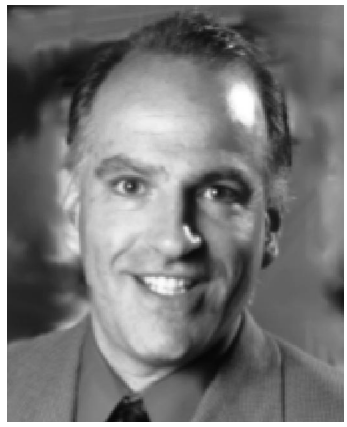

Matt Neurock is currently the Alice M. and Guy A. Wilson Professor of Chemical Engineering and Professor of Chemistry at the University of Virginia. He joined the faculty in Chemical Engineering at the University of Virginia in 1995 after receiving his Ph.D. degree from the University of Delaware and working as a postdoctoral fellow at the Eindhoven University of Technology and at the DuPont Corporate Catalysis Center. He has received various awards for his research in Computational Catalysis including the 2007 R. H. Wilhelm Award in Chemical Reaction Engineering, the 2007 Distinguished Visiting Professor of the University of Montpellier, the 2005 Paul H. Emmett Award in Fundamental Catalysis from the North American Catalysis Society, and the 2006 Johansen-Crosby Lecturer at Michigan State University. He has also been the recipient of an NSF Career Development Award, a DuPont Young Faculty Award, and a Ford Young Faculty Award. He has coauthored over 145 publications, 2 patents, and 2 books. He is currently an editor for the *Journal of Catalysis*. His main research interest is in the area of elucidating catalytic mechanisms and modeling catalytic reaction systems.

Sharan Gurupad Shetty obtained his Master's (M.Sc.) degree in Physical Chemistry from the University of Pune, India, in 1999. In 2001 he started his Ph.D. research at the National Chemical Laboratory (NCL), Pune, India, under the supervision of Dr. Sourav Pal (NCL) and cosupervision of Professor D. G. Kanhere (University of Pune). His Ph.D. research was related to the application of density functional theory to zeolites and metal clusters. He obtained his Ph.D. degree in 2006 from the University of Pune and started as a postdoctoral researcher at the Eindhoven University of Technology with Professor Rutger van Santen. His current research deals with the molecular understanding of the Fischer−Tropsch and ammonia synthesis on metal surfaces and nanoparticles.

change of the reaction energy, δE_r, for different surfaces via a constant factor α, which is based on the particular reaction type. The activation energy which is a kinetic parameter can then be deduced from the reaction energy, which is a thermodynamic parameter. A number of papers have justified the applicability of eq 1 for a wide range of different surface reactions. The first demonstration of DFT methods to the development of BEP analysis of surface-catalyzed reactions was the work by Pallassanna and Neurock,[9] who showed the direct correlation between the activation barriers and the reaction energies for both ethylene hydrogenation and ethylene dehydrogenation over bimetallic Pd alloys. In addition, they showed that similar molecules that fall in the same reaction family could also be described. In a seminal work, Hammer and Nørskov[5] extended such ideas to the development of Universal BEP relations for dissociation of diatomic molecules such as CO, N_2, NO, and O_2 with the same value of α. Michaelides et al.[10] proposed a very similar result for the elementary reaction steps in which CH, NH, or OH bonds are activated.

In this review, we will provide a detailed analysis of the activation of CO, NO, CH_4, and NH_3 on group VIII transition-metal surfaces. This is based on the application of plane wave gradient-corrected DFT results obtained using periodic slab models of metal surfaces. We will not discuss these methods here but refer the interested reader to an introductory review with extensive references in the appendix of ref 7.

It will appear that for a proper understanding of the conditions of applicability of the BEP relation a detailed nature of the reacting molecules as well as the active sites involved in the complex surface reactions are very important. We are interested here in understanding two specific questions. First, how the reaction path or activation barrier is affected with respect to the changes in the electronic or structural properties of the metal surface? Second, whether these changes in the surface properties can categorize the reactions into structure-sensitive and insensitive reactions? The concepts of early and late transition states are critical complements to the BEP analysis as they provide the basis for the proportionality factor α.[11] An early transition state occurs when the transition state is structurally close to the initial reactant state along the reaction coordinate. On the contrary, a late transition state refers to the case where the transition state is close to the product state. For instance, dissociation of a diatomic molecule such as CO, for which α is approximately 0.9, implies that the transition-state geometry is close to that of the dissociated product state. The mobility of the molecule in such a transition state will be small, demonstrating a strong interaction to the surface. Such a transition state has also been called a tight transition state, which is in contrast to a loose transition state which has a high mobility and weak interaction with the surface.[4b,12] An analysis of computational results for the activation of CH bonds in methane or NH bonds in ammonia indicates that such an intuitive interpretation of the value of α and the nature of transition states does not often hold. A more detailed atomistic analysis is needed, which will be presented below.

In order to provide a conceptual frame for our discussion, we will first present an analytic derivation of eq 1 using a Marcus-type analysis.[13] The physical chemistry of the surface reaction then is viewed as a potential-energy curve crossing problem. The limiting conditions will be identified such that α in eq 1 can be considered independent of the reaction free energy and under which conditions it will be near 0 or 1. We will find that surface electronic factors require a modification of this simple potential-energy crossing model. It will appear that the BEP relationship only holds when the activation energy changes are related to the interaction energies of the separated product or intermediate states. We will present a detailed analysis of the reaction path that leads to the dissociation of CO, CH_4, and NH_3

molecules. The analysis is made easier by a comparison of these and related reactions on different surfaces and metals. The activation of ammonia is considered in detail including activation by coadsorbed oxygen atoms and hydroxyl fragments.

An important question that we will discuss is whether there is an analogy between oxidative addition and dissociation of molecular bonds on surfaces. In the case of oxidative addition, the transition state is lowered because of the significant electron back-donation in the antibonding molecular orbital from the localized d orbitals of the metal surface. An alternative process is more similar to the heterolytic bond cleavage reaction. Formation of the new bonds with catalyst atoms then overcomes the cleavage energy of breaking of the molecular bond by an electronic push−pull mechanism. In the bond activation process, electron donation to one of the atoms of the dissociating bond is assisted by electron back-donation of the other atom.

A fundamental issue that we address in this paper is whether, in general, one can expect to find such a relationship between transition-state properties and those of the initial and final states. According to statistical mechanics there is a firm foundation of thermodynamic equilibrium properties but not for time-dependent phenomena. Irreversible thermodynamics provides expressions for rate constants, only valid within specific physical conditions. Similarly, we will see that the BEP-type relations are only applicable under stringent conditions.

The BEP relationship is directly analogous to the linear free-energy relationship widely used throughout physical organic chemistry which is known as the Hammett[14] relationship.

$$\log \frac{k_{ij}}{k_{oj}} = \rho_j \log \frac{K_i}{K_0} \tag{2a}$$

Hammett originally showed that the reactivity of an aromatic molecule, such as the rate of hydrolysis of an aromatic ester, is related to the acid strength of its corresponding benzoic acid. Hammett-type relationships are typically found when the rates and equilibrium constants are compared for molecules that come from a particular "family" whereby the changes arise as the result of substituent effects. For example, when the relationship in eq 2a is applied to the reactivity of meta- and para-substituted benzene, K_o is to be taken as the acidity constant of benzoic acid and K_i the acidity constant of substituted benzoic acid. Then, k_{ij} is the rate constant of reaction j for substituent i and k_{oj} the corresponding reaction rate when the substituent is absent. The parameter ρ_j can be identified with parameter α in the BEP relation and depends, of course, on reaction type. This is illustrated in Scheme 1.

A more classical relation is the Brønsted relation[15] that relates the rate of a catalytic reaction (k), a kinetic property, to the acid−base strength of the corresponding catalyst (K), which is an equilibrium property

$$k = GK^{\alpha} \tag{2b}$$

The equilibrium constant here determines the ionization degree of the organic acid used. The Brønsted relation has been widely used to correlate concentration of the organic anions derived from organic acids with the rate of a particular reaction. The reaction originally studied was the decomposition of nitramide in benzoate buffers.

Scheme 1. Hammet Relation between the Rate of Hydrolysis and the Equilibrium Constant for Deprotonation

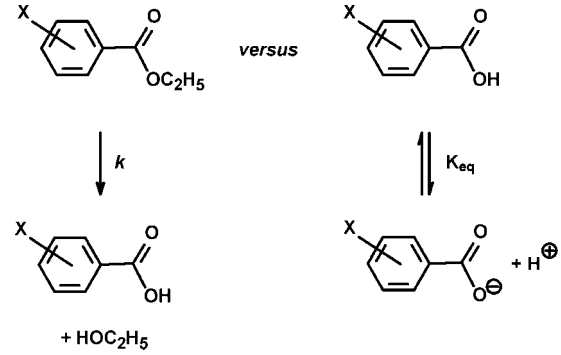

In catalytic science, the Langmuir−Hinshelwood relation[16,17] or its complementary relation in enzyme catalysis the Michaelis−Menten[18] provides similar relationships. Here, the equilibrium constant refers to the surface concentration of adsorption complex or reactant intermediate and the rate (r) refers to the turnover frequency of the overall catalytic step as indicated in eq 2c for the rate of monomolecular reaction r

$$r = k_e\theta = k_e \frac{K_{ads}p}{1 + K_{ads}p} \tag{2c}$$

According to eq 2c, the rate is related to the adsorption equilibrium K_{ads} between reactant phase and surface and the rate constant k_e of the elementary reaction constant that is assumed to be rate limiting. In the above equation, θ is the coverage of the reaction sites and p is the partial pressure of the reactants. A linear relationship between the apparent activation energy and the adsorption energy results at low surface coverage

$$E_{act}^{app} = E_{act} + E_{ads}(1 - \theta) \tag{2d}$$

Changes in the catalyst or the reactant will directly affect r. As long as the elementary reaction step is considered, a linear relationship between the apparent activation energy of the overall catalytic reaction and the adsorption energy can be established. This relationship is valid for solid acid reactions catalyzed by zeolites with different micropore structure and dimensionality[19] or for reactions with varying length of reactant alkane molecule.[20]

Langmuir−Hinshelwood-type equations, such as eq 2c, can be used to understand the Sabatier principle.[7,21−24] The Sabatier principle explains the often found volcano-type curves of the rate of a catalytic reaction as a function of changing the interaction strength with reactants or reaction intermediates.[22] This again is the result of the relationship between a kinetic parameter, the overall rate of the catalytic reaction, and a thermodynamic parameter, measured by the strength of the adsorbate chemical bonds. We will discuss this in detail in section 5.

The BEP relationship is employed to a much more constraint situation. It applies to the elementary reaction step, k_e (eq 2c), itself. It aims to deduce the rate of its reaction from the reaction energy of an elementary reaction step. A very successful theory that provides such a relationship for electron-transfer reactions between coordination complexes in water has been described by Marcus[13]

$$\Delta G^{\ddagger} = W(r) + \wedge\left(1 + \frac{\Delta G}{4\wedge}\right)^2 \tag{3a}$$

An analogous relation has also been used for reactions involving transfer of atoms and protons.[25] In eq 3a, $\Delta G^{\ddagger}$ is the activation Gibbs free energy, $W(r)$ the energy change within the molecular reaction complex, and $\wedge$ the reorganization energy or molecules in the liquid phase due to charge displacement. When the ligands in the coordination complexes change, $\Delta G^{\ddagger}$ is affected. From eq 3a one calculates

$$\frac{\delta \Delta G^{\ddagger}}{\delta \Delta G} = \frac{1}{2}\left(1 + \frac{\Delta G}{4\wedge}\right) = \alpha \tag{3b}$$

Equation 3b gives an explicit expression for the BEP parameter α.[17] However, one should note that according to eq 3b the proportionality constant α also depends on the reaction free energy. In the next section, we will use adapted forms of the Marcus expression to provide an analysis of the BEP relation applicable to surface reactions and deduce an expression for α.

Determination of α is an important practical issue that is necessary in the development of BEP relationships. A successful BEP relationship enables prediction of the rate constants for reactions comprised of the same family and other related reactions without the need to perform laborious transition-state searches to determine all of the activation barriers for each of them.

2. Crossing of Potential-Energy Surfaces: Analytical Considerations

In this section we analyze the reaction paths and corresponding barriers for both bond scission and bond formation reactions using two different but complementary approaches. To explain this we use the model of crossing potential-energy surfaces. In section 3, we investigate the quantum-chemical bonding models of dissociation and recombination reactions. The results presented here are subsequently used in later sections to analyze computed data on surface reaction rates.

The interpretation of a reaction in terms of crossing potential-energy curves was first proposed by Horiuti and Polanyi.[26] This follows from a seminal paper by Eyring and Polanyi[1] where they used the crossing of potential-energy curves model, approximately computed from the quantum-chemical theories, to deduce expressions for the transition-state energy. Evans and Polanyi[2] then formulated eq 1 for an elementary chemical reaction step. Herein, we follow some of the arguments discussed in the book of Bell.[25] A very good introductory treatment of this topic is also given by Masel.[6]

A two-dimensional representation of the changes in the potential energy of a surface reaction is given in Figure 1. Curve V_1 represents the potential energy of the one-dimensional system before reaction, i.e., the initial state; curve V_2 follows that of the product state. The local minima of the initial and final states are separated by x_0 as indicated in Figure 1. The crossing point of the two curves is regarded as the transition state. This model is rather similar to that used by Marcus[13] and Bell[25] in their analysis of electron- and proton-transfer reactions, respectively. For harmonic potentials with equal force constants, one can derive eq 4a

$$E_{act} = E^{\circ}_{act}\left(\frac{\Delta E_r}{4E^{\circ}_{act}} + 1\right)^2 \tag{4a}$$

$$\alpha = \frac{\delta E_{act}}{\delta \Delta E_r} = \frac{1}{2}\left(1 + \frac{\Delta E_r}{4E^{\circ}_{act}}\right) \tag{4b}$$

E°_{act} is the activation energy of the thermodynamically neutral reaction. When ΔE_r is equal to $-4E^{\circ}_{act}$ the activation energy as well as α are equal to zero. When the value of α is near zero, the transition state can be considered to be early. The crossing point of the two potential-energy curves is now near the minimum of V_1, the initial reactant state. The activation energy is at a maximum when ΔE_r is equal to $4E^{\circ}_{act}$. Now the minimum of curve 2 has been shifted upward to the point where the transition-state energy and this local minimum of the second potential-energy curve coincide. The transition state can be considered late, and α is close to one. It should be noted that eq 4a has only a physical meaning for $0 \leq \alpha \leq 1$. Masel provides an interesting analysis analogous to the derivation of eq 4b for harmonic potentials by the linearization of the potential-energy curve crossing.[6] Interestingly, one should note that in the above analysis we assume that x_0, i.e., the distance between the local minimum of the initial and final states, is kept fixed during the change in the reaction energy ΔE_r. For example, if the minimum of the final state is away from the initial state then the point of the curve crossing, i.e., the transition state, can increase. Hence, the direct correlation between the ΔE_r and E°_{act} will be invalid if x_0 is varied from one reaction to the other. An alternative definition of early and late transition states is found when one considers the crossing of potential-energy curves with very different force constants as sketched in Figure 2. As is illustrated in Figure 2, when the reaction energy changes there is little shift in the activation energies, implying a BEP α value near zero. In contrast, in the reverse situation there is a large change in E°_{act} with ΔE_r, implying a BEP α value near 1. The corresponding equations can be readily solved and are given in eq 5a. k is the force constant of potential V_1; k' is that of potential V_2.

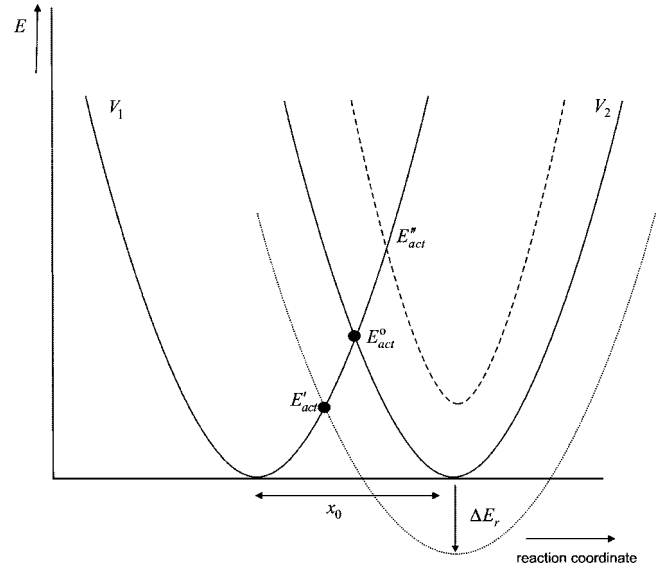

Figure 1. Crossing of two potential-energy surfaces: a one-dimensional model of a dissociation reaction.

$$E_{act} = A(-1+\sqrt{1+\delta})$$
$$A = \frac{1}{2}\frac{kk'^2x_0^2}{(k-k')^2};\ \delta = \frac{|k-k'|}{k'x_0^2}\left(x_0^2 + 2\frac{\Delta E_r}{k'}\right) \quad (5a)$$

$$\alpha = \frac{k}{k'-k}\frac{(1-\sqrt{1+\delta})}{\sqrt{1+\delta}}$$
$$\lim \frac{k}{k'} \rightarrow o : \alpha = 0 \quad (5b)$$
$$\lim \frac{k}{k'} \rightarrow \infty : \alpha = 1$$

BEP-type behavior is found independent of the ratio k/k' only as long as $\Delta E_r/k' \ll x_0^2$.

As indeed follows from relation 5b, when $k/k' \ll 1$, α approaches zero even when the potential-energy crossing point is far from the reactant energy minimum. Hammond-type identifications of the transition states are only valid when $k = k'$. When force constants of reactant and product states are very different, we find that early transition-state behavior does not necessarily require a transition-state location that is close to the energy minimum of the initial reactant state. The definition of an "early" transition state as being when $\alpha \approx 0$ now tends to lose its meaning. Figure 2b illustrates the reverse case to be interpreted as "late" transition-state behavior but with the same argument as applied for the previous case. We now find that the activation energy is a strong function of reaction energy. When $k/k' \ll 1$, α is close to 1. The transition-state position remains quantitatively the same and is independent from the location of reactant or product states.

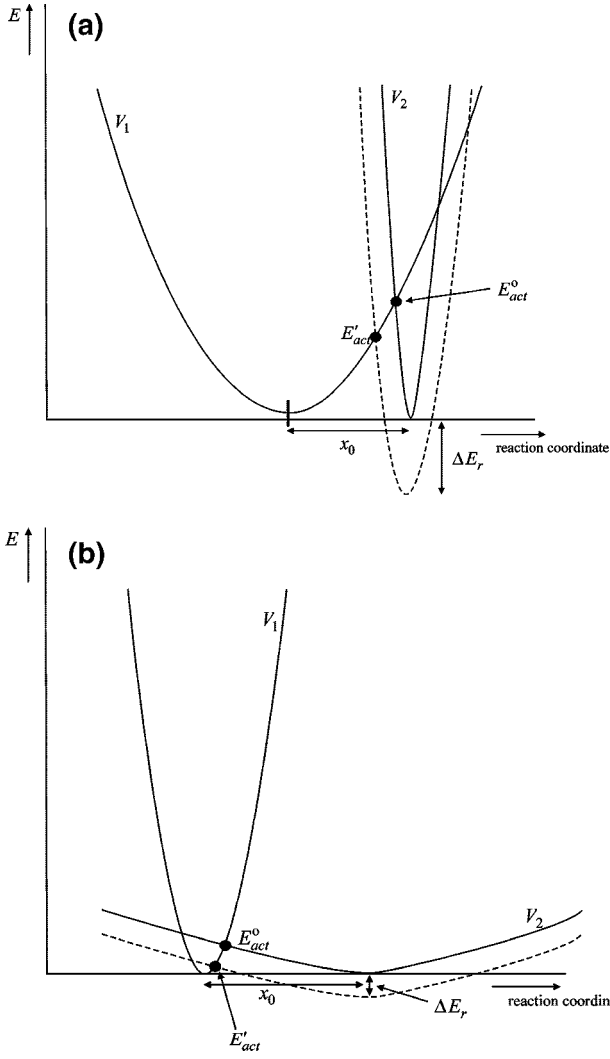

Figure 2. (a) Curve crossing of potential-energy surfaces of the initial and final states with different second-derivative, i.e., different force, constants. (b) Curve crossing of potential-energy surfaces. The final state has a smaller second derivative than the initial state.

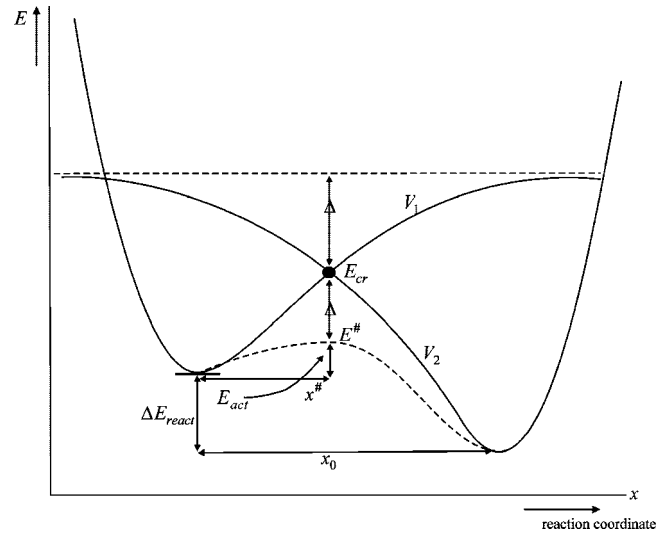

Figure 3. Energy diagram of curve-crossing potentials based on additive atom−atom interactions.

In order to advance further we have to analyze the corrections to the harmonic approximation used to deduce eqs 4a and 5a. This potential-energy picture is based on cleavage of a chemical bond which is succeeded by formation of a new chemical bond. When Lennard−Jones types of potentials are used and curve crossing occurs in the attractive parts of the potentials, the curve crossing potential-energy curves change as sketched in Figure 3. Moreover, the energies V_1 and V_2 described in Figure 3 cannot be considered completely independent. Dissociation of ammonia adsorbed on a metal surface through its nitrogen atom presents a useful example of the system sketched in Figure 3. The initial part of the reaction path is determined by the stretching of the NH bond. In Figure 3, V_1 refers to activation of NH_3 with removal of the H atom in the gas phase. The second potential-energy curve V_2 is determined by bond formation of the H atom with the metal. Obviously the correction to the curve crossing energy sensitively depends on the position of the transition state along the reaction coordinate path. The activation energy depends on the relative position of V_2 and V_1 potentials. We return to this issue in later sections.

So far we have not considered any factors that might result in potential energies to be nonadditive as well as features that are specific to the activation of the molecules by a transition-metal surface. This requires a more detailed consideration of the electronic structure involved in chemical bonding, which is discussed in the next section. An important consideration is whether potential curve crossing actually occurs in the attractive part of the potentials as we discussed so far or whether a repulsive barrier has to be overcome as found in early quantum-chemical studies (see ref 27, pp 195−203).

3. Quantum Chemistry of Molecular Bond Activation on Surfaces

The models described so far do not provide a theoretical description of the chemical bonding features that determine the structure of the transition state. In the one-dimensional models used so far, the detailed electronic structure was congregated into the term α, which represents the value of the derivative of the potential-energy curve with respect to the reaction energy. Quantum-chemical considerations are necessary to not only quantify α but also predict the validity region of α.

The analogue to the activation of chemical bonds on surfaces and organometallic complexes is the single-center oxidative addition or reductive elimination of reactant molecules.[28] The alternative push−pull mechanism which involves a cooperative Lewis-base−Lewis-acid type of activation, which is more common on protonated solid surfaces, will also be considered.[7,29]

3.1. Quantum-Chemical Preliminaries

3.1.1. Oxidative Addition and Reductive Elimination

A prototype oxidative addition reaction (dissociative adsorption) is the dissociation of H_2 over different metal surfaces. The electronic structure model of this reaction involves repulsive as well as attractive interactions. In the present context, an interesting question would be what is the nature of the surface−adsorbate interaction in the transition state? An important consideration is the relation between this electronic interaction with that in the initial or final states. We will use computed first-principle quantum-chemical results on H_2 adsorption and activation on transition-metal surfaces to present an insightful tight-binding-type model of the essential orbital interactions.[30−33] The essential observation of many quantum-chemical studies of chemisorption on transition-metal surfaces is that often a surface complex of adsorbate and directly interacting surface atoms is formed that can be considered to be embedded on the surface through weak embedding interactions.[7] This is the basic reason for the generally observed analogy between the surface chemistry and the corresponding coordination complexes.[34] Quantum chemists sometimes call this view of chemisorption the surface complex or molecule limit.[7] The important difference between molecular complexes and surface-embedded clusters is that in the latter case the chemical potential equalizes due to the conductive contact electron flow between the surface-embedded cluster and the bulk metal. This also causes the local electron density distributions in the surface to be broadened into bands when these are degenerate with metal valence electron energies.

For the case where H_2 is adsorbed to an isolated transition-metal atom and the metal atom is located on the z axis perpendicular to the molecular H_2 bond, the elementary orbital interaction scheme is shown as in Figure 4. Before adsorption, the electronic structure of the H_2 molecule consists of a bonding orbital symmetric with respect to the z axis (α orbital) that contains two electrons and an unoccupied antibonding orbital antisymmetric with respect to the z axis (σ^*). These orbitals can only interact with orbitals on the metal atom of the same symmetry. The σ orbital will interact with s, p_z, and d_{z^2} metal atom orbitals and the σ^* orbital with a metal d_{xz} or d_{yz} atomic orbital. In Figure 4 the interaction of the H_2 σ orbital is considered to be interacting with only one surface atomic d orbital. One should note that this is an approximation. However, on the surface or with the free atom it will interact with a linear combination of the metal atomic orbitals. The σ orbital becomes part of a bonding and antibonding orbital pair, ε_1^+ and ε_2^+. Similarly the H_2 antibonding σ^* orbital becomes also part of bonding and antibonding orbital pairs ε_1^- and ε_2^- but now through combination with an antisymmetric metal d atomic orbital.

To indicate the embedding of the surface-molecular complex in Figure 4, the open line indicates the relative position of the Fermi level (E_F). The orbitals are occupied when their energy is below the E_F, while the orbitals above E_F are empty. The essence of the orbital and their occupation energies upon oxidative addition or reductive elimination is contained in the simple situation as sketched in Figure 4. Calculations certainly will show additional features due to the presence of metal valence electrons that are broadened into bands. Also, the adsorbate surface interaction will be described by more complex features broadening the orbital energy distributions. Typically, on a transition-metal surface the number of sp valence electrons in the broadened band will be one per surface metal atom. The E_F may be positioned in the d valence electron band, implying a partial filling of

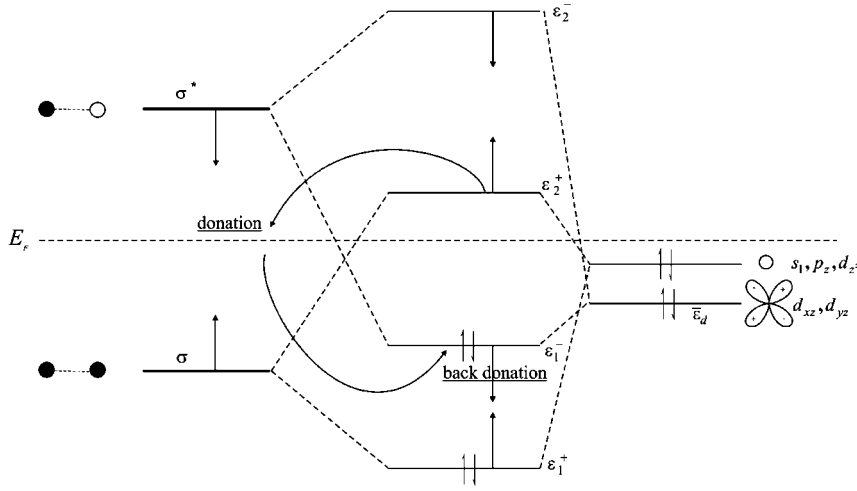

Figure 4. Schematic representation of the molecular orbital interaction scheme of H_2 with a surface metal atom. The curved arrows represent the donation and back-donation of the electrons from the metal atom to the H_2 and vice versa, respectively. The straight arrows represent the moving of orbitals as the H_2 molecule stretches.

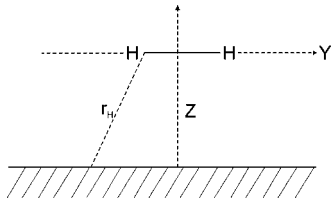

Figure 5. Potential-energy curves of the dissociating H_2 molecule. The z axis represents the approach of the H_2 molecule perpendicular to the surface normal, and the y axis represents the stretching of the H_2 molecule parallel to the surface normal.

this valence band. As we will argue below, the relative position of the d valence band with respect to the E_F is important to determine the actual efficiency of the donative and back-donative interactions.

Electron occupation of the bonding surface orbital interactions ε_1^+ and ε_1^- implies a bonding attractive interaction between the hydrogen molecule and the metal surface. In contrast, electron occupation of the antibonding surface orbitals ε_2^+ and ε_2^- implies a repulsive interaction between the H_2 molecule and the surface. This orbital occupation is controlled by the relative position of the E_F. When the E_F is higher than ε_2^+, both bonding and antibonding orbitals that are formed from the H_2 σ orbital are occupied and the result is a repulsive interaction. This repulsive interaction is counteracted by the attractive interaction due to occupation of the bonding ε_1^- surface orbital. Since this orbital is a linear combination of the σ^* orbital of H_2 and surface metal atomic orbitals, its occupation implies that the σ^* orbital, which initially is unoccupied, becomes occupied by electrons. This implies that an electron flow from the metal surface into the σ^* antibonding H_2 orbital can be termed as a back-donative interaction. This is in contrast to the donative interaction of electrons from H_2 into the unoccupied metal valence orbitals that arise when at a lower position of the E_F electrons in the surface interaction orbital ε_2^+ are depleted. The relative position of the antibonding orbital ε_2^+ and E_F determines significantly the relative position of the transition state as a function of z and r_H coordinates as shown in Figure 5. When the molecule approaches the surface, i.e., along the z axis, the r_H distance shortens. The increased overlap between adsorbate and surface orbitals results in a maximum splitting of the respective bonding and antibonding orbital pairs. Whereas at a large distance the surface interaction orbital ε_2^+ will be located below the E_F, when the distance between H_2 and the surface decreases there will be a distance z at which ε_2^+ will become positioned above the E_F. Consequently, the interaction energy inverts sign from repulsive to attractive. The interaction between the H_2 σ^* orbital and the surface is always attractive since the ε_2^- orbital is above the E_F. Hence, the initial repulsive interaction between the metal surface and H_2 is converted into an attractive one by a combination of the two attractive interactions that results from the shifting of the antibonding ε_2^+ orbital above the E_F and occupation of the bonding ε_1^- orbital.

In addition to these factors that cause changes in the surface interaction orbitals, there is an ongoing change of the H_2 bond distance when z decreases. This lengthening of the H_2 bond is due to two factors. One is the occupation of the H_2 σ orbital that is antibonding with respect to the H_2 bond energy, which causes the H_2 bond to stretch. The other factor is the lowering of the relative position of this H_2 σ^* orbital with respect to the interacting metal valence orbitals; the larger this back-donating interaction will be, the more

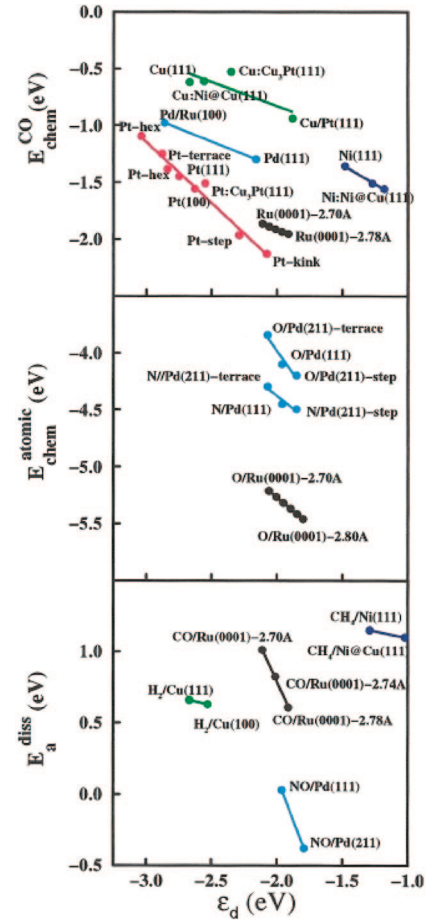

Figure 6. (Top and middle) Molecular CO and atomic species binding energies as a function of the d band center. (Bottom) Dissociation barriers of various molecules on different metal surfaces as a function of d band center.[35]

weakening of the H_2 bond will take place. In our simplified model this is essentially determined by the average position of the surface d valence electrons, ($\bar{\varepsilon}_d$). The smaller the distance between surface orbital energy $\bar{\varepsilon}_d$ and the σ^* orbital of H_2, the stronger they interact and the lower the relative position of ε_1^- will be. We note that in addition to the relative position of the E_F, the relative position of $\bar{\varepsilon}_d$ determines the strength of the back-donating interaction. The higher the average d valence electron band energy $\bar{\varepsilon}_d$, the stronger this interaction. This correlation between the chemisorption energy and $\bar{\varepsilon}_d$ position has been emphasized, especially by Mavrikakis et al.,[35] as illustrated in Figure 6.

Chemisorption energies of atoms to metal surfaces that differ in topology relate to changes in $\bar{\varepsilon}_d$. This results from the dominance of the back-donating interaction. As we explained in more detail elsewhere,[7] this change in the $\bar{\varepsilon}_d$ position with surface relates to differences in the coordination of the surface atoms with nearest neighbor surface atoms. The upward shift of $\bar{\varepsilon}_d$ with decreasing surface atom coordination number (increased reactivity) is due to the decreased screening of the repulsive interactions of the d valence electrons when the number of neighbors decreases.[33] In addition, there is also a small increase in d valence electron occupation on the surface with decreasing surface atom coordination number. These effects correlate with the decrease in electron delocalization, and hence, the reactivity of the surface atom increases. This implies that the H_2 molecule will also interact more strongly with surfaces of increasing corrugation or with step edges. The increased

coordinative unsaturation of the surface atoms is reflected in an upward shift of the $\bar{\varepsilon}_d$ and hence in an increasing contribution of the back-donating interaction. The back-donating interaction causes the H_2 σ^* orbital to become (partially) occupied with electrons. The antibonding nature of the orbital with respect to the H_2 bond energy implies a weakening of the H−H bond when the σ^* orbital becomes occupied. The stronger the back-donating interaction, the more significant the H−H bond weakening will be. As a consequence, the H−H bond length will increase. The increased bond length in turn will decrease the overlap of the H atomic orbitals. This decreases the difference in energy between the σ and the σ^* orbitals of H_2. The orbitals in Figure 4 then shift in indicated directions. The decreasing position of H_2 σ^* lowers also ε_1^- and hence increases the back-donative contribution to the bond energy. The ε_1^+ levels shift upward, and hence, the z distance at which the ε_2^+ level crossed the E_F will be earlier. Since beyond this point the Pauli repulsive interaction between H_2 and the surface does not increase any more, there is a driving force to decrease further the z distance. The resulting orbital changes will increase the H−H bond distance further until the H−H bond is broken. The ε_2^- and ε_2^+ and the ε_1^- and ε_1^+ orbitals then become degenerate. The difference between the σ orbital energies no longer exists. In this process of oxidative addition, combinations of two electrons from the metal with two electrons from the H_2 molecule have been used to form the MH bond. Near the transition state, electrons have been transferred to form a H_2, x anionic intermediate, with x close to 1. This is the original Nørskov view of the dissociation of H_2, which was initially developed while studying this process on Mg.[32]

Thorn and Hoffmann[28a] emphasized the importance of the crossing of the ε_1^- level and the E_F. Their analysis starts with the opposite situation of two hydrogen atoms recombining to form a H_2 molecule. This is the analogue of reductive elimination. The initial situation is degeneracy of orbitals ε_1^- and ε_1^+ representing the two occupied bonding MH orbitals. When the H atoms recombine, bonding and antibonding orbital combinations are formed, which now transform into the occupied ε_1^+ and ε_1^- orbital combinations. With respect to the original separate MH ground states this orbital pair gives a repulsive interaction. As mentioned earlier, at the transition-state orbitals ε_1^- and ε_2^+ become nearly degenerate. On continued H_2 formation, orbital ε_1^- splits into the unoccupied H_2 σ^* orbital and metal d orbital. Consequently, a repulsive interaction develops between H_2 and the metal surface due to electron occupation of the ε_2^+ orbital.[33] In the process electrons have been donated out of the MH bond into the metal valence bands. This can be viewed as "reduction" of the initially oxidized metal atoms.

The interesting question that arises is the location of the transition state with respect to the change in the position of the z or y coordinate. In the above discussion we note that there are two ways in which one can locate the transition state. Let us start again with the nondissociated H_2 molecule parallel to the surface. Upon a decrease in the z distance, at some specific point along the z direction the repulsive interaction is converted into an attractive one (ε_1^- crosses E_F). The energy required to overcome the repulsive interaction into an attractive one creates a small barrier as represented by the crossing of regime I and II as indicated in Figure 7a. Alternatively, the transition state is located in the regime where the H_2 bond stretches (i.e., along the y direction). The position of the transition state then is dominated by a change in the y direction (Figure 7b). It is important to note that the H_2 activation would have a negligible barrier along the z axis, i.e., the transition from repulsive to attractive, but would have a barrier for the stretching along the y axis. However, in other case H_2 will dissociate without any barrier along the y axis and would have a negligible barrier along the z axis. A classic example is the work by Hammer and Norskov.[30] The dissociation barrier required for H_2 on the Au and Cu surfaces would follow the earlier case, and on Pt and Ni it is the latter situation, where the H_2 molecule stretches without barrier.[30] Interestingly, both situations have been found to occur simultaneously on the Fe(100) surface. In Figure 8 calculated potential-energy contour plots are shown for the dissociation of H_2 parallel to the surface on the (a) atop and (b) bridge sites of the Fe(100) surface.[36] One notes that the transition state for H_2 dissociation on the atop and bridge sites is located at the same z position. However, interestingly, on the top site the activation barrier of H_2 is located in between regimes II and III of Figure 7, dominated by stretching of the H_2 bond. On the contrary, on the bridge site the transition state is located in the cross-section of regimes I and II, dominated by changes in the z distance.

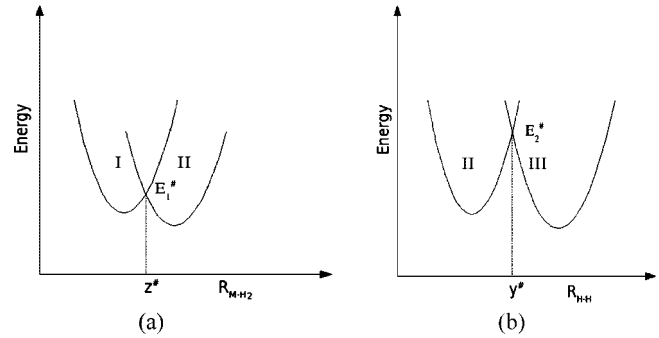

Figure 7. Schematic representation of the two possible transition states of H_2 dissociation. (a) Activation energy ($E_1^{\ddagger}$) due to the repulsive intreraction between the H_2 and the metal surface as the H_2 molecule is approaching the surface along the z axis. $R_{M\text{-}H2}$ is the decreasing distance between the metal surface and the H_2 molecule along the z axis. (b) Activation energy ($E_2^{\ddagger}$) with respect to the stretching of the H_2 molecule on the metal surface (along the y axis). R_{H-H} is the distance between the two H atoms. $E_1^{\ddagger} \ll E_2^{\ddagger}$. The z and y axes are defined in Figure 5. Regions I, II, and III are explained in the text.

Hammer and Norskov used the DFT results to investigate the activation of H_2 over different metals.[30] Their results indicate that in the chemisorbed state for H_2 over both Cu and Au the antibonding ε_2^+ state is occupied. Since the ε_2^+ state remains below the E_F, there is a substantial degree of repulsive interactions with the metal orbitals of the surface. This results in the higher activation barrier for H_2 over Cu and Au surfaces. In the case of H_2 interaction with the Ni and Pt surfaces, the ε_2^+ state is pushed above the E_F and therefore experiences less repulsive interaction compared to the Cu and Au surfaces. Obviously the $\bar{\varepsilon}_d$ position in Ni and Pt and partial depletion of the Ni and Pt d valence electron band are responsible for this difference. The results are consistent with experimental evidence which shows that the activation of H_2 over group Ib metals is activated while that over the group VIII metals has no barrier. This difference relates to the relative position of the d valence electron band with respect to the E_F in these metals.

We emphasized the important role of the Pauli repulsion to the interaction energy of the H_2 molecule with the metal

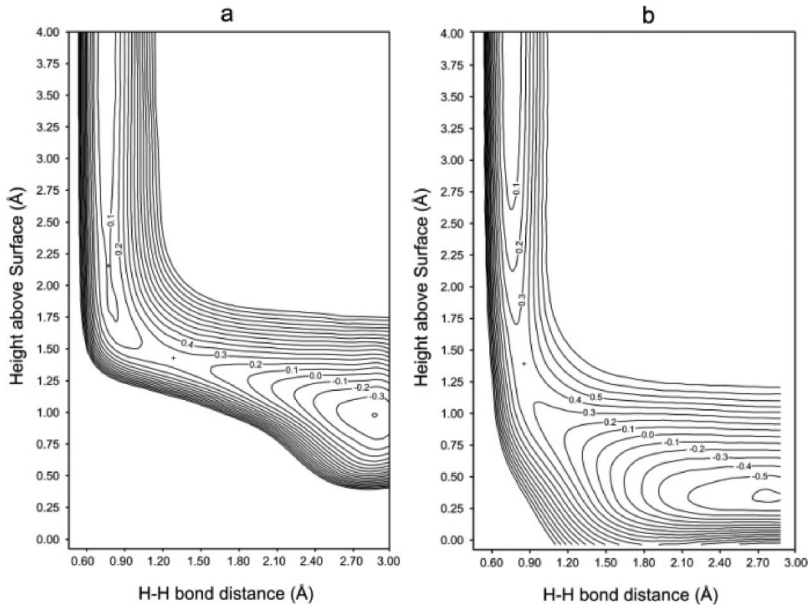

Figure 8. H_2 dissociation on a clean Fe(100) surface. (a) Dissociation of H_2 on the top site with H atoms ending up on the bridge sites. (b) Dissociation of H_2 on the bridge site with H atoms ending up in the hollow sites.[36]

surface. Whereas H_2 adsorption to the metal surface usually occurs parallel to the metal surface, this is not always the case for adsorption of H_2 to a small metal cluster. One important reason for this is that on a metal cluster electron back-donation can be expected to be less than on a surface because the ionization potential (work function) of a metal is lower than that of a small cluster. Consequences of differences in Pauli repulsion for different adsorption modes become apparent when comparing different adsorption modes for small clusters. Calculations of H_2 interacting with an Ir_4 cluster show[31] that instead of the expected parallel, μ_2, attachment of H_2 with two of its atoms attached to the Ir cluster, the H_2 molecule is found to be adsorbed end on, interacting through only one of its H atoms. Pauli repulsion is proportional to the number of interacting atoms. It is twice more repulsive in the side-on coordination mode than in the end-on one. Due to the weakness of the back-donating interactions, the increased back-donating interaction in the side-on mode does not compensate for the enhanced Pauli repulsion in the same adsorption mode. This is confirmed by comparing with the situation where the Ir_4 cluster is interacting with a cation. This could be the situation of Ir_4 adsorbed in a cationic zeolite. It is now found that the H_2 molecule adsorbs side on on the site of the cluster opposite of the interacting cation. In contrast, where there is no interaction of the cluster with the cation., now there is a significant electron occupation of the H_2 σ^* orbital.

The cation polarizes the metal particle such that the negative charge is pulled toward the cation, and hence, there is less density between the H_2 molecule and the cluster. As a consequence, Pauli repulsion decreases (the lowered electron density also creates low-energy metal cluster orbitals that allow reduction of Pauli repulsion through polarization of electron density away from the adsorbate−cluster interaction location) and the H_2 molecule can approach the cluster closer. In the side-on mode the H_2 antisymmetric unoccupied σ^* orbital now can develop significant overlap with the antisymmetric occupied cluster orbitals, for instance, the atomic d orbitals. Due to increased overlap, significant occupation of the ε_1^- orbital of the adsorbate−cluster complex becomes possible for side-on adsorption of H_2. For end-on adsorbed H_2 there is now no interaction with occupied antisymmetric surface orbitals because now also the H_2 σ orbital is σ symmetric with respect to the interacting atom(s), which are most relevant for the stable back-donating interaction. Hence, the side-on-bonded mode is preferred over the end-on one. We will see in the next section that this becomes very different when π-type orbitals of the adsorbates are involved in the interaction. Whereas the deformation of the reactant molecule in the transition state is very similar, the interaction energy with an atom that is part of the metal surface is much lower than that with an isolated atom. This corresponds to the energy cost to localize electrons in the surface Pd atom.[7]

Diefenbach et al.[37] analyzed the change in energy of a dissociating methane molecule in contact with a Pd atom. They defined the strain energy for a dissociating molecule to be the energy change that occurs along the reaction coordinate from the isolated molecule in the gas phase. The activation energy is the sum of this strain energy cost and the energy gain due to the increased interaction of the dissociated fragments with the metal atom (see Figure 9). No repulsive barrier is found in this activation energy path. The study by Diefenbach et al.[37] on methane activation over a Pd atom concludes that in the transition state the occupation of the C−H antibonding orbital increases by 0.36 electrons, while the occupation of the C−H bonding orbital decreases by 0.29 electrons. This weakens the C−H bond. The electrons that back donate are accommodated by the empty Pd 5s atomic orbital. The overall charge on the dissociating molecule is found to be slightly negative. This redistribution of electrons over the bonding and antibonding orbitals of the dissociating molecule is consistent with the simple model presented above.

A very similar result as Diefenbach et al. was found by Bunnik and Kramer.[38] They analyzed dissociation of methane over the top of a surface Rh atom on the Rh(111) surface. At the transition state, the strain energy of the methane molecule is 140 kJ/mol. The interaction energy is close to 50% of that value. Although the deformation of the reactant molecule in the transition state is very similar, the interaction energy with an atom that is a part of the metal surface is

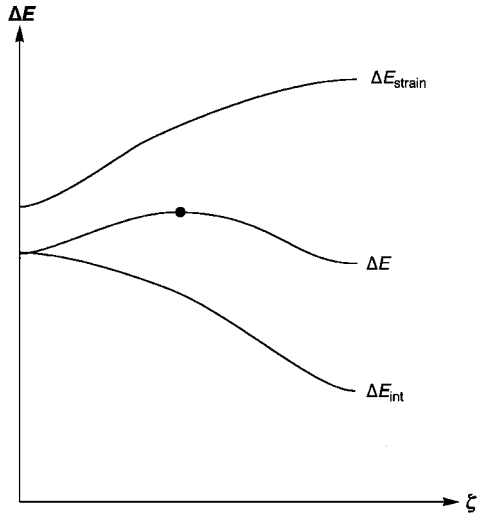

Figure 9. Schematic representation of a typical reaction energy profile for oxidative insertion of CH_4 in Pd.[37] ΔE_{strain} is the deformation energy of methane, ΔE_{int} the interaction energy of deforming methane with a Pd atom, and ζ the reaction coordinate.

much lower than that with a single isolated atom. This corresponds to the energy cost to localize electrons with a single Pd atom.

3.1.2. Cleavage of Molecular π Bonds: Rehybridization

The key difference between the activation of σ and π bonds is their surface coordination criteria. Whereas activation of σ bonds as in H_2 and methane will usually proceed atop of a metal atom, this is very different for the activation of molecules such as CO or NO. This is notwithstanding the finding that in the case for CO the differences in the adsorption energies between atop or 2-fold or 3-fold coordination are within 10−20 kJ/mol. This is very small compared to the adsorption energies, which are typically of the order of 200 kJ/mol.

The main reason for the differences in the surface coordination requirement is the difference in the preferred adsorption sites of atoms as C, O, or N compared to that of CH_3 or H.[39] The latter adsorption energies are not very sensitive to coordination. Adsorption energy differences of adsorbed C, O, or N atoms depend strongly on the local coordination of the site. These atoms prefer strong adsorption in high coordination sites. This is due to the dominance of the interaction with the π-type adatom orbitals parallel to the surface. In high coordination sites they will strongly interact not only with metal surface d atomic orbitals but also with antisymmetric surface metal s and p atomic group orbital combinations.[7] For this reason, dissociation of adsorbates consisting of π-type chemical bonds require an ensemble of surface atoms to react. The size of such a surface ensemble may vary between five and eight surface atoms. This makes chemistry on surfaces unique with respect to organometallic complexes. The nature of the electronic structure and the chemical bonding between the molecular adsorbates and the metal surface is well understood. An excellent reference is the chapter by Nilsson and Pettersson[8] that summarizes chemical bonding insights obtained from a comparison of high-quality photoemission spectroscopic data and quantum-chemical calculations.

One of the most crucial electronic features to consider is the rehybridization of the adsorbate molecular orbitals upon

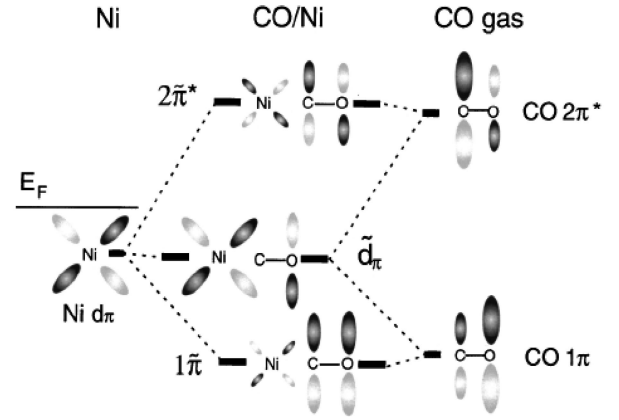

Figure 10. Schematic representation of the interaction of the π orbitals of CO and the metal d orbital of Ni.[39b]

contact with the metal surface. This is not only valid for the orbital structure but also for changes in the spin states. The latter has been demonstrated for adsorption of ethylene on Cu single-crystal surfaces.[8,39a] It was observed that the changes in the geometries of adsorbed ethylene, from the planar configuration in the free molecule to the approximately sp^3-hybridized state of the adsorbed molecule, are very similar to the eclipsed configuration of free ethylene in the triplet state. The small adsorption energies found result mainly from the compensation of the singlet−triplet transition energy by the relatively large M−C bond energy corrections. Exchange between metal electrons and ethylene π molecular electrons is responsible for this spin-forbidden transition to the relatively low triplet excited state of the molecule. Overall, there is negligible electron transfer between the molecule and the surface. Adsorption of ethylene is preferentially di-σ, as has also been found for many of the group VIII metals.[40] The analysis by Nilsson and Petterson attributes the distortion of the benzene configuration adsorbed on the Cu(110) surface to the changes in the triplet state of the benzene.[8]

The balance between Pauli repulsive interactions and back-donating chemisorption bond energy stabilizing interactions also controls the coordination of diatomic π-bonded molecules. On most of the group VIII metals CO tends to adsorb end on through its carbon atom. However, on a low work function metal such as Fe, CO adsorbs side on. The tendency of NO to be adsorbed end on is less than that for CO. For instance, NO also adsorbs side on on the Rh(100) surface.[41] O_2 with its lower electron affinity will adsorb side on on most metals. In contrast, N_2 adsorbs end on on metals such as Ni. In all these cases the occupied π molecular orbital causes increased Pauli repulsion in high coordination sites that is counteracted by back-donating interactions favoring high coordination sites. In the end-on adsorbed mode Pauli repulsive interactions are reduced with the molecular π bonds, but now these interactions are replaced by repulsive and partially repulsive interactions with occupied 4σ and 5σ orbitals that in this mode have large interactions with the metal surface. The adsorption of the molecule leads to the mixing of symmetry-adapted orbitals of the metal surface and the adsorbate. Effectively this leads to a rehybridization of the orbitals of the adsorbate. This has been very well illustrated in Figure 10.

Föhlisch et al. in a combined experimental and theoretical work elegantly explained the electronic and bonding nature of the CO adsorption on different sites of the Ni surface.[39b,42]

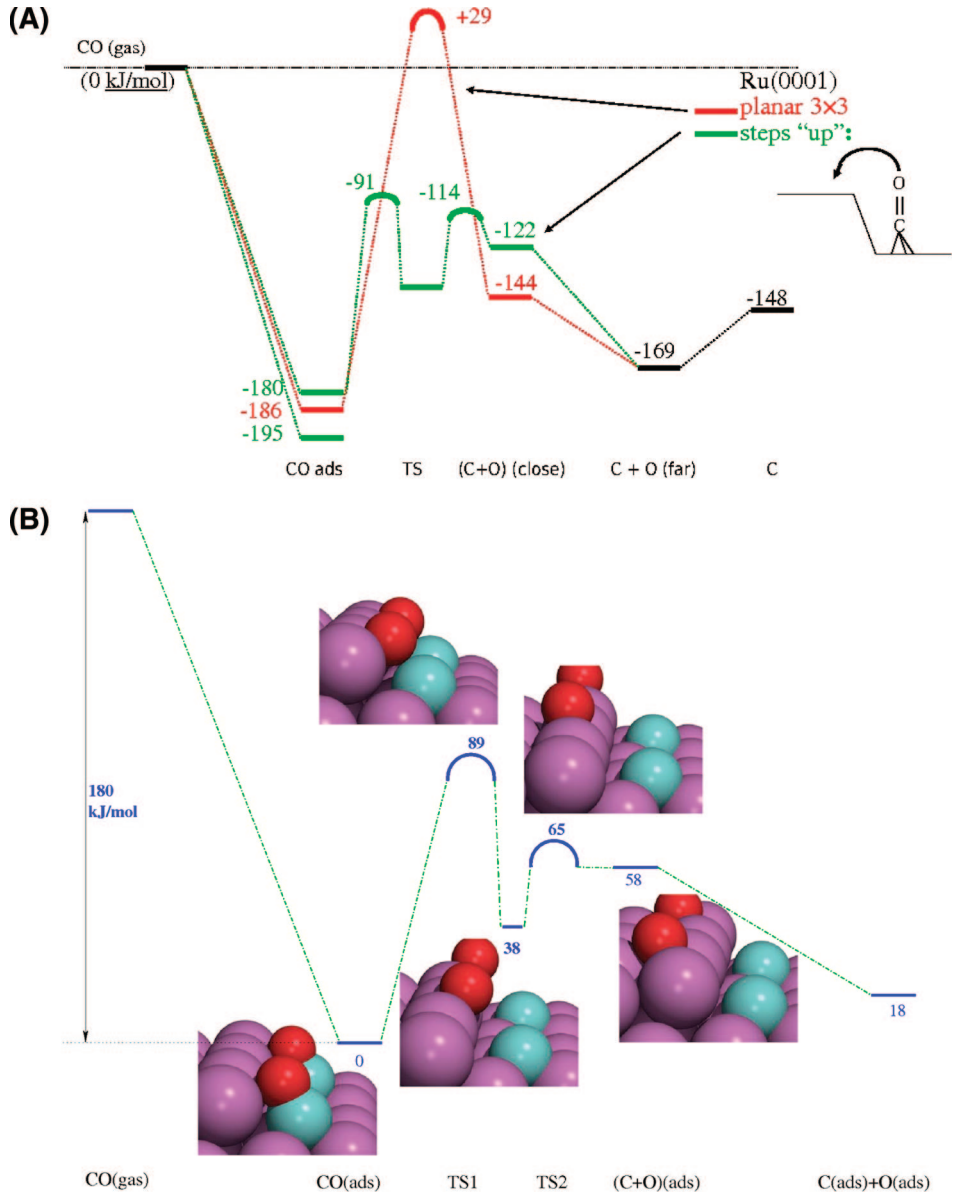

Figure 11. (A) Reaction energy diagram of dissociation of CO on Ru. A stepped and nonstepped surface is compared.[42] (B) Structures of CO dissociating at a stepped surface at potential-energy saddle points and local energy minima positions.[42]

The schematic representation shown in Figure 10 depicts the interaction of CO through its C atom with the Ni d_{z^2}, d_{xz}, or d_{yz} atomic orbitals. Consequently, rehybridization of σ- as well as π-type molecular orbitals occurs. The interaction with the doubly occupied σ orbitals reduces the electron density in this orbital system. Since the 5σ orbital is antibonding with respect to the CO bond, it increases the internal CO bond energy. The donation of electrons from the 5σ CO molecular orbital into the empty d valence metal orbitals reduces the Pauli repulsion between initially doubly occupied orbitals. Rehybridization of the π electronic system and substantial back-donation of electrons into the empty $2\pi^*$ orbital contributes to the weakening of the CO bond. Electron density gets more localized on O due to the rehybridization. The weakening of the CO bond by electron back-donation into the CO $2\pi^*$ orbital critically determines the height of the activation barrier for CO dissociation. This is similar for the other diatomic molecules. The weakening of the CO bond increases when CO adsorbs in high coordination sites due to the increase in the overlap of the π orbitals, also when oriented end on. Consequently, electron back-donation increases and the CO bond weakens. It is important to realize that this does not necessarily imply an increase in the overall adsorption energy. The attractive contribution to the adsorbate bond energy is counteracted by the increase in the Pauli repulsive interactions. During dissociation the CO bond has to stretch. Increasing back-donation of electrons from the metal will help as well as the lowered π^* position. The CO molecule undergoes a significant stretch from its initial upright position, which is nearly perpendicular to the surface normal, to the one in which there is a significant decrease in the angle with which the adsorbate binds to the surface. Figure 11 illustrates the energetic and structural changes for a CO molecule that dissociates on a terrace and step of the Ru(0001) surface.[43] We will first discuss the dissociation of CO on the Ru(0001) terrace. Although CO prefers the 3-fold (3-fold) fcc adsorption site, it has to diffuse to an atop site on the Ru surface in order to reach the transition-state configuration. This diffusion from the 3-fold site to the atop site, which costs 25 kJ/mol, can be considered as a pre-transition state. This energy must be added to the intrinsic barrier to activate CO from the atop site in order to calculate

the overall activation barrier for the reaction. The transition-state energy with respect to the pre-transition state (the activation from the atop site) $E^{\ddagger}_{diss}$ is equal to 209 kJ/mol. The first local minimum of the dissociated molecule is a state where O_{ads} and C_{ads} still significantly interact. The direct attractive interaction between O and C within the CO molecule is replaced by a repulsive interaction that occurs indirectly through the surface metal atom that they share. The C═O bond can be considered to be nearly broken. This state can be considered to be a post-transition state (this can also be considered to be a pre-transition state for the reverse recombination reaction to form CO from the C_{ads} and O_{ads}). With respect to the final separate state of C_{ads} and O_{ads} the post-transition-state energy is repulsive and amounts to 25 kJ/mol. As can be observed from Figure 11 for the stepped surface, the transition-state configuration is already close to the structure of the post-transition state. This indicates the late nature of this transition state. Dissociation at the step edge results in a significant lowering of the reaction barrier. As observed from Figure 11a, there is a small pre-transition-state energy cost that is required to move the molecule close to the step edge. The molecule adsorbs initially at the bottom of the step. The transition state to activate CO is again near its final state. The first minimum that is reached is the pre-transition state where carbon atom of CO is bound at the bottom of step. The oxygen atom interacts with the 2-fold site that exists at the top of the step edge (Figure 11b). The energy for this pre-transition state is 56 kJ/mol higher than the most stable state. From this initial minimum the oxygen and carbon atoms move from the step edge to a second less stable pre-transition-state configuration.

Interestingly, the low barrier for dissociation at the step edge compared to that on the terrace does not correlate with the corresponding reaction energy differences for the dissociated state. The adsorbed C and O atoms that result near the step edge are in a less stable configuration than in the corresponding pre-transition state on the terrace. Recombination of C and O atoms at the step-edge sites will also show a lowered activation energy barrier. The lowering of the barrier at the step edge is due to increased opportunity for back-donation of electrons into antibonding orbitals of CO, which results from the additional interaction of CO with d atomic orbitals at the step edge, as demonstrated initially using extended-Hückel-type studies.[44] The stretching of the CO bond required to reach the transition state is also much less than what is required on the terrace because of the close proximity of the oxygen atom to the Ru atoms at the top of the step. An additional reason for the lower energy barrier at the step edge is the structural difference of the transition state. At the step edge the dissociating atoms do not share binding to the same surface metal atom.[45] This reduces the repulsive interaction of the adspecies. Additionally, on a terrace the CO molecule has to bend from a perpendicular to a parallel configuration to activate the CO bond. This is not the case at the step edge.

The observation of low transition-state energies for dissociation as well as the reverse reaction for recombination on sites that circumvent formation of shared bonds of the dissociating or recombining fragments with the same surface metal atom is general. As we will see later, this feature is also responsible for the large difference in the reactivity of fcc(100) surfaces compared to the (111) surfaces. The square arrangement of atoms on the (100) surfaces cause low dissociation and recombination barriers of π molecular bond

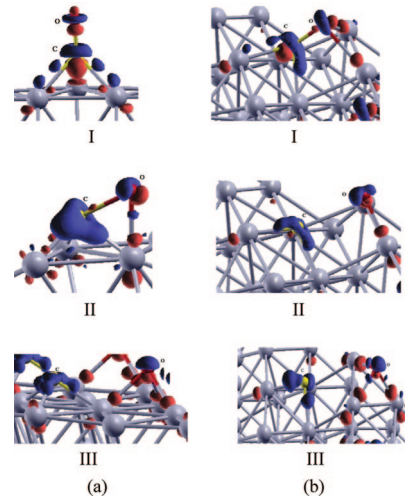

Figure 12. Charge density difference plots of CO on the Ru(0001) surface (a) and stepped Ru(1015) surface (b): I, initial state; II, transition state; III, final state. The red and blue regions indicate the charge lost and gained, respectively.

diatomic molecules in which the fragments interact with the surface metal atoms through the opposite sites of the squares, i.e., not sharing the metal atoms.

Figure 12 illustrates changes in chemical bonding within the CO molecule by showing the changes in CO electron density upon dissociation for CO dissociating on a Ru(0001) surface and the stepped Ru surface. In Figure 12 two features are noteworthy: The large rehybridization features on C and O through the dissociation process, and the differences in the CO interaction when comparing the dense and open stepped surface. One clearly observes the complete rupture of the CO bond on the stepped surface compared to the dissociation on the terrace. Even in the transition state the interaction of CO with the terrace site, in which sharing of metal atoms with C and O occurs, is weaker than on the step site in which no such sharing takes place. This relates to the previous observation, made for ethylene, that a molecule that interacts through a π bond with the metal and is adsorbed side on prefers di-σ over π (single metal atom coordination). This enhances back-donative interactions significantly. For molecular adsorption on the Ru(0001) surface, CO shows the earlier described changes on C and O. Compared to the stepped surface (Figure 12b) one observes less dramatic changes and the still largely intact CO bond. In the respective transition states, prominent rehybridization on the atoms is seen to occur. Both O and C show electron density features close to those of the adsorbed atoms. The CO bond appears completely broken on the stepped surface.

The late nature of the transition state and its closeness to the structure of the final state implies that in the crossing part of the potential-energy curves there is no memory of the initial state. For such a case, a useful choice for the transition-state energy is to take its value with respect to the gas phase, $E^{\ddagger}_{g}$, and to study how it correlates with the energy of the product state computed also with respect to the same gas phase state (E^{prod}_{g})

$$\Delta E^{\ddagger}_{g} = \alpha' \Delta E^{prod}_{g} \qquad (6)$$

For surface reactions, BEP plots applying eq 6 are often established.[5] Reaction sites of the same structure but on a different metal are compared. For diatomic molecules such

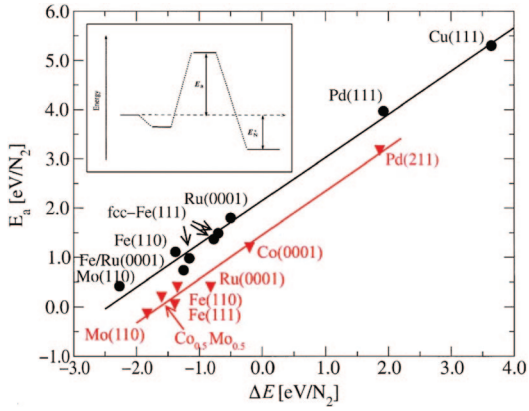

Figure 13. Calculated activation energies (transition-state potential energies) for N_2 dissociation (E_a) on a range of metal surfaces plotted as a function of the adsorption energy for two nitrogen atoms (E_{N^*}). All energies are relative to N_2(g). Results for both close-packed surfaces (circles) and more open surfaces are shown (triangles). (Inset) Sketch of the energetics for the N_2 dissociation reaction.[24b]

as CO, N_2, NO, and O_2, the values of α' are close to 1. This is consistent with the identification of these transition states as late with respect to the initial state on the reaction coordinate for dissociation reactions. An example of such BEP plots for N_2 dissociation is shown in Figure 13.[5,24b] The data have been plotted using eq 6. The two different lines that result correspond to dissociation on a surface with a topology similar to that of the (111) surface of an fcc crystal and on a stepped surface along the (100) directions.

While the resulting lines are parallel with α values of around 0.9, they are shifted with respect to each other. This energy shift corresponds to the energy difference of the activation energies E°_{act} (Figure 1) for the two topologically different dissociation sites. This difference is indeed a constant. This is consistent with the general linear free-energy relationships which suggest that reactions which belong to the same families will have the same slope but may have different intercepts due to differences in the initial states. This very well agrees with the interpretation made in section 2, where we mentioned that the distance between the minimums of the initial and the final states on the reaction coordinate should remain constant. Hence, one cannot apply the BEP relationship obtained for the dense surfaces with the stepped surface because the distance between the minimums of the initial and final states on the reaction coordinate differs.

In essence, this means that the difference in the energies of the transition state and product state remain approximately constant when there are changes in the metal. Such late transition states can also be considered tight transition states. There is no mobility of the atoms in the product as well as in the transition state. The entropy of the transition state in such a case is thus very low and close to that of the final dissociated state.[46] It is important to realize that often intermediate states are present between the reactant, transition, and final product states which are adsorbed at a distance whereby they do not interact. The corresponding reaction energy diagram for this type of system is schematically drawn in Figure 14. This can be illustrated by following the reaction coordinate for dissociation of CO along a terrace. CO is activated late along the reaction coordinate to form a late transition state. The path from the transition state continues down along the potential-energy surface to a first local

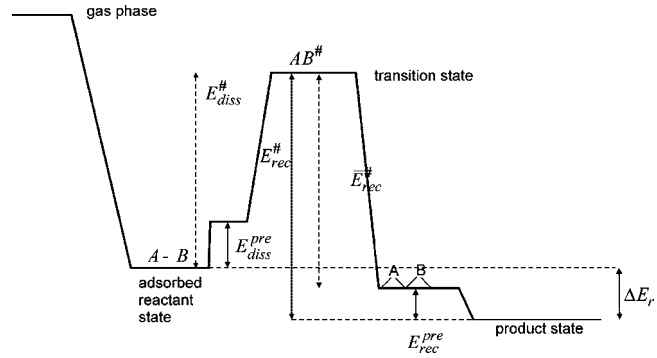

Figure 14. Schematic representation of the reaction energy diagram for the dissociation of a molecule AB into fragments A and B; $\bar{E}^{\ddagger}_{rec} = E^{\ddagger}_{rec} - E^{pre}_{rec}$.

minimum which is an intermediate, where the carbon and oxygen atoms are in an equilibrium configuration but can interact strongly when they share coordination to the same surface metal atom. This interaction is usually repulsive (see ref 6, p 144). This is in contrast to the situation on the step edges, where the carbon and oxygen adatoms are fully separated and do not interact with one another, thus resulting directly in the stabilization of the energy.

With respect to recombination, the intermediate state is considered as a pre-transition state. The pre-transition-state energy E^{pre}_{rec} of the repulsive state on a fcc(111) terrace is typically of the order of 30−70 kJ/mol due to the sharing of a metal atom. The overall activation energy for recombination can be written as

$$E^{\ddagger}_{rec} = E^{pre}_{rec} + \bar{E}^{\ddagger}_{rec} \tag{7}$$

$\bar{E}^{\ddagger}_{rec}$ is the transition-state energy with respect to the recombinative pre-transition state. The potential-energy curve crossing model suggests that the energy of the transition state now should not correlate with the overall reaction energy but as

$$\delta\bar{E}^{\ddagger}_{diss} = \alpha''\delta(E_r - E^{pre}_{rec} + E^{pre}_{diss}) \tag{8a}$$

where

$$\bar{E}^{\#}_{diss} = E^{\#}_{diss} - E^{pre}_{diss} \tag{8b}$$

As we will see, no appropriate linear relationships are found between reaction energies defined for coadsorbed states and transition states with respect to the reactant state. This is because of the assumption in eq 8a that $\bar{E}^{\ddagger}_{diss}$ and E^{pre} are independent variables. This turns out not to be a valid assumption as we will see in later sections. The explanation can be given within a simple quantum-chemical model.

The quantum-chemical basis for this is explained by the simple interaction model shown in Figure 15a and the orbital interaction schemes presented in Figure 15b. In Figure 15b the molecular orbital changes are sketched for the simplified quantum-chemical interaction scheme shown in Figure 15a. In the pre-transition state, all orbitals below the E_F are doubly occupied. A metal atom is represented by the d_{xz} atomic orbital. For two coadsorbed atoms, the interaction between the p_z atomic orbitals and the d_{xz} orbitals of the metal is analyzed. Both the pre-transition- and transition-state configurations are considered. In the pre-transition state the orbital interaction of the metal atom d_{xz} atomic orbital and adatom p_z atomic orbitals are assumed to dominate ($|\beta_{p_z,d}| > |\beta_{p_z,p_z}|$). In the transition state (Figure 15b2) the π-type

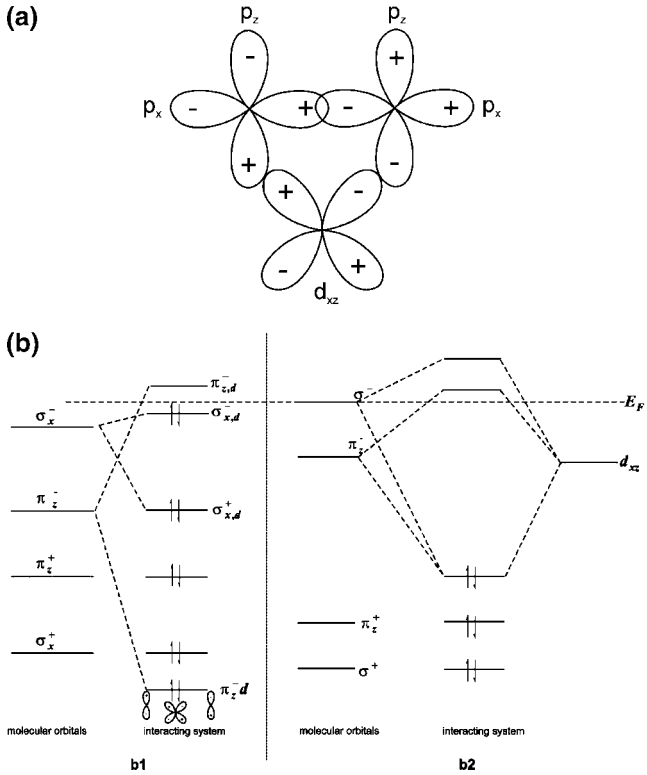

Figure 15. (a) Schematic illustration of the interaction of two p-type orbitals from the two recombining surface atoms with a d orbital of the transition-metal atom over which the recombination is carried out. (b1) Schematic molecular orbital energy diagram at the pre-transition state of reductive elimination (coadsorbed state). (b2) Schematic molecular orbital energy diagram at the transition state of reductive elimination.

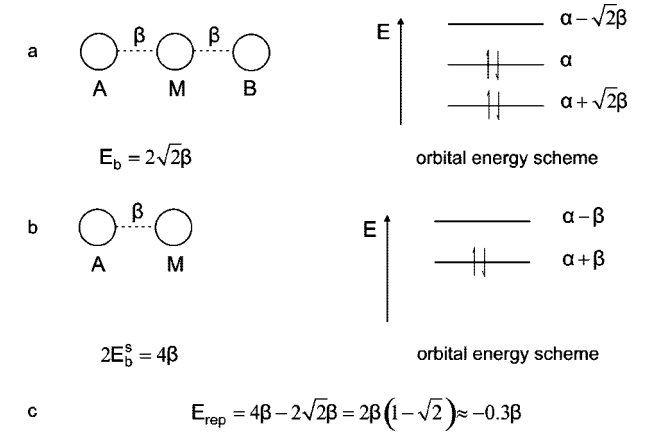

Figure 16. (a) Tight-binding orbital energies of a chain of three atoms. Each atom has an s-type orbital. The overlap energies β as well as orbital energies are assumed to be equal. (b) Tight-binding orbital energies of the separately interacting atoms. (c) Repulsive energy.

molecular orbital interaction between the coadsorbed atoms dominates (β_{p_x,p_x}, $\beta_{p_z,p_z} > \beta_{p_z,d}$). E_{pre}^{rec}, the repulsive coadsorption energy, is seen to depend on two interaction components that are both repulsive. The through-metal interaction is mediated by the metal atom to which the recombining atoms are connected. This repulsive interaction can be readily understood by a comparison of the interaction in a linear chain of three atoms with that of the separated components (Figure 16). In accordance with bond order conservation principle one can ascertain from Figure 16 that sharing of bonds with the same atoms decreases the individual bond energies. In Figure 16b the orbital with energy $\alpha + \sqrt{2}\beta$ corresponds to the bonding orbital component π_z^-d of Figure 15b1. In addition to this bonding interaction, which is less than the sum of the interaction of the separate atoms, there is also a repulsive interaction with molecular σ-type interactions.

The direct interactions of coadsorbed adatoms give rise to both bonding and antibonding π_z-type as well as σ_x orbitals (the molecular orbitals shown in Figure 15b). When bonding as well as antibonding molecular orbitals are occupied by electrons, these interactions are repulsive. The interaction with the d metal atomic orbital may however push the antibonding component above the E_F, which reduces the overall repulsive interaction. In the transition state the strong interaction between the adatoms pushes the antibonding σ as well as π-type orbitals further higher in energy. Ultimately when pushed above the E_F, the antibonding π orbital and σ orbitals may donate their electrons into empty metal orbitals. This analysis illustrates that $\bar{E}_{rec}^{\ddagger}$ and E_{rec}^{pre} cannot be considered independent quantities. The different behavior of E_{rec}^{pre} for CO and NO formation has to relate to the occupation of the antibonding π orbital in the free molecule. In CO this antibonding π orbital is not occupied. As a consequence for NO, the direct π repulsive interactions between the coadsorbed atoms in the pre-transition state are relatively small and changes in E_{rec}^{pre} are dominated by the adatom interactions through the shared surface metal atom. These are found to be more significant for the stronger interacting Ru than Pd surface. We infer from the above theoretical analysis that BEP-type relations are only useful when a direct comparison is made between the activation energies and the reaction energies obtained from the reactant and separated product state. We conclude this section with an analysis on how the activation energy of an H_2-type molecule depends on the position of an antibonding surface−adsorbate orbital with respect to the E_F.

We start by analyzing the dissociation of a homonuclear diatomic molecule, A_2, over two metal atoms to form the activated surface complex as shown in Figure 15. The two metal atoms are considered to be embedded in the Fermi sea of a conductive metal. We consider the simple quantum-chemical model in which each of the four atoms is described by a 1s atomic orbital. The electron affinities of all atoms are assumed to be equal. The atoms in A_2 interact initially with each other with an overlap energy β. The interaction of the metal atoms with the molecule is ignored. After reaction they each interact with one of the adsorbate atoms with overlap energy β'. The orbital scheme and energies are given for the nonembedded system in Figure 15a. The reaction here is assumed to be thermodynamically neutral. The transition state is defined as the state where the overlap energies are similar. The intramolecular overlap energy at the transition state is substantially reduced due to stretching of the A_2 bond. We assume that the M−A bond overlap energies are reduced to one-half their final-state values. In Figure 4 the two situations are compared where in the transition state of the antibonding surface interaction orbital is either lower or higher than the metal E_F. In the latter case a lower transition-state energy is found because electrons are donated from the surface complex to the metal. Interestingly, the dissociation reaction according to the interaction scheme sketched in Figure 17 is a Woodward−Hoffmann[27b] forbidden reaction. Such a scheme is always expected to generate a significant reaction barrier when only orbitals of

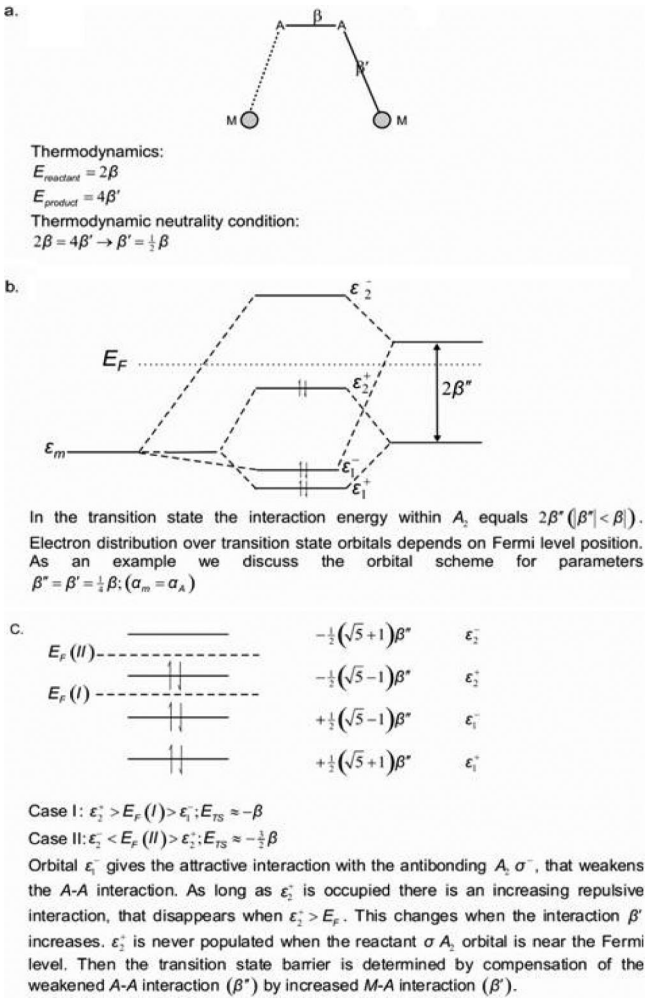

Figure 17. Schematic representation of the molecular orbital view of homonuclear diatomic molecule dissociation. (a) Interaction scheme of the σ bond of a diatomic molecule, A_2, with s atomic orbitals of two metal atoms (4 electron occupation). (b) Molecular orbital view of the transition-state orbitals. Orbital occupation depends on the relative position with respect to the Fermi level. (c) Energies as a function of the relative position with respect to the Fermi level.[33]

the same symmetry in A_2 and M_2 are occupied. This repulsive energy is due to population of the bonding and antibonding surface orbital combinations ε_1^+ and ε_2^+. The resulting Pauli repulsion is proportional to $-\beta' S$ (S being the overlap of the atomic orbitals).

Embedding in the Fermi sea of the metal reduces this barrier when the ε_2^+ state is pushed above the E_F. The orbital is depleted by donation of electrons into the empty metal orbitals. This determines the difference of the cluster and surface. The relevant barrier is usually the energy cost to cleave the A−A bond. In the transition state it is typically weakened to one-quarter of its predissociation state value. The energy cost of this reduction $-3/2\beta$ (the A−A bond before reaction is 2β) is reduced by the interaction energy with the metal surface $4\beta''$. In the transition state we choose $\beta'' = 1/2\beta'$. $2\beta'$ is the energy of the product M−H bond. It would give an overall activation energy of $-1/2\beta$. These interpretations hold when the energy changes of A_2 bond stretching and the interaction with the metal surface are considered to be additive. In Figure 17c quantum-chemical solutions for this model are presented.

Case I results in a lower activation barrier as a result of the depletion of the antibonding orbitals that are pushed above the E_F. Whereas the additive interaction model would give an energy of $6\beta''$ for the transition-state system, quantum-chemical delocalization reduces this to $4\beta''$. It increases the activation barrier to $-\beta$. The interaction energy of $4\beta''$ is equal to the sum of the energies of the two M−H bonds, assuming that the A−A bond is completely broken. This is in agreement with the decomposition proposed by Hu et al. to be discussed in section 3.2.2. In contrast, the quantum-chemical model indicates that the strength of the A−A bond is weekend compared to its gas-phase value but is still one-sixth of the energy before reaction is compared to the transition-state M−H bond energies.

Within our model, case II describes a further increase of the activation barrier to $-3/2\beta$. The decreased stabilization of the transition state is due to occupation of antibonding adsorbate−surface orbitals that gives a repulsive contribution. The relatively high barriers computed within this model results from the one-quarter reduction of the initial bond energy assumed between the A atoms in the transition state to approximately one-quarter of its original value. When instead we choose a reduction of only one-half of the original bond energy, case I would not result in any barrier whereas case II would give rise to a barrier of $-1/2\beta$ instead of $-3/2\beta$. Typical activation barriers of surface bond cleavage reactions are 10−20% of the initial bond energy. For a low barrier, Pauli repulsion has to be reduced and the antibonding σ*-type A_2 orbital has to become occupied. Oxidative addition or reductive elimination of molecular σ bonds is analogous to similar reactions in metal organic complexes. It is expected to preferentially occur atop of a surface metal atom. Then optimum stabilization of antibonding σ*-type molecular orbitals is possible through back-donative interactions with the metal surface d atomic orbitals that are also antisymmetric with respect to metal surface.

3.2. Analysis of Transition States

3.2.1. Push−Pull Mechanism

According to the oxidative addition mechanism, bond stretching is the consequence of the lowering of the antibonding orbitals of the molecular bond that is to be broken. This increases electron back-donation into this antibonding adsorbate orbital and lowers the energy cost for bond dissociation. The barrier is finally overcome by the increasing interaction of the product fragments with the surface. Alternatively the initial repulsive interaction between adsorbate and surface is overcome by the polarization of the electrons in the molecule or within the metal. This push−pull model describes activation of CH bonds by soft Lewis-acid cations. A system that illustrates this model is provided by the activation of a CH bond in ethane by Ga cations adsorbed in the micropore of a zeolite. The corresponding energy diagram is shown in Figure 18.[47] Although oxidative addition to Ga is thermodynamically preferred over heterolytic bond cleavage, the actual reaction path proceeds via a heterolytic pathway. The latter pathway illustrates the Lewis-base−Lewis-acid push−pull model. Oxidative addition, according to the back-donation model, requires electron back-donation from the atomic orbitals of Ga^+, asymmetric with respect to the axis between the Ga and the center of the dissociating bond into the antibonding CH orbitals. In Ga^+, the HOMO is the symmetric 4s atomic orbital that does not interact with asymmetric orbitals. The occupied 3d atomic orbitals that have the right symmetry for electron back-donation are too

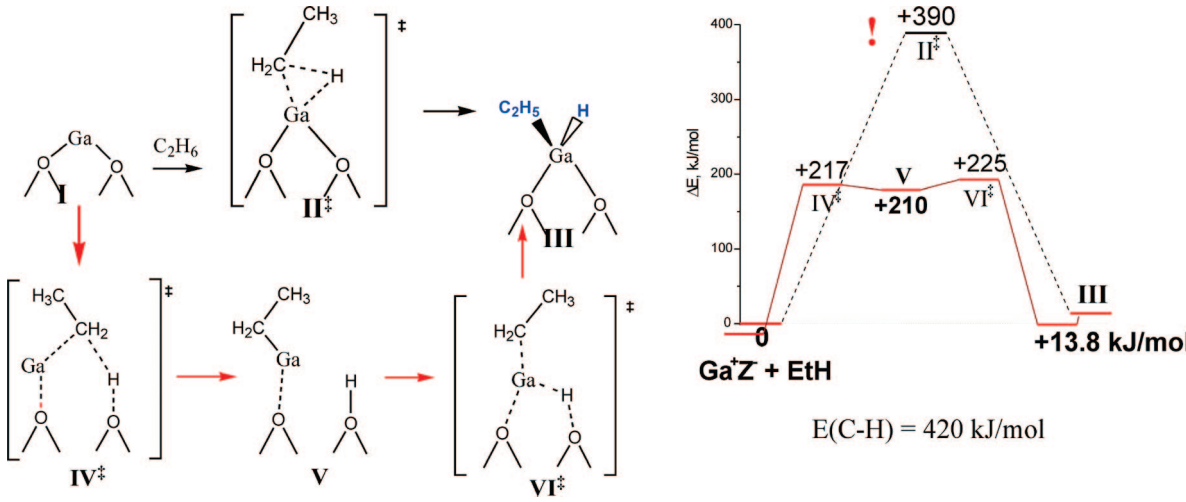

Figure 18. Reaction intermediates and reaction energies for the heterolytic dissociating of CH on Ga^+ zeolite centers.[47]

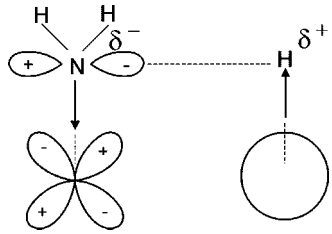

Figure 19. Schematic representation of the push−pull model of NH_3 dissociation.

low in energy to interact. Hence, extensive back-donation cannot occur and the dissociation barrier found for "back-donative" dissociation (oxidative addition) is close to the noncatalytic gas-phase bond cleavage energy of the CH bond. On the other hand, the push−pull model proceeds through a transition-state barrier that is heterolytic. Now the transition-state energy is close to that of the more favorable heterolytic dissociated state. In this state, the hydrogen atom is adsorbed "proton" like to a Lewis-base oxygen atom in the zeolite lattice and the alkyl fragment is adsorbed as a negatively charged carbanion to the Ga^+. In the second step, the proton transfers and oxidizes Ga^+ to Ga^{3+}.

The analogy to this push−pull mechanism is represented by the activation of ammonia by coadsorbed atomic oxygen atoms on a metal to form $NH_{2,ads}$ and OH_{ad}, which will be discussed in detail later. In the transition state the NH bond can be considered essentially broken and the OH bond of the water product is close to its final-state value. There is no direct activation by the metal. Contact of the NH bond with oxygen polarizes the NH bond. It leads to the formation of negatively charged $NH_2^{\delta-}$ and $H^{\delta+}$, which is schematically illustrated in Figure 19. Analogous to the heterolytic dissociation state of ethane by Ga, the NH_2 adsorbed to a single metal atom is a metastable state. It is stabilized in a consecutive step as it moves to a 2-fold coordination site. In classical studies of CH and OH activation of hydrocarbons by coadsorbed oxygen on Ag and Cu, this push−pull mechanism has been extensively explored. A relation between the gas-phase acidity of alcohol and the rate of activation by coadsorbed oxygen has been established.[48] The question that arises is whether the push−pull model as schematically visualized in Figure 19 is also applicable to the activation of CH or NH bonds on metal surfaces. It implies a view of the metal surface, where the metal is considered to have Lewis-acid−Lewis-base properties.

3.2.2. Three Ways To Analyze Transition States

In this section we will describe three ways to decompose energy changes of the chemical bonds that are formed or broken on the reaction path that connects reactant and product states. An important outcome of this analysis is the determination of the position of the transition state with respect to the chemical bond characteristics of the initial or final state.

In section 3.1.1 we already met Bickelhaupt's activation strain model when discussing activation of methane.[49,50] According to this method the energy at the transition state is decomposed into two terms (see Figure 20): the strain energy (ΔE_{strain}) is the deformation energy of reactant changing its original gas-phase structure to that of the transition state and the interaction energy is the difference between the energy of the transition-state complex and that of the separate fragments.

An interesting interpretation from the activation strain model is that there is a negligible change in the strain energy when one compares the activation of methane on many different systems. Changes in the coordination number of the reacting

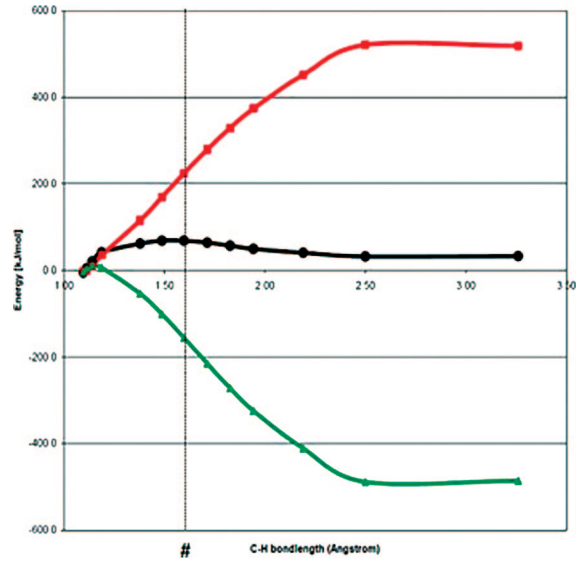

Figure 20. Activation strain model analysis of the CH_4 dissociation on the Rh(111) surface. (Black line) Interaction energy as a function of reaction coordinate. (Red line) ΔE_{strain} of the CH_4 molecule as a function of reaction coordinate. (Green line) ΔE_{int}.[38] # indicates the position of the transition state.

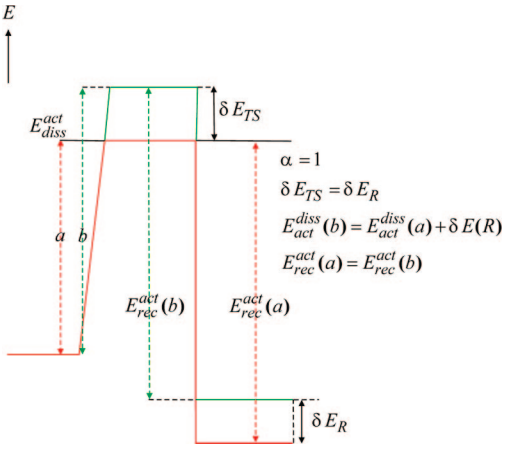

Figure 21. Brønsted−Evans−Polanyi analysis of the relation between activation energy changes in the forward and backward direction as a function of reaction energy changes when $\alpha = 1$ in the forward direction.

surface atom mainly alter the interaction energy. This generally increases with decreasing surface atom coordination number due to the increasing degree of electron localization. Whereas the activation strain model discusses reactivity with respect to the nondissociated state, for surface reactions it appears often to be very useful to analyze energy changes with respect to the dissociated state. This intuitively seems most natural for those reactions in which the transition states are late with respect to the initial nondissociated state. We have seen that dissociation of diatomic molecules with π bonds belongs to this category. Transition and product states are already close in electronic structure. In the transition state the reactant chemical bond is almost broken. This justifies the value of α in the BEP equation being close to 1.

illustrated in Figure 21, a large value of α implies that the activation energy for dissociation varies linearly with the reaction energy but the activation energy for recombination ($E_{\mathrm{rec}}^{\mathrm{act}}$) is constant. When one uses the microscopic reversibility relation

$$E_{\mathrm{R}} = E_{\mathrm{diss}}^{\ddagger} - E_{\mathrm{rec}}^{\ddagger} \tag{9a}$$

and BEP relation

$$\delta E_{\mathrm{diss}}^{\ddagger} = \alpha \delta E_{\mathrm{R}} \tag{9b}$$

the BEP relation for $\delta E_{\mathrm{rec}}^{\ddagger}$ becomes

$$\delta E_{\mathrm{rec}}^{\ddagger} = -(1-\alpha)\delta E_{\mathrm{R}} \tag{9c}$$

Liu and Hu[51] suggested that the transition-state energy for recombination, $E_{\mathrm{rec}}^{\ddagger}$, which is determined by the energy differences between the dissociated state and the transition state, corresponds mainly to the energy changes due to the shifting of adatoms from high- to low-coordination sites during the activation process. In the transition state, not only are some of the adatoms surface bonds stretched but also there is often a reduction in the coordination number of the adatoms with the surface metal atoms. The changes in energy will be proportional to the binding energies of the atoms. As we will see in section 4.1, for the recombination of nitrogen atoms, the low BEP proportionality constant determined implies that only a fraction of the adatom bonds with the surface are weakened in the transition state.

The barrier decomposition model is illustrated in Figure 22.[52] The recombination of surface fragments of coadsorbed

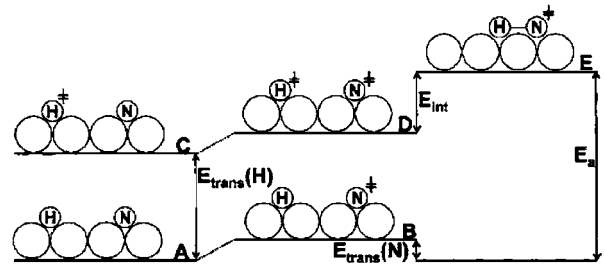

Figure 22. Schematic illustration of the barrier decomposition analysis. In state A the reactants are far apart on the surface at their equilibrium geometries and not interacting with each other. In state B the reactants are still far apart, though N has been activated to its transition-state geometry. State C is similar to state B only H is activated. In state D both reactants are activated to their respective transition-state geometries but are not interacting. In state E the reactants are at their transition-state locations and interacting.[65]

H and N atoms are considered. The activation energy for recombination is considered to consist of two energy terms

$$E_{\mathrm{rec}}^{\ddagger} = E_{\mathrm{trans}} + E_{\mathrm{int}} \tag{10}$$

The above equation is slightly different than eq 7 presented before. Whereas this expression is also a decomposition into two terms, the transition-state energy is computed with respect to the difference between the energy of the coadsorbed recombinative pre-transition-state and transition-state energy. In the barrier decomposition model, the bond energy between the recombining fragments is assumed to be zero. Thus, it strictly applies to late transition states with respect to the nondissociated state. In eq 10, E_{trans} refers to the energy cost to transfer adsorbate fragments into the configuration they have in the transition state while remaining separate. When one compares the transition-state geometries with that of the dissociated fragments, one finds that the strength of the interaction energy between reactant and surface is reduced in the transition state. This was the essential assumption used in the quantum-chemical model illustrated in Figure 17. E_{int} in eq 10 is the energy change that results when the two activated fragments are positioned into the actual transition-state complex. This term is to be compared with the relative energy of the pre-transition state of recombination but is slightly different because of the stretched adatom−metal atom distances. The barrier decomposition model works remarkably well when applied to late transition states. However, as we will see below, this is partially accidental due to a significant attractive interaction between the atoms of the adsrobate in which a chemical bond is broken or formed.

A third method to analyze transition-state energies is the symmetric transition-state analysis introduced by Bunnik, Kramer, and van Santen.[53] In this method, all bond energy changes are computed as two-body interactions and their sum is compared with the transition-state energy. In agreement with the earlier presented quantum-chemical models it is found that in the transition state the interaction energy changes are nonadditive. Different decomposition schemes can be used. As an example, Figure 23 shows a decomposition scheme for CH_4 activation based on the activation strain model. Results of the symmetric transition-state analysis are shown in Figure 24. This analysis is based on DFT quantum-chemical calculations for dissociation of CH_4 on a Rh(111) surface.[38] The intriguing result is that although the interactions are additive in the reactant and product state the maximum nonadditivity is found when the system has not

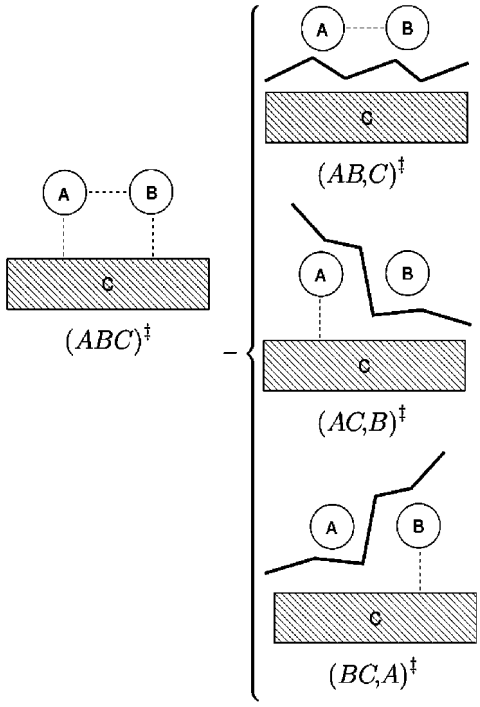

Figure 23. Schematic representation of symmetric transition-state analysis of an association/dissociation reaction consisting of parts A, B, and C. The left picture indicates the full system, and the right pictures indicate the decomposition schemes.[53]

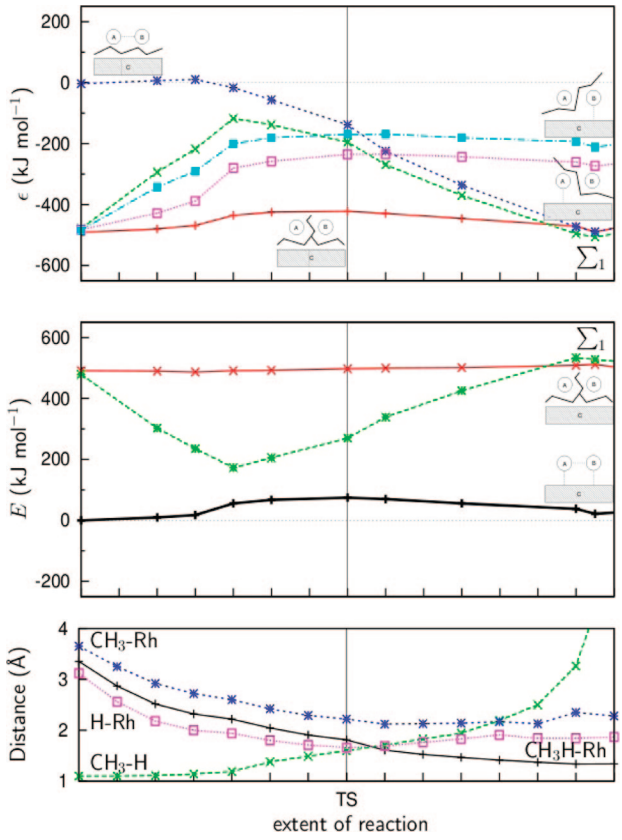

Figure 24. Symmetric transition-state analysis of the activation of CH_4 to form CH_3 and H on the Rh(111) surface. A, B, and C in the top and middle pictures are CH_3, H, and Rh surface, respectively. Σ_1 represents the sum of the decomposition energies.[53]

yet reached its transition-state value. It implies that the transition state is more than halfway on its path to the product state.

Table 1. Bond Orders of the Bonds Involved in the Methane Activation C−Rh, C−H, and H−Rh at the Reactant, Transition, and Product States[54]

bond	reactant state	transition state	product state
C−H	0.99	0.29	<0.2
C−Rh1		0.43	0.54
H−Rh1		0.38	0.42
H−Rh2		<0.2	0.49

Since the nonadditivity in interactions is still substantial, the transition state of methane dissociation is best described as on its way to become late. In section 4.1 we will discuss what this implies for the BEP α value. An indication of the relative strength of the MC, CH, and MH interactions in the transition-state geometry can be obtained from a calculation of their bond orders. The bond orders are calculated using the definition by Mayer[54] and presented in Table 1. In the transition and final states CH_3 and H remain attached to the metal atom that activates the CH bond. The numbers in Table 1 clearly indicate that there is still considerable chemical bonding present between CH in the transition state.

It is interesting to compare the activation strain model presented by Bunnik and Kramer for methane activation over the Rh(111) surface as presented in Figure 20 with the barrier decomposition analysis illustrated in Figure 22 by Crawford and Hu. The corresponding values for the surface interaction energies of the separated $CH_3^{\ddagger}$ and $H^{\ddagger}$ surface intermediates in their transition-state structures with respect to the gas phase are 203 and 263 kJ/mol, respectively.[53] The energy of the transition-state complex $CH_4^{\ddagger}$ in the gas phase shows a reduction of the strength of the CH bond from 490 to 245 kJ/mol. This is calculated from the deformation energy of CH_4 in its transition-state configuration in the gas phase. In the transition state the interaction energy of 180 kJ/mol is computed with respect to the surface. If one assumes that these energies remain unaltered when $CH_4^{\ddagger}$ interacts with the surface, then a repulsive interaction energy of 41 kJ/mol is computed between $CH_3^{\ddagger}$ and $H^{\ddagger}$ fragments in the transition state. Due to the interaction with the surface, the attractive interaction of 245 kJ/mol between $H^{\ddagger}$ and $CH_3^{\ddagger}$ in the gas phase is converted into an effective repulsive interaction of 41 kJ/mol.

It should be noted that the values one obtains for the different interactions are dependent on the particular partitioning of bonding interactions. A simple quantum-chemical model illustrates how this effective weakening of the three bond energies involved ($CH^{\ddagger}$, $HS^{\ddagger}$, and $CH_3S^{\ddagger}$, where S denotes the metal surface) is distributed. The tight-binding model is demonstrated in Figure 25. We approximate the transition state to a model of three interacting atoms, each with one s atomic orbital. The orbital (α) and overlap energies (β) are assumed to be equal. It agrees with the earlier proposition that the interaction energies in the transition state between the partitioned fragments are very similar. The weakening of the $CH^{\ddagger}$ bond energy depends again

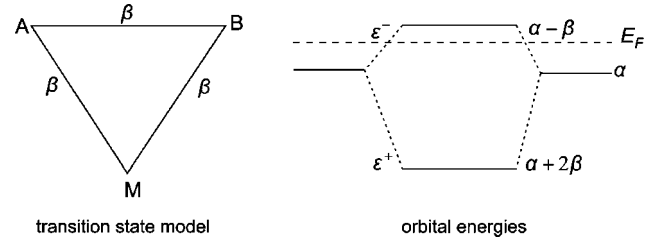

Figure 25. Transition state model for dissociation of molecular σ bond over the metal s orbital.

on the relative position of the antibonding orbitals of the transition state and the E_F.

In the case where the E_F is lower than these orbitals, electrons flow from antibonding orbitals ε^- to E_F and the total energy is 4β. The energy per bond is then $4/3\beta$, which can be compared with the energy 2β for the $CH_3-H^{\ddagger}$ bond of the free transition-state molecule. One can conclude that the $CH^{\ddagger}$ bond in the transition state is reduced to 164 kJ/mol, which is 33% of its gas-phase value. The $H^{\ddagger}S$ and $CH_3{}^{\ddagger}S$ bonds are also weakened by one-third of their noninteracting values. This analysis leads to the interesting conclusion that the bond strength of a dissociating C−H bond is still significant in its transition state, when dissociation occurs over a (111) terrace. The choice of the relative position of the E_F level versus antibonding orbitals corresponds to the reductive elimination model[28] that locates the transition state where the antibonding orbitals and E_F cross. A high transition-state barrier corresponds to a low value of the transition-state complex energy with respect to the energies of the free components.

4. Trends in the Activation Energies of the Diatomic Molecules

4.1. Diatomic Molecules

As a further introduction to the dissociation of diatomic molecules we extend our discussion from CO to N_2 and examine in detail the reaction path for the recombination of 2 N atoms to form N_2 on the Rh(111) surface[55] following the barrier decomposition approach of Liu and Hu.[51] Figure 26a describes the changes in energy that occur when two surface nitrogen atoms recombine from an initial coadsorbed state. The corresponding surface geometries are shown in Figure 26b. Basically two steps can be considered. The two nitrogen atoms initially are brought together in a pre-transition recombinative state where they are adsorbed in the hcp sites (a2 configuration in Figure 26a and 26b). The recombinative pre-transition, a2, state is 105 kJ/mol (Figure 26a) less stable than the more stable a1 state. This justifies the strong repulsive interaction between the two N atoms in this pre-transition state. The reaction proceeds by stretching the M−N bonds from the coadsorbed state. In the transition state, one nitrogen atom moves to a 2-fold configuration with a cost of ~80 kJ/mol; the weakening of the other bonds contributes an additional 70 kJ/mol. This energy cost is 16% of the total interaction energy of the nitrogen atoms before recombination. This number corresponds approximately to cleavage of one of the six bonds of the two N atoms in the reactant state. Compared to the dissociated state there is very little change in the entropy at the transition state. This indicates a very rigid transition state. This is consistent with the general observation that in the transition state the N−N bond interaction is still rather weak and the interaction with surface metal atoms dominates. The repulsive pre-transition-state energy as well as the bond weakening of surface adatom bonds can be expected to relate to the adsorption energies of the nitrogen atoms. If one assumes a linear dependence, this results in the following

$$E^{\ddagger}_{rec} = (1-\alpha)E_R \quad (11a)$$

$$\approx \frac{1}{6}(2E_N - E_{N_2}) \quad (11b)$$

$$\alpha \approx 0.8 \quad (11c)$$

We will return later to the question of the validity of the proposed linearity between the transition-state energy of recombination and the adsorption energies.

It is interesting to compare the energy diagram of N_2 recombination with that for NO recombination on a stepped and nonstepped Pt(111) surface (Figure 27).[7] On the Pt(111) terrace, NO recombination proceeds through formation of a pre-transition state with a repulsive energy of 67 kJ/mol. Note again the double counting of the interactions due to the limited size of the unit cell; this reduces the repulsive interaction per N−O interaction to ~35 kJ/mol. The transition state for NO recombination has a very similar structure to that for the N-atom recombination reaction that was just considered. An additional energy input of 162 kJ/mol is required. Interestingly, this energy value is very similar to that found for N_2 recombination on Rh. The recombination

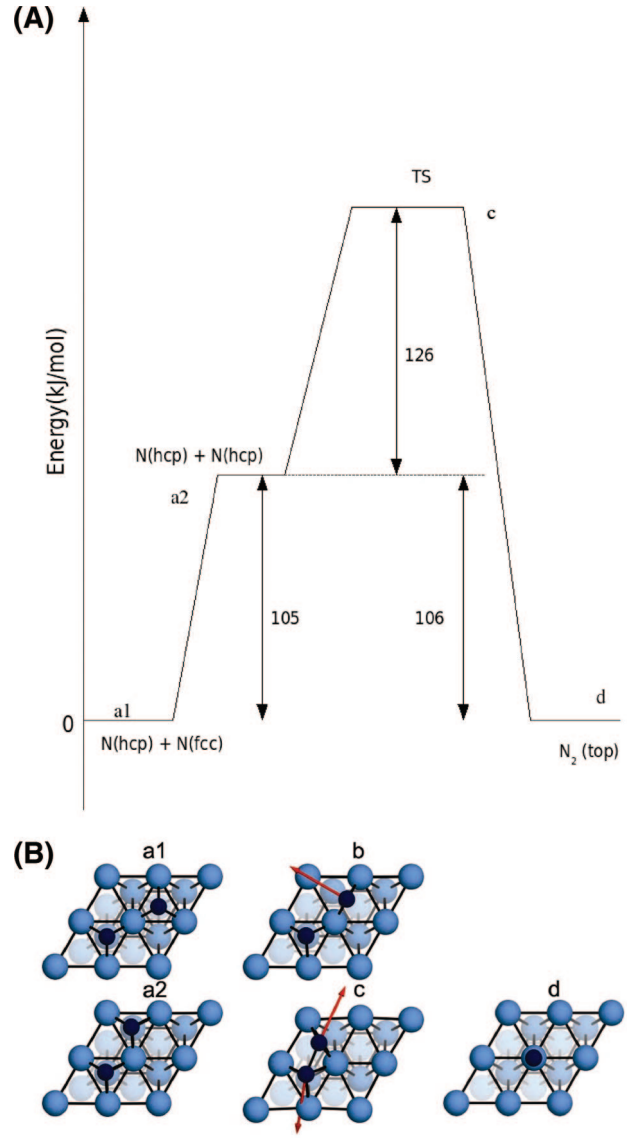

Figure 26. (A) Reaction energy diagram for the recombination of two nitrogen atoms on a Rh(111) surface.[55] The notations a1, a2, c, and d are structurally described in Figure 26b. (B) Surface configurations that belong to the different energy states of Figure 26a. a, Pre-transition-state configurations; b, transition state between state a1 and a2; c, transition state for recombination; d, hinal molecular state.[55] The blue and black spheres correspond to the Rh and N atoms, respectively.

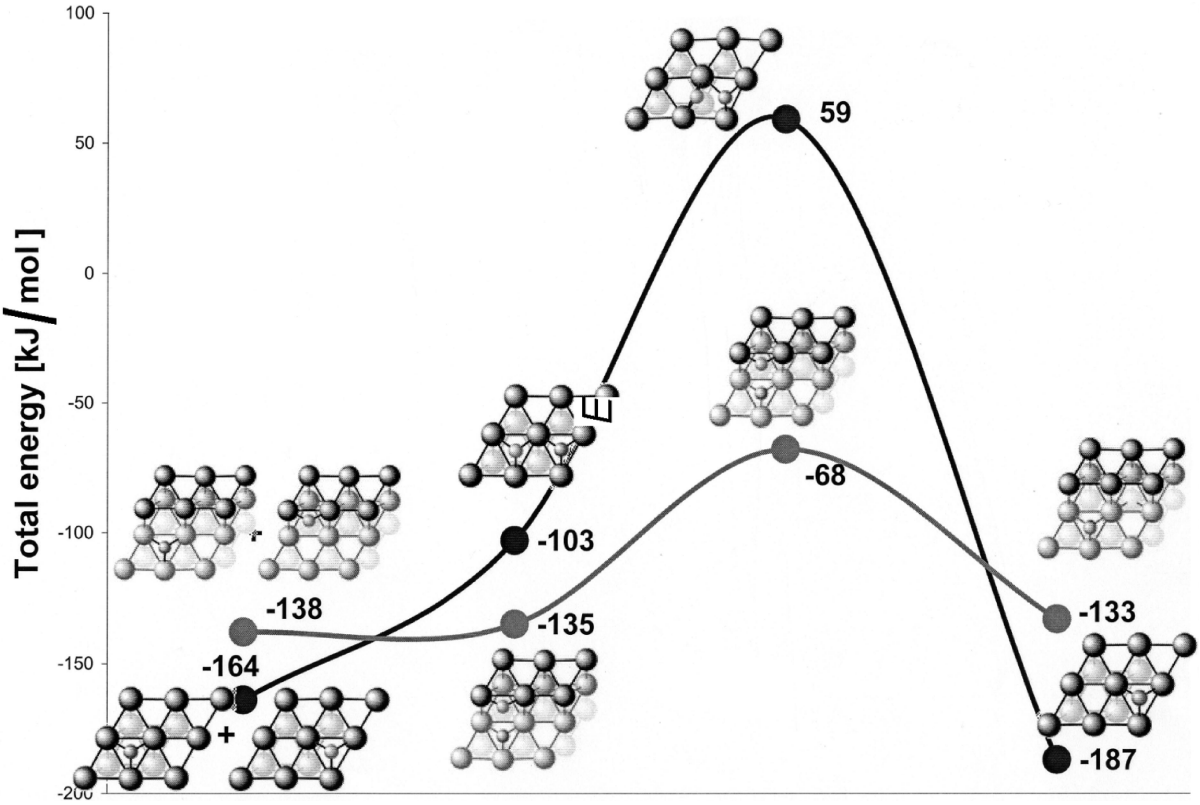

Figure 27. Reaction energy diagram for N_{ads} and O_{ads} recombination on a (111) terrace and stepped Pt surface.[7]

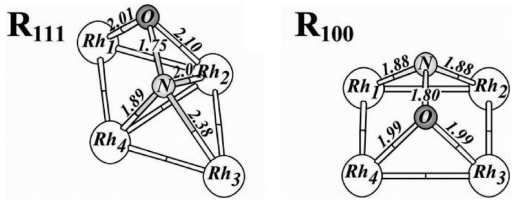

Figure 28. Transition states for NO dissociation computed for Rh(111) and Rh(100) surfaces.[57a]

over the stepped surface also proceeds through a pre-transition state; however, there is a characteristic difference. The pre-transition-state energy is 26 kJ/mol lower on the steps than on the terrace. There is no repulsive energy to form the pre-transition state since there is no surface metal atom sharing. However, there is a gain in energy as the pre-transition state moves from a low to a high coordination site. With respect to this pre-transition state, the activation energy for recombination is now reduced to 67 kJ/mol. As we discussed earlier for CO dissociation on a stepped surface, this lowering of the energy is attributed to the increased back-donation of electrons in the transition state. Such differences are not only present on terraces with steps and kinks but can also appear on surfaces which do not require the reacting fragments to share metal atoms in their transition-state configurations. A well-known example is the low activation barrier found for NO dissociation on the Pt(100) surface.[56]

Similar results have also been found for dissociation of NO on Rh or Pd.[57] The relevant prototype transition-state structures are shown in Figure 28. On the Rh(100) surface the activation energy for NO dissociation is decreased by 110 kJ/mol compared to that on the Rh(111) surface. This difference in activation energy is nearly equal to the difference in the energies of coadsorbed N_{ads} and O_{ads} in the pre-transition recombination state. This reduction in energy results from the strong repulsive interaction between N_{ads}

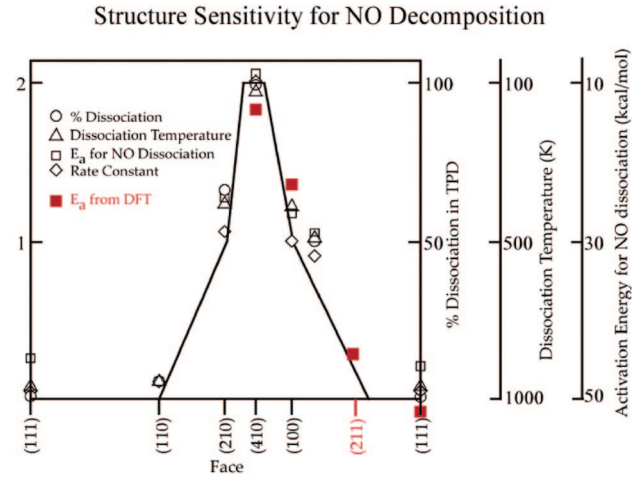

Figure 29. Comparison of the DFT-calculated NO dissociation activation energies for different faces of platinum with experimental results, as shown in the structure sensitivity diagram constructed by Masel. Adapted with permission from ref 56a. Copyright 1996 Wiley & Sons, Inc.

and O_{ads} on the Rh(111) surface, in which they share bonds to the same surface metal atom, compared to the corresponding state on the Rh(100) surface in which no sharing of surface metal atoms occur. Ge and Neurock[56a] discovered this to be the basis to a rather remarkable surface dependence for the NO dissociation on various Pt surfaces. Their results are reproduced in Figure 29. Reactions with even lower activation energies than the (100) surfaces correspond to step edges as formed on the (410) surface. The topology of the reaction site on top of the step edge is similar to that of the (100) surface. The lowered barrier is due to the increasing stabilization of adsorbed nitrogen and oxygen atoms in the product state due to binding to coordinative unsaturated edge atoms.

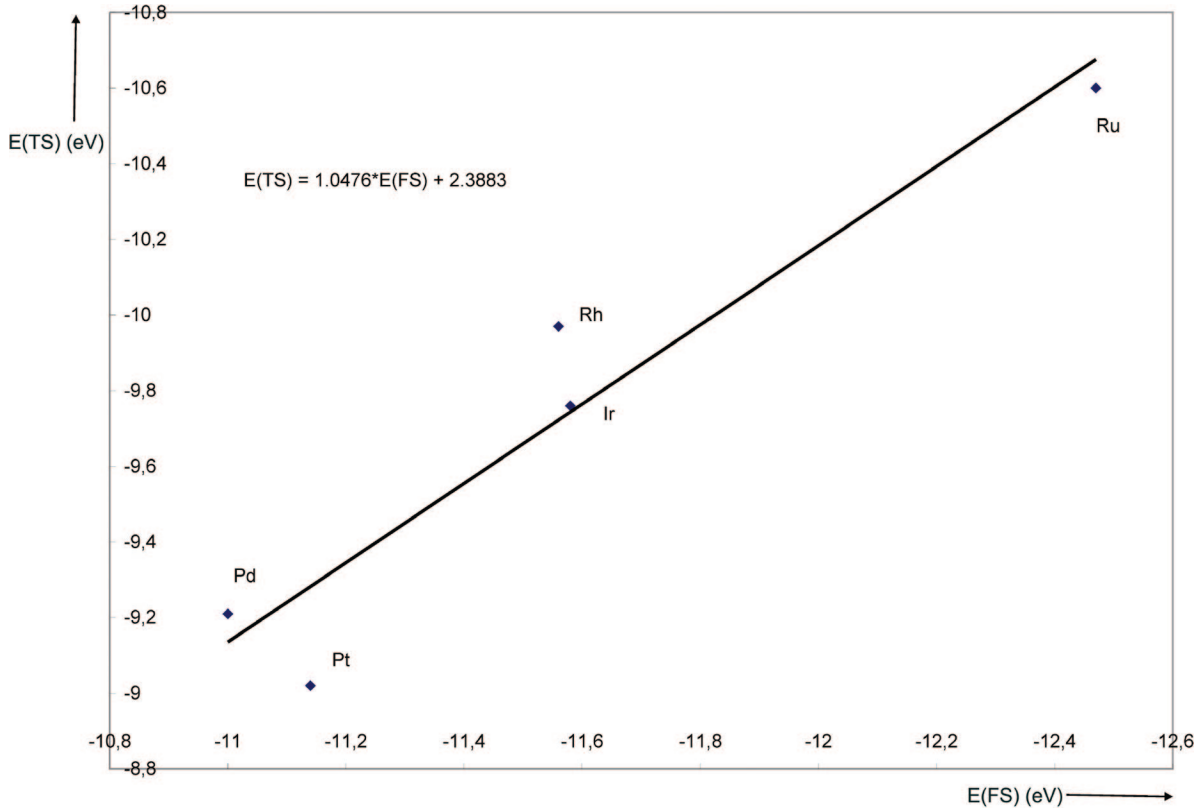

Figure 30. BEP plot of transition-state energies (E(TS)) versus the product-state energies (E(FS)) for the dissociation of CO. Data obtained from ref 60b.

The activation of CO is also known to depend significantly on the structure as was shown earlier for CO dissociation over Ru. Similarly, Ge and Neurock[58] showed significantly different activation barriers for the activation of CO over different Co surfaces. They found a difference of over 120 kJ/mol for the activation energy of CO on the terrace of the Co(0001) surface verses that on stepped Co(1124) surface. Chemisorbed carbon, a product from the dissociation, is strongly bound to the surface and prefers to adsorb in 4-fold coordination sites on Co.[59] Surfaces without these 4-fold Co sites were found to reconstruct upon dissociation to create these 4-fold sites provided that the energetics were favorable. As a result of the reconstruction, the direct relationship between the transition-state complex structure and final-state structure is lost, and as such the BEP correlation does not hold in comparing the dissociation over the four Co surfaces. Ge and Neurock did show, however, that the BEP relationship was found if the transition-state energies were correlated with product-state energies on the nonrelaxed surfaces.[58]

Several recent papers provide detailed information on transition- and product-state energies, i.e., $E^{\ddagger}_{diss}$ and E_{prod} respectively, for the activation of CO[60a] as well as NO[61] over the dense terraces of several metals. In Figure 30 reported transition-state energies $E^{\ddagger}_{diss}$ are plotted as a function of E_{prod} for CO on different closed packed (111) fcc-type transition-metal surfaces. A similar plot is given in Figure 31 for dissociation of NO. In comparing these two systems one finds two different slopes in plotting E(TS) vs E(FS) for dissociation of CO and NO. In the case of CO activation the BEP value of α determined from the slope in Figure 30 is equal to 1. For NO dissociation the value of α determined from the slope in Figure 31 is equal to 0.77. For an evaluation of α it is very important that comparable product states are considered. One expects to find a linear relation between the activation energy and the energy of the product states. However, the question is what is the most appropriate product state? Upon dissociation, the fragment atoms occupy intermediate local minima between the transition and the final state in which they typically share the metal atoms. If the neighboring surface sites are not fully occupied they can ultimately move to more favorable final product states where there is no metal atom sharing. This is simply the microscopic reverse of associative recombination of C_{ads} and O_{ads} to form CO_{ads} or N_{ads} and O_{ads} to form NO_{ads}. The intermediate state for the dissociation reaction which involves metal atom sharing is known as the pre-transition state for the associative recombination reaction. In Figures 30 and 31 we plot the activation barriers against the final product states where the product adatoms or adfragments are separated by a distance such that they do not interact with each another. The relevance of this proposal becomes quite clear if we plot E^{pre}_{rec}(CO) against E^{pre}_{rec}(NO) as shown in Figure 32.

Figure 32 illustrates that not only do the values of E^{pre}_{rec} vary for different metals but also the variations also depend on the atoms that recombine. While the values for E^{pre}_{rec} recombination of C_{ads} and O_{ads} increase as we move from Ru to Rh to Pd (i.e., left to right in the periodic table), the reverse trend is observed for N_{ads} and O_{ads} recombination. Interestingly, the activation energies for recombination of C_{ads} and O_{ads} increase as we move from Pd to Rh to Ru (i.e., right to left in the periodic table). The increase in $\bar{E}^{\ddagger}_{rec}$ compensates for the decrease of E^{pre}_{rec} in this comparison. One can then conclude that the variation of E^{pre}_{rec} and $\bar{E}^{\ddagger}_{rec}$ with metal surface cannot be considered independent from each other.

By comparison with eq 7, we can also decompose the transition-state energy into $\bar{E}^{\ddagger}_{rec}$ and E^{pre}_{rec}. The results summarized in Figures 30 and 31 as well as BEP results for CO

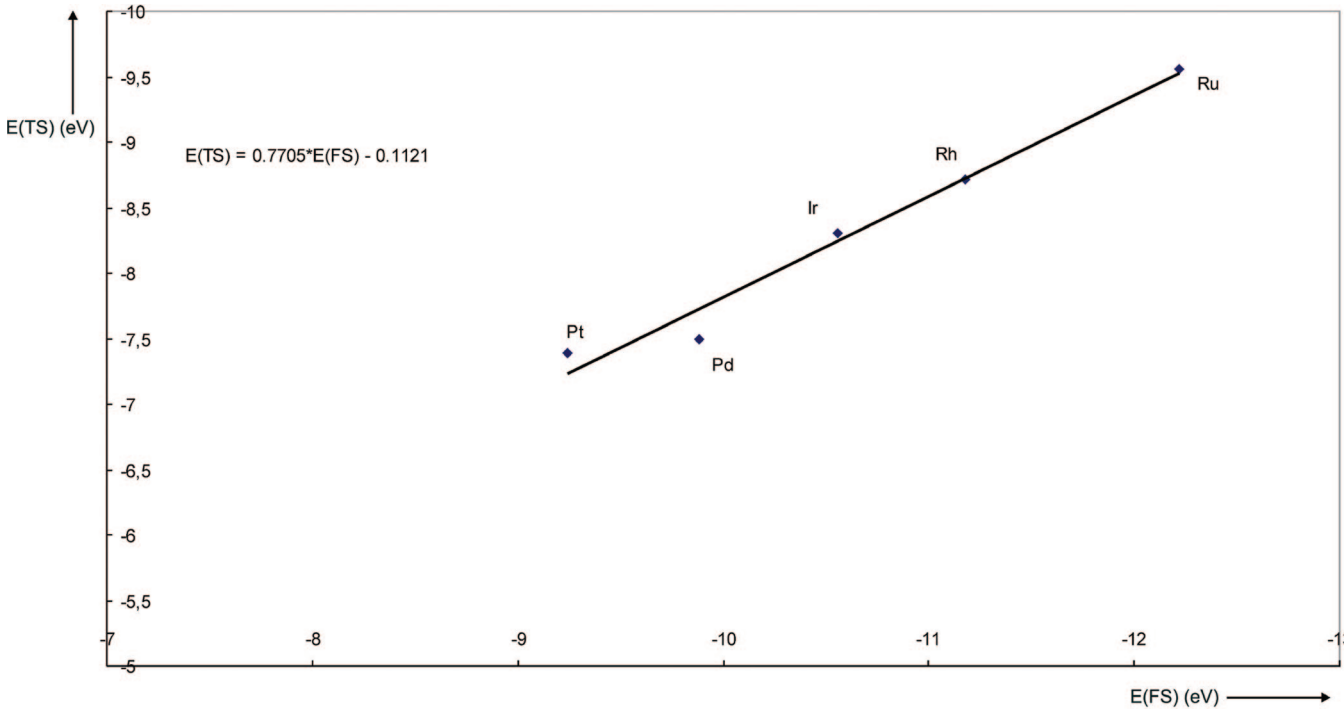

Figure 31. BEP plot of the transition-state energy (E(TS)) versus the product-state energy (E(FS)) for the dissociation of NO as a function of transition metal. Data obtained from ref 61.

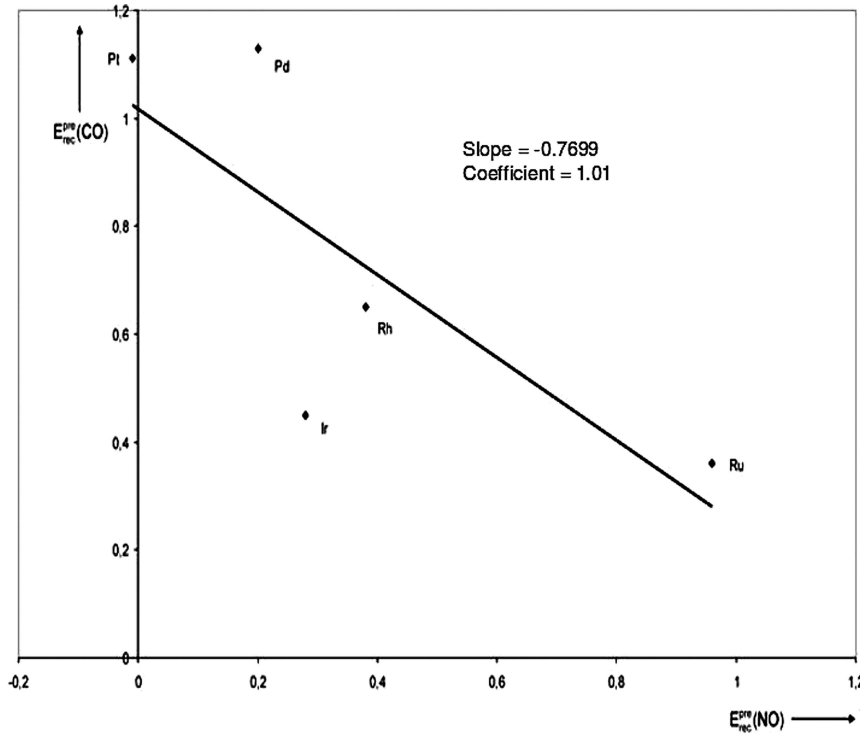

Figure 32. Repulsive interactions in the pre-transition state for NO and CO recombination plotted for different transition metals. Energies are given in eV.

and NO activation discussed earlier[62] all confirm the conclusion that $E^{\ddagger}_{rec}$ is usually close to E_{trans}, as defined in the barrier decomposition model. E_{trans} is approximately $(1 - \alpha)E_{prod}$, which helps to explain the BEP result. No successful BEP-type relation however can be found when one attempts to correlate the variations in the overall reaction energies or in the recombination barriers, $E^{\ddagger}_{rec}$ with the changes in $\bar{E}^{\ddagger}_{rec}$. As we noted earlier, this is because of the correlation between $\bar{E}^{\ddagger}_{rec}$ and E^{pre}_{rec}.

In this context, Liu and Hu[63] proposed two classes of surface reactions that are of interest. They proposed that oxidation of CO_{ads} by O_{ads} is a surface reaction of class 1. Then E^{pre}_{rec} is small and the activation energy is mainly defined by energy changes of E_{trans}. In their terminology E^{pre}_{rec} is the energy of the coadsorbed product state of the dissociated fragments. On the contrary, they defined recombination of H_{ad} with coadsorbed C_{ads} or N_{ads}, which is discussed later, as class 2, which is controlled by what they refer to as the

Table 2. CO Transition-State Energies According to the Brønsted−Evans−Polanyi Relation (kJ/mol) for (111)-Type Surfaces of fcc Crystals, $\delta E_{TST} = 0.85\delta E_R$[7]

	Fe 166	Co 251	Ni 355	Cu 517
	Ru 227	Rh 315	Pd 424	Ag 592
Re 122	Os 227	Ir 336	Pt 416	Au 581

bonding competition effect. In our terminology, this is defined by the energy change E_{rec}^{pre}. It is the large repulsive interaction that develops when coadsorbed atoms share bonding with the same surface atoms. This, according to our model, is the result of bond order conservation.[7,64] Perhaps the most important result from the CO and NO dissociation studies that we report here is that the class 1 and 2 behavior may strictly depend on the surface topology. Terrace sites tend to show class 2 behavior, whereas sites along stepped surfaces tend to show class 1 behavior. We note that one should be careful in applying this general classification. Whereas on terraces E_{rec}^{pre} for CO and NO recombination is significant, the trends in $E_{rec}^{\ddagger}$ still follow the trends in E_{trans}. There is generally no relationship with changes in E_{rec}^{pre}.

From this analysis, we reach a critical conclusion: if in the transition state E_{int} is considered negligible, the overall activation energy for recombination will strongly correlate with E_{trans}. In this case, one can relate the energies of the stable product state, where the fragments do not interact, with the activation energies. We are now in a position to understand the trends in the activation energies as a function of metal position in the periodic systems. The transition-state energies for different metal surfaces are reported in Table 2. A BEP value of $\alpha = 0.85$ has been used.[5] The barriers for CO dissociation are higher over metals such as Pd, Pt, or Cu. In essence, the activation energy barrier correlates mainly with the relative stability of C_{ads} and O_{ads} in the product state, since the adsorption energy of CO varies only slightly. The reactivity with respect to CO activation decreases moving from left to right in a row of the periodic table. We also note the increase of the activation energy for CO dissociation moving down along a column of the periodic system.

Crawford and Hu[65] correlated the activation energy for N_2 activation with the electronegativity difference of nitrogen and metal surface. The electronegativity difference provides a measure for the tendency for back-donation of surface metal electrons into the antibonding molecular orbital as well as for the strength of the metal−nitrogen bond. As we discussed earlier, lower activation barriers for CO dissociation are expected on the metals with lower electronegativity. This is because a metal possessing low electronegativity favors a larger electron back-donation compared to the high-electronegativity metals.

To summarize this section it is useful to consider the differences in the activation energy of CO dissociation on the Rh (111) stepped surface[63] that are very similar to those discussed earlier for Ru (Figure 33). The activation barrier at the step is reduced by 87 kJ/mol compared to that on the (111) surface. The activation energies for both the forward dissociation and the backward recombination reactions are reduced. Therefore, as expected for reactions that follow different reaction paths, there is no BEP relation between the two reactions. As explained earlier, the low barrier on the stepped surface is among others due to increased electron back-donation into the unoccupied antibonding CO orbital. The weakened CO bond does not have to stretch far, and in the transition-state complex there is no sharing of the surface metal atoms of the dissociating atoms. On the (111) surface, E_{pre}^{rec} is calculated to be 110 kJ/mol. This is due to the through-metal as well as direct repulsive interactions. In contrast, the energy to bring the C and O atoms from an infinite separation distance to the step edge where C is bound to a site along the terrace below the step edge and O is bound at the top of the step edge is only 17 kJ/mol.

As a general conclusion, one finds that activation and formation of chemical bonds as the result of π-type interactions is preferred along the step edges. This type of relation between the forming and breaking of molecular π bonds with the structure of the active site has an important implication on the elementary reactions on the particle size. In general, a decrease in the particle size results in an increase in the ratio of step edges and corner sites to those of terrace sites. However, when a particle becomes very small it will only have edge or corner sites available. The terraces which are necessary to form step-edges disappear. Moreover, the electronic properties of the particle also change with respect to the size. As a consequence, the maximum in the overall rate of a catalytic reaction (normalized per exposed surface atom) appears at a particular particle size which is typically on the order of 3 nm.

Figure 34 depicts such a particle as it helps to explain the maximum in the turnover frequency for ammonia formation from nitrogen as a function of Ru particle size.[62] This appears to be general for reactions which involve dissociation of π molecular bonds in the rate-determining step. A similar particle size effect on the maximum rate is also found for

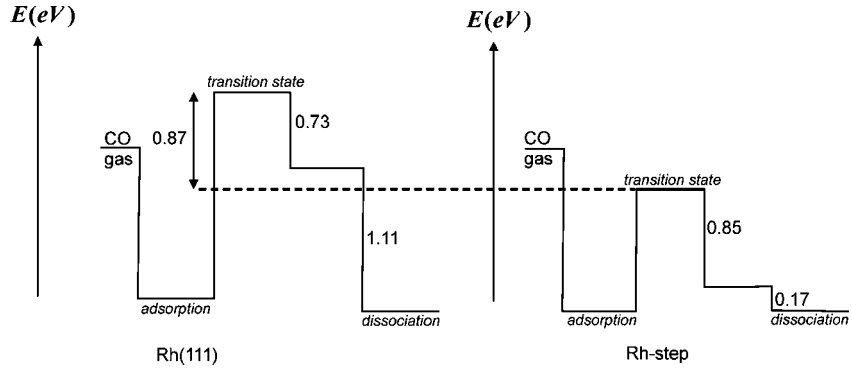

Figure 33. C_{ads} and O_{ads} recombination as well as the dissociation step is edge dependent. Schematic representation for Rh(111) and stepped Rh surfaces.

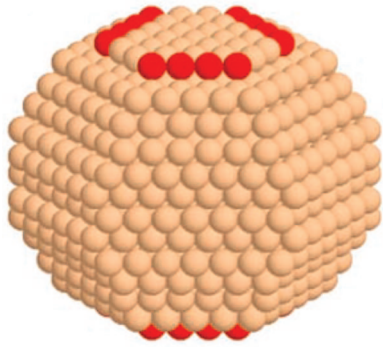

Figure 34. Typical Ru particle with an average diameter of 2.9 nm. Step sites are indicated with red.[62]

the F−T reaction,[66] which requires activation of CO over supported Co particles. Since CO dissociation also requires step-type sites, dissociation of CO over particles below a particular particle size will be difficult due to the loss of step-edge sites. The drop in activity may implicate that CO dissociation now becomes rate limiting. As a final example we mention the activation of the O_2 molecule over supported Au particles. Again, at a particle size of 2.5 nm the TOF of a reaction reaches a maximum.[67]

4.2. Activation of CH and C−C σ Bonds

4.2.1. Methane Activation

Methane activation requires cleavage of a σ-CH bond, which is essentially different than activation of a π bond such as CO, NO, or N_2. This difference is very well demonstrated in Figure 35, which highlights the changes in the activation of methane that occur in moving from a terrace to a step edge. Methane activation only requires interaction with a single metal atom. The reaction path does not vary when the surface is altered. Therefore, changes in the activation barrier scale linearly with the changes in the overall reaction energies and thus precisely follow the BEP relationship. While there is a large decrease in the activation energy for the forward C−H bond-breaking reaction, the activation energy for the reverse hydrogenation reaction appears to be insensitive to changes in structure. The BEP α value is 0.85. The activation energy for dissociation is found to be reduced at a step, which is accompanied by a large change in reaction energy. For the reverse C−H bond-forming reaction, the calculated E_{pre}^{rec} values were found to be comparable. Methane activation involves a metal insertion into the C−H bond and occurs over most transition-metal surfaces and organometallic complexes over the top of a single metal atom. This is in contrast to CO activation and recombination, which are structurally sensitive and require larger and more specific structural ensembles. The activation of methane only appears to be sensitive to the coordination of the single metal atom that results in insertion. While activation of a C−H bond is structure sensitive, the reverse reaction, i.e., the hydrogenation of $CH_{3,ads}$ to form methane, can be characterized as a structure-insensitive reaction. This is a consequence of α being close to the value of 1 for the dissociation step. Microscopic reversibility requires that the BEP proportionality constant for the recombination reaction is equal to $(1 - \alpha)$. CH bond activation reactions occur most readily along the edge of a step. Since these reactions predominantly occur at single site present along step edges, the rates for this reaction will increase as the number of these sites increase per surface area. The turnover frequency for this reaction should uniformly increase as the size of the particle decreases since the number of these sites increases. Note that in contrast the reverse hydrogenation reaction rate will be unaffected by such particle size effects because of the structure insensitivity.

Figure 36 and Table 3 reveal that the reactivity of different transition metals is not the same. These results indicate that the correlation between the activation energies and fragment adsorption energies is quite complex. Figure 36 summarizes the activation barriers and reaction intermediate energies for the decomposition of CH_4 in CH_x and $(4 - x)$H adsorbed reaction fragments. Data are collected for the densest surface of the respective metals. We note a rough parallel between the activation barrier changes and the binding energies for the carbon and hydrogen product fragments. Noteworthy is the relative stability of the CH_{ads} intermediate over that of C_{ads}.

An interesting observation is the comparable barrier for CH_4 activation over Ru compared to Rh, whereas the C adsorption energies as well as CH_3 adsorption energies on Ru are comparatively higher. Although C_{ads} tends to prefer adsorption in high coordinated sites, for $CH_{3,ads}$ site preference strongly depends on the metal as well as the surface topology. A much better correlation, however, is found if one compares the activation energies with the energies of a

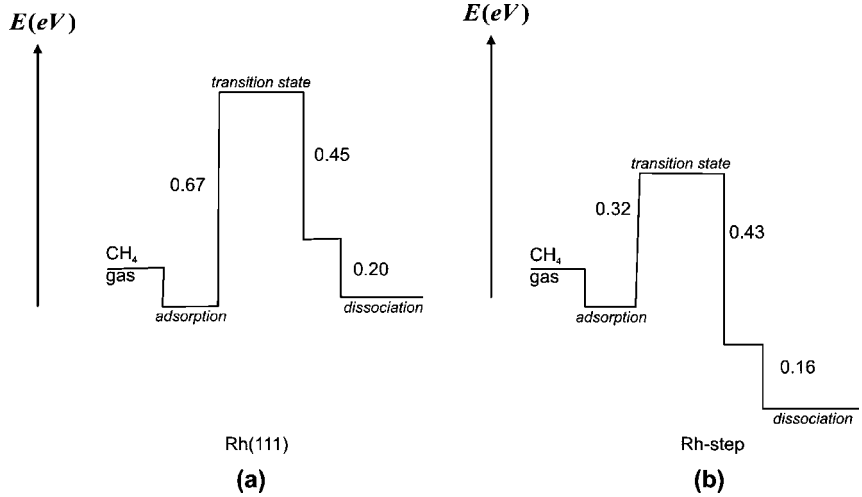

Figure 35. Comparison of methane activation energies (a) by Rh terrace atoms compared with (b) Rh step atoms.[63]

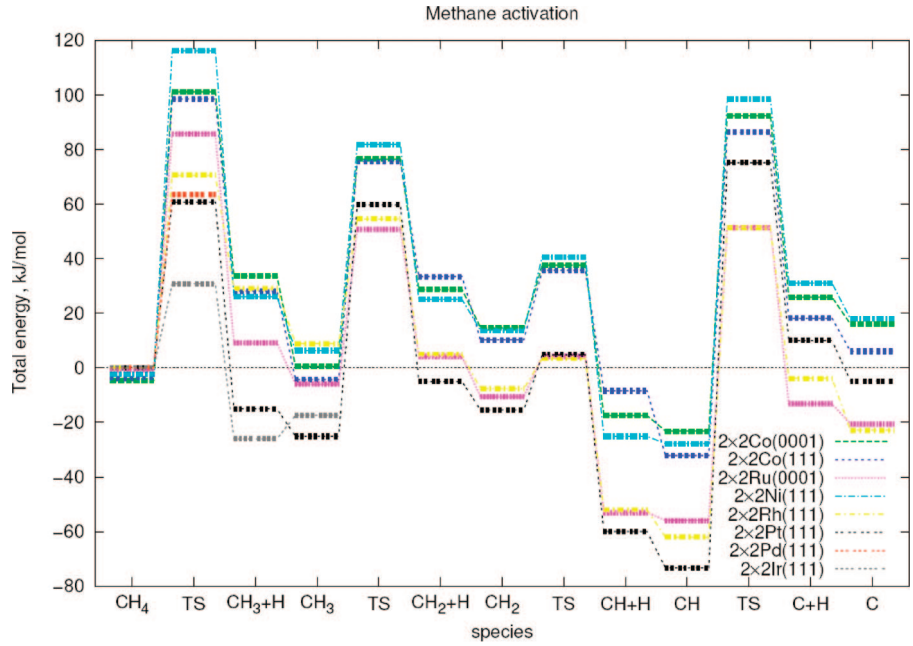

Figure 36. Comparison of methane activation energies on the dense terrace fcc(111)-type surfaces.

Table 3. Comparison of Computed CH_4 Activation Energies

	100	118
	Co(0001)[a]	Ni(111)[a]
77	67	80
Ru(0001)[b,c]	Rh(111)[d,e,f]	Pd(111)[g]
	~40	75
	Ir(111)[d]	Pt(111)[b,g]

[a] Kratzer, P.; Hammer, B.; Nørskov, J. K. *J. Chem. Phys.* **2006**, *105*, 5595. [b] Michaelides, A.; Hu, P. *J. Am. Chem. Soc.* **2001**, *123*, 4235. [c] Ciobica, I. M.; van Santen, R. A. *J. Phys. Chem. B* **2002**, *106*, 6200. [d] Henkelman, G.; Jansson, H. *Phys. Rev. Lett.* **2001**, *86*, 664. [f] Liu, Z.-P.; Hu, P. *J. Chem. Phys.* **2001**, *115*, 4977. [e] Bunnik, B. S.; Kramer, G. J. *J. Catal.* **2006**, *242*, 309. [g] Michaelides, A.; Liu, Z.-P.; Zhang, C. J.; Alavi, A.; King, D. P.; Hu, P. *J. Am. Chem. Soc.* **2003**, *125*, 3704.

hydrogen atom and the CH_3 adsorbed on an atop of a metal atom. While CH_3 is more strongly bound to Ru than to Rh in its most stable high coordination sites, the adsorption energy on the atop of Ru is comparable to that on Rh. Since dissociation takes place on the atop site, the activation energy correlates much better with this CH_3 adsorption state. This issue highlights the important question of the relevant product states to be used to interpret the transition-state energies. We will later show that in the case of ammonia dissociation the stable product site of NH_2 is not the right state for correlation but rather an atop site similar to methane activation.

The main difference between the metals of the third row compared to the fourth or fifth row of the periodic table is the extension of the d atomic orbitals. Whereas on Ni and Co the d atomic orbitals are contracted, on metals which lie in the lower 4d and 5d transition-metal rows of the periodic table the spatial extension of the d atomic orbitals is larger. The tendency of adsorbed intermediates such as CH_3, CO, or NH_3 to preferentially adsorb atop relates to this spatial extension of the d atomic orbitals.[33] Because of the high electron occupation of these orbitals, as follows from the previously discussed Nilsson and Pettersson model,[8] the interaction is repulsive with the doubly occupied orbitals of adsorbing molecules or molecular fragments. Adsorption on the atop site minimizes this interaction. In CH_4 it promotes

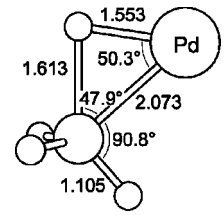

Figure 37. Transition state for CH_4 activation by a Pd atom.[37]

back-donation into antibonding adsorbate orbitals. Therefore, interaction with highly occupied d atomic orbitals atop of an atom is highly beneficial. It explains the low barrier for CH_4 activation over metals in rows 5 and 6. The contracted nature of the d atomic orbitals on Ni and Co results in substantially higher activation barriers than those in the 4d and 5d series. In addition, C−H activation occurs over a hollow site on both Ni and Co. In agreement, on these metals the activation energy of CH_4 activation now correlates with the energy of CH_3 adsorbed in high coordination sites.

Surface metal atom coordination affects the C−H bond activation significantly. It is instructive to compare the different reported barriers for methane activation over a single Pd atom and Pd(111) surface and along a Pd step edge. The activation barriers tend to decrease with a decrease in the coordination number of the activating Pd atom. The calculated barriers for the activation of methane over a single Pd atom, a Pd kink site, and Pd within the Pd(111) surface were found to be 24,[37] 40,[68] and 64 kJ/mol,[68] respectively. The geometries of the dissociating molecule in each of these transition states were found to be very similar. Comparison of the transition-state structures of CH_4 activation on a Pd atom (Figure 37) with a Rh surface (Figure 19) shows that the relative stretching of the CH bond in CH_4 in the transition state on the surface is comparable to that of CH_4 on a Pd atom. The main difference in the activation energies arises from what Bickelhaupt has defined as the Δ_{int} energy component (see Figures 9 and 19). Hence, in an elementary quantum-chemical sense, the difference in activation energies relates to differences in the localization energies of electron density on the atoms involved in the activation of CH_4 (see ref 7, p 117). This agrees with the relation between activation

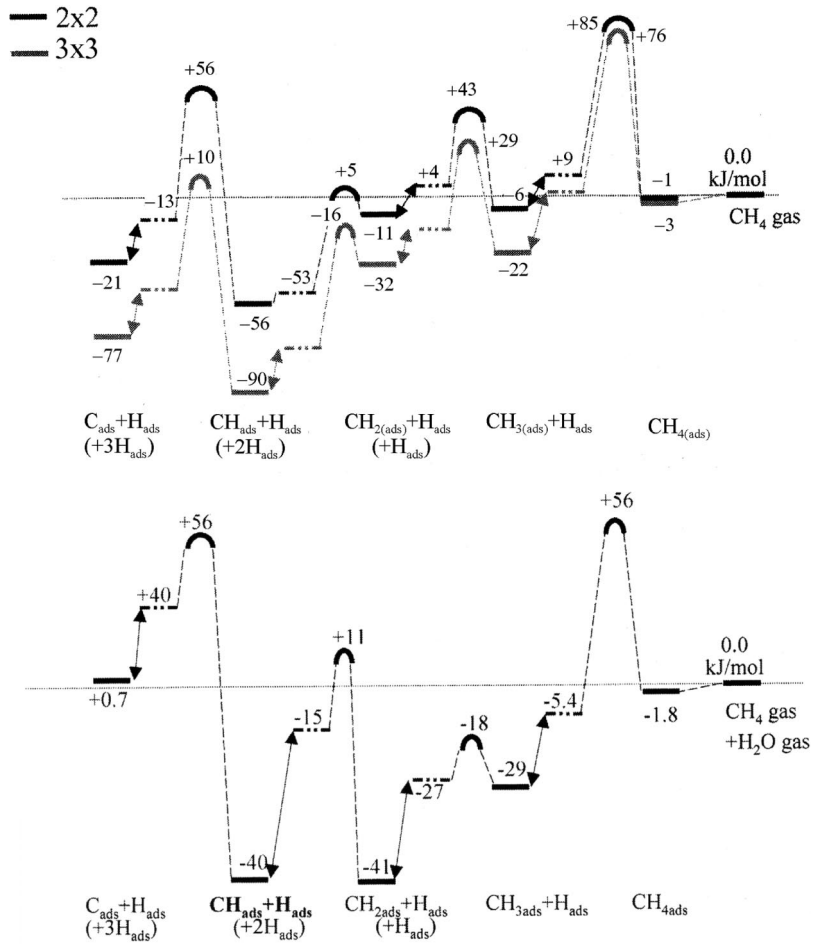

Figure 38. (Top) Reaction energy diagram for CH_4 formation (left to right) and decomposition (right to left) over the Ru(0001) surface at different coverages.[69a] Top and below curves refer to 25% and 11% coverage, respectively. (Bottom) DFT-calculated reaction diagram of CH_4 decomposition with 25% coverage on the Ru (1120) surface.[69b]

energies for CH_4 activation by surface metal atoms with varying coordination number. A comparison of Tables 2 and 3 illustrates that CH_4 and CO activation displays characteristically different trends as we move across the periodic table. These trends are due to the very different interaction energies observed for adsorbed oxygen versus that of adsorbed carbon. For instance, whereas C adsorbs more strongly to Pt than Ni, the reverse is true for oxygen (see ref 7, p 106). The differences relate to the changes the Pauli repulsion and bond ionicity.

A comparison of the activation energies for CH_3 activation on Ru(0001) and Ru (1120) shows no BEP-type behavior (see Figure 38).[69] The activation energies for the forward and reverse reaction are both decreased over the more open surface. The significant decrease in activation barriers relates to the specific corrugated structure of the Ru(1120) surface. On the Ru(1120) surface the hydrogen atom which results from activation of the C−H bond of CH_3 sits very closely to the resulting CH_2 fragment, and as such there is little stretching of the CH bond needed for dissociation. Similarly, the reverse reaction proceeds rather easily as a result of the small displacement of the hydrogen atom that is necessary. Formation of this initial noncovalent metal−hydrogen interaction is familiar from organometallic complexes and is known as an agostic interaction.[70] This results in a "push−pull"-type mechanism. This idea was introduced earlier in section 3.2. This is illustrated in Figure 39a and 39b. There is an increase in the C−H bond length of CH_2 adsorbed to the metal atoms along the edge of the Ru(1120)

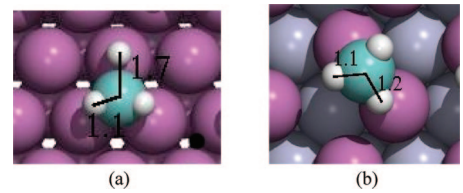

Figure 39. (a) Transition state of CH_3 activation on Ru(0001).[69a] (b) Transition state of CH_3 activation on Ru(1120).[69b] The purple and light blue represent the first and second layer of the Ru surfaces. The blue and white spheres represent the C and H atoms, respectively. The values of the C−H bond lengths are in Angstroms.

surface due to the nearby position of neighboring atoms located on the zigzag structure at the edge. There is now much less stretching required to reach the transition-state geometry than on the Ru(0001) surface. The activation barrier in the forward as well as reverse direction of the reaction is therefore enhanced. It is interesting to mention that a decrease in the coverage can affect the barrier as shown in Figure 37a. The barriers calculated with 25% coverage are relatively higher than the 11% coverage. This is due to the increase in the lateral interactions resulting from high coverage.

Furthermore, it is interesting to analyze the relative stability of $CH_{x,ads}$ species on different surfaces. This is also of interest in view of our later discussion on the relative stability of $NH_{x,ads}$ or $OH_{x,ads}$ species. As is clear from both Figure 38 for CH_4 activation and the latter Figure 40a for NH_3 activation, the relative stability of $CH_{x,ads}$ and $NH_{x,ads}$ species

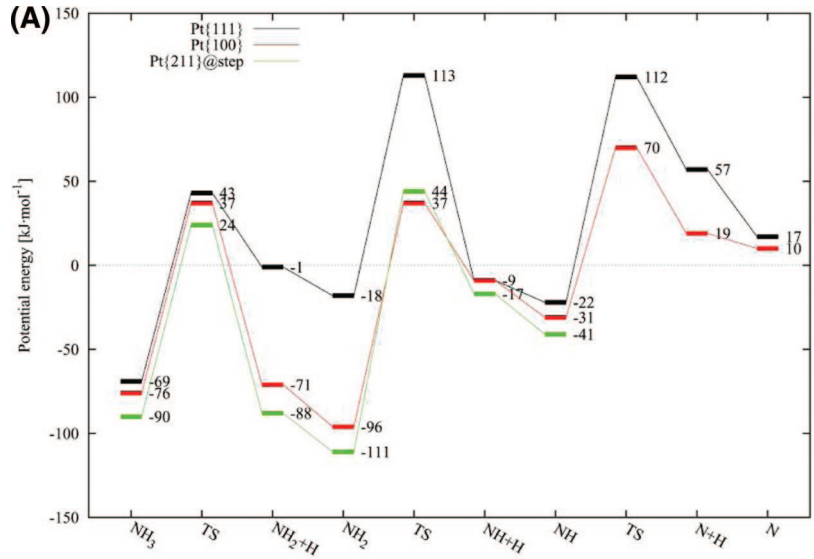

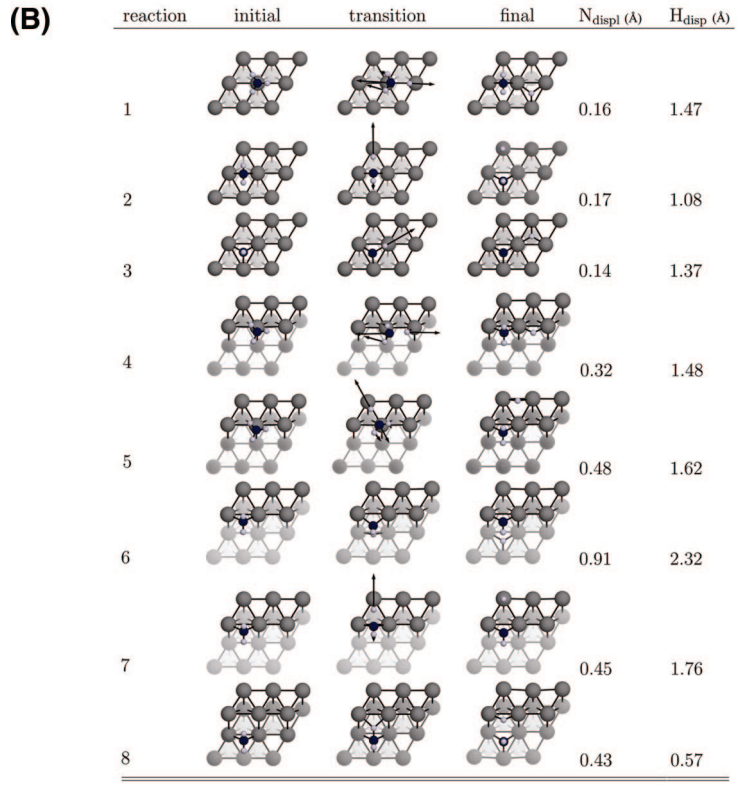

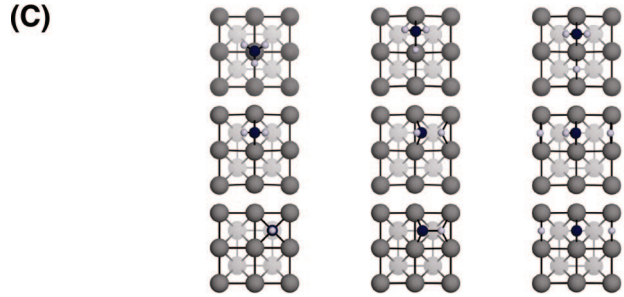

Figure 40. (A) DFT-calculated reaction energy diagram for the dissociation of NH_x = 1, 2, 3 over Pt(100), Pt(111), and stepped Pt(211). (All calculations were carried out using a 2 × 2 unit cell with 25% coverage).[84] The energies are with respect to NH_3 in the gas phase. (B) NH_3 and NH_2 reaction intermediates for the Pt(111) shown panels 1−3 and the stepped Pt(111) surfaces shown in panels 4−8. Black, white, and gray spheres indicate N, H, and Pt atoms. The second layer of the Pt surface has been shaded for clarity. The energies are shown in Figure 39a.[84] (C) Transition states for NH activation on the Pt(100) surface.[86] Black, white, and gray spheres indicate N, H, and Pt atoms. The second layer of the Pt surface has been shaded for clarity.

varies strongly with the type of surface. Note that in these figures the reaction energies are compared. It should be noted that the relative energy difference is partially contributed by the strength of the hydrogen−metal interaction energies. The adsorption energies of the $AH_{x,ads}$ intermediates tend to decrease with increasing x. This is chemically relevant and explained by the bond order conservation principle.[71] It is also consistent with recent studies by Abild-Pedersen et al.[72] They deduce bond order conservation type behavior for different $CH_{x,ads}$ and $NH_{x,ads}$ species from a statistical comparison of the respective adsorption energies with respect to the gas phase. Abild-Pedersen's analysis is based on data for the (111)-type surfaces of the fcc structures.

$$AH_{x,ads} \rightarrow AH_{x-n,ads} + nH_{ads} \tag{12}$$

Abild-Pedersen et al.[72] conclude that the interaction energy of a XH_n fragment with the surface increases with decreasing number of H neighbors. The proportionally constant with varying adatom energies is 0.25, 0.5, or 0.75 for CH_3, CH_2, or CH, respectively. According to bond order conservation principle,[7,72] in a molecular complex the strength of a single chemical bond $E_b(n)$ relates to the corresponding bond energy E_b in a two atomic fragment as

$$E_b(n) = E_b\left(\frac{2n-1}{n^2}\right) \tag{13}$$

In the molecular complex a central atom (as C or N) has n neighbors, which are assumed to be similar. As long as adsorbate coordination does not change, eq 13 can be readily adapted to analyze the interaction energy of a XH_n species with a surface metal atom.

$$E_{ads}(n) = E_{ads}(n=0)\left[\frac{2n+1}{(n+1)^2}\right] \tag{14}$$

$E_{ads}(n = 0)$ is the interaction energy of a single atom such as C or N with a surface atom; $E_{ads}(n)$ is the decreased adsorption energy for the adsorbed fragment CH_x or NH_x. Equation 14 is valid if we make an additional assumption that all bond strengths are the same.

The adsorption site generally changes when fragment bond number n varies. With $n = 0$ the adsorption fragment maximizes its number of metal atom contacts and completes to satisfy the valence of X. For example, when $n = 3$ the adsorption fragment tends to adsorb to a single atom. For strongly adsorbing species the adsorption strength tends to vary with respect to $\sqrt{N(7)}$. N is the coordination number of the adsorbate with the surface atoms. For adsorbates that change coordination with n, eq 14 then becomes

$$E_{ads}(n) = a(n)E_{ads}(n=0)\left[\frac{2n+1}{(n+1)^2}\right] \tag{15a}$$

where

$$a(n) = \sqrt{N(n)} \tag{15b}$$

Interestingly, one finds the following relations

$$\frac{E_{ads}(n=3)}{E_{ads}(n=0)} \approx \frac{1}{4} \qquad (N(3)=1, N(0)=3) \tag{16a}$$

$$\frac{E_{ads}(n=2)}{E_{ads}(n=0)} \approx \frac{1}{2} \qquad (N(2)=2, N(0)=3) \tag{16b}$$

$$\frac{E_{ads}(n=1)}{E_{ads}(n=0)} = \frac{3}{4} \qquad (N(1)=3, N(0)=3) \tag{16c}$$

The adsorption strength follows a trend that one also would find when adsorption is determined by the number of sp^3-type bonds that an XH_n species are available. Adsorption to Pt(111) follows this behavior energetically as well as topologically. We ascribed this before to the importance of a strong interaction with spatially extended d atomic valence orbitals.[33]

4.2.2. Activation and Formation of Alkane Molecules

The strong dependence of the activation energies for methane activation on the coordinative unsaturation of the surface metal atoms, especially as reflected in the preference of activation along step edges or at kink sites, is also found for CH activation in alkanes[60] and even for the C−C bond cleavage and formation reaction.[73] The bond dissociation energy for a covalent σ C−C bond in the gas phase, which is 88 kcal/mol, is weaker than that of the CH bond corresponding to 99 kcal/mol. The activation energy to dissociate the bond over a metal surface, however, is higher. This is found even for activation by a single Pd metal atom (22.2 versus 6.4 kcal/mol).[37] On a metal surface part of this increased activation energy can be ascribed to contribute to the deformation of the alkane molecule to access the C−C bond. This steric hindrance, however, is significantly smaller for activation over a single metal atom. The difference, however, still persists and, in part, is related to the fact that results from HOMO−LUMO-type interactions in the transition state between the two fragments that form is much smaller for C−C activation than for C−H activation. Consistent with the weaker C−C bond energy, the longer bond length of the C−C bond compared to CH (1.532 versus 1.099 Å) requires less relative stretching of the bond in order for a M−C bond to be formed. We showed earlier that dissociation of a diatomic molecule with a π bond or its microscopic reverse associative recombination reaction preferably occurs over a step edge where one of the atoms is attached below the step while the other sits on top of the step edge.

We just discussed here that the activation of σ bonds such as C−H or C−C preferentially occurs along the step edges. The larger space around a step edge will further decrease the steric inhibition required for a metal atom insertion into the C−H or C−C bond. The low-coordinated metal atoms on the surface behave similar to the metal atom centers in organometallic complexes with open ligand sites to assist bond activation. We include in this section a discussion on the implications of the general rules for activation of molecules and their reverse associative recombination reactions that we discussed so far to mechanistic issues in heterogeneous catalysis. We briefly describe the application of these rules to alkane hydrogenolysis and F−T synthesis.

Scheme 2 summarizes some of the proposed elementary reaction steps involved in the hydrogenolysis of an alkane molecule to short-chain hydrocarbon intermediates. For an extensive treatment of the classical heterogeneous catalytic view of this reaction, we refer to an important paper by Garin.[74] Two essential mechanistic steps have to be distinguished: cleavage of the C−C bond between atoms α and β (Scheme 2, b3) and cleavage of the C−C bond through metal−carbon contact of atoms α and γ (Scheme 2, II). On

Scheme 2. Mechanistic Pathways for C−C Bond Cleavage in Hydrocarbons[a]

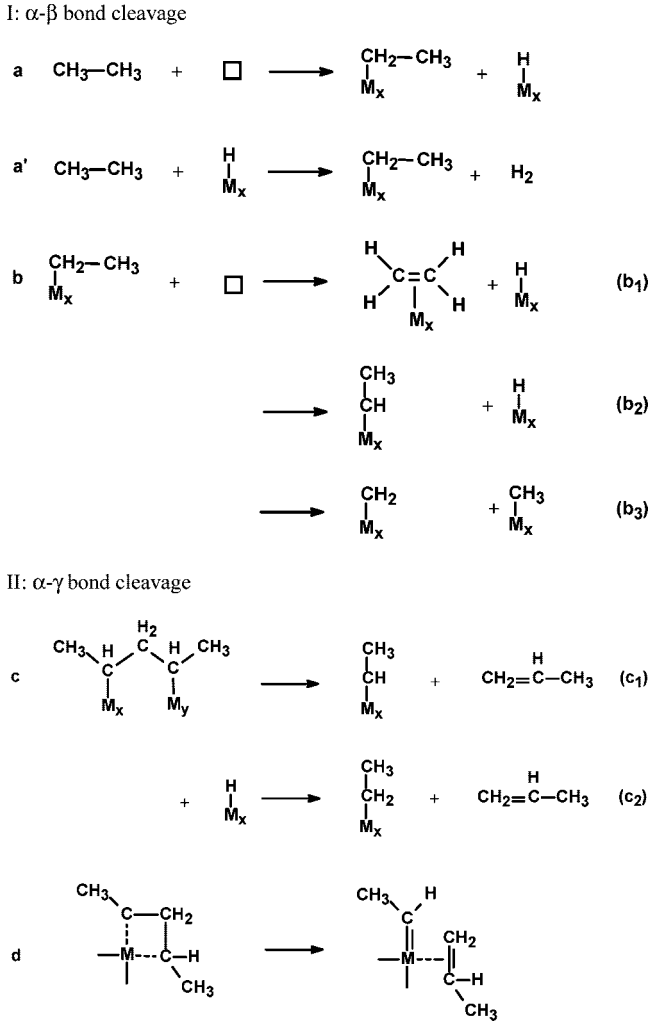

[a] (I) Direct cleavage of a C−C bond and competitive reaction steps. (II) Activation by a surface ensemble of metal atoms (IIc) or through a single metal atom by way of a metallocycle.

the basis of an analysis of catalytic data, it has been proposed that the initial C−H activation occurs by direct interaction with vacant surface metal atom sites such as those we discussed so far or in an associative reaction with adsorbed hydrogen to give adsorbed alkyl and H_2 (Scheme 2, Ia′). The latter reaction likely proceeds through a push−pull mechanism, similar to activation of N−H bonds by coadsorbed oxygen that we will discusse later. Reaction Ia (Scheme 2) will be favored when the M−H bond is weak as on the dense surfaces of Ni or Pt. After the initial C−H bond activation step and formation of M−C bonds, several reaction paths are possible. We will first analyze the α, β C−C cleavage path and then the α, γ cleavage path.

The reactivity of the adsorbed alkyl intermediates has been extensively studied both experimentally as well as theoretically, and the surface chemical information is summarized by Garin.[74] The adsorbed alkyl intermediate can react via various different paths. The major routes are outlined in Scheme 2, I.b. They include the following: (1) β C−H activation of the CH_3 group to form ethylene, (2) α C−H bond activation of the CH_2 group to form the alkylidene intermediate, and (3) C−C bond activation to form adsorbed CH_2 and CH_3 intermediates. Watwe et al.[73] showed that the reactions occur most favorably on Pt at step edges as opposed to terrace sites. At the step edge of Pt, β C−H bond activation (b1) was found to be most difficult (E_{act} = 193 kJ/mol), whereas α C−H bond activation (b2) had the lowest barrier on the step edge. The C−C bond activation reaction (b3) at the step edge had a barrier of 100 kJ/mol, which is 73 kJ/mol lower than that found on the (111) surface. The latter reaction is the analogue of the $CH_{3,ads}$ dissociation reaction that was discussed earlier, which also takes place at the step edges.

The α−γ C−C bond activation proceeds on a terrace as indicated in Scheme 2, IIc. C−C bond activation proceeds either through β C−C bond cleavage, reaction IId, with formation of the carbene and the olefin or via a hydrogen atom addition to give the adsorbed alkyl and the olefin. A large surface ensemble of metal atoms is required to accommodate the product fragments that form in this reaction. The carbene species are stabilized at a step edge (see also the relative stability of adsorbed NH_2 in section 4.4). In addition to the multiple adsorption site contact shown in path C1, the step edge can also accommodate a reaction path that proceeds by formation of a metallocycle attached to a single metal atom and its subsequent activation (see IId). Such intermediates are known to form in organometallic chemistry[70a] and can subsequently decompose, forming a strongly bound carbene species along a more weakly coordinated olefin. On a metal surface, the subsequent C−H bond cleavage steps can occur, thus leading to formation of CH_{ads} or C_{ads} intermediates. Recombination of reaction intermediates as shown in Scheme 2 can also lead to isomerization or chain growth. Many of the chain growth reaction steps proposed in the F−T synthesis can be considered as a reverse of these hydrogenolysis reactions. We can therefore use some of the above-mentioned computational results to analyze key elementary reaction steps as a function of site geometry for F−T synthesis.

F−T synthesis proceeds via reaction of CO with H_2 to produce methane and higher hydrocarbons (C_2^+). A main processing issue concerns the selectivity for production of C_1 versus C_2^+ species.[75,76] One can distinguish elementary reaction steps that are site dependent from those that are independent of site geometry. As we have seen, recombination of H_{ad} with $CH_{3,ads}$ to form methane proceeds preferentially over a single metal atom with an activation energy that is independent of the local environment of the metal atom. Methanation and hydrocarbon chain growth termination through hydrogenation can therefore be considered to be site independent. Chain growth can proceed via recombination of various different CH_x intermediates.[77,78] The relative rates of these reaction steps will depend upon the strength of the metal−CH_x bond and the concentration of different CH_x intermediates under reaction conditions. In recent years several computational studies have proposed various elementary steps.[77] It appears that recombination barriers of different CH_x intermediates sensitively depend on surface type. Whereas CH and CH_3 recombination preferentially occurs on surface terraces, CH_2 and CH or CH_2 and CH_3 recombination on Co has been shown to occur on step edges.[78] C−C coupling, ultimately leading to coke, appears to be preferred on the terraces of group VIII transition metals.

A general kinetic condition for chain growth to initiate through $CH_{x,ads}$ insertion is that the rate of CH_x formation should be fast compared to the termination reaction by which gas-phase hydrocarbons are generated.[79] This requires the

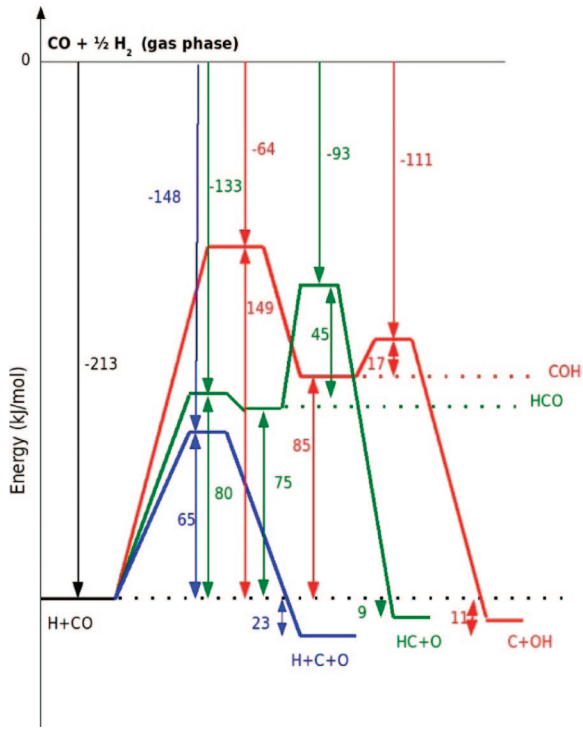

Figure 41. Energetics of CO dissociation in the presence of coadsorbed H on the Ru(1121) surface. (Blue line) Direct CO dissociation. (Green and red lines) CO dissociation via HCO and COH intermediates, respectively.[81]

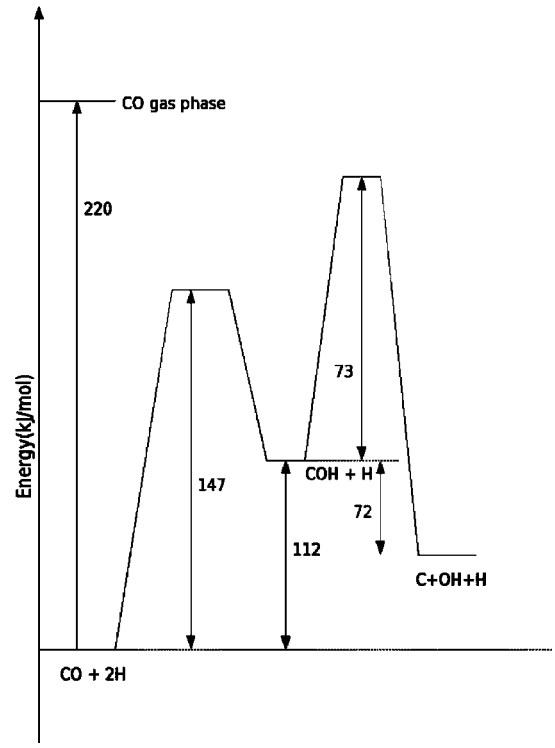

Figure 42. CO dissocation path through the COH intermediate on the Rh_6 cluster.[82]

activation barrier of CO to be lower than 80 kJ/mol. We earlier discussed the lowering of the activation energy for the CO bond at step edges to values about 100 kJ/mol. This is still higher than the lower activation energies reported for the chain growth and termination reactions, whereas we recently reported on the open Ru (11$\bar{2}$1) surface an activation barrier of 65 kJ/mol.[45] An alternative dissociation path for CO bond cleavage is of interest. This will be discussed in the next section.

4.3. CO Activation by H_{ads}

We have seen how critically important a low barrier to generate CH_{ads} species is to the selectivity of the F−T reaction. This requires a low CO activation energy as well as low barrier for CH formation. The activation energy to form CH_{ads} from C is typically between 60 and 80 kJ/mol. This is a borderline with respect to the criterion of a maximum barrier of 80 kJ/mol for CO activation energy as mentioned earlier.

On the Ru(0001) terrace, we find that the barrier to formyl formation is 140 kJ/mol.[42] Consecutive cleavage of the CO bond now has only a barrier of 40 kJ/mol. Obviously on the Ru(0001) terrace the reaction path for CH_{ads} and O_{ads} formation via intermediate formation of formyl is preferred over direct CO dissociation with a barrier of 220 kJ/mol. Very similar results have been found by Inderwildi et al.[80a] for the Co(0001) terrace. In view of the large reduction of the barrier for direct CO dissociation on a step-edge site, a comparative study has to be made for H_{ads}-assisted CO dissociation. For the open Ru(1121) surface the results are shown in Figure 41. One finds that on this corrugated surface, which consists of active 6-fold sites, direct CO dissociation has a lower barrier than the H-assisted paths.[81] This is mainly due to the high barriers to form HCO_{ads} or COH_{ads} intermediates. This observation has to be contrasted with a study by Andersson et al.[80b] on the cleavage of the CO bond on Ni stepped and flat surfaces. They conclude that H-assisted CO cleavage is preferred in both cases.

CO activation on Ru and Ni surface data are consistent once it is realized that the activation energies for direct CO dissociation even for the stepped Ni surfaces are relatively high. For these systems typical values of the activation energies are around 160 kJ/mol for direct CO activation on a stepped surface, whereas H-assisted CO activation has only an overall barrier of 115 kJ/mol. This implies that when one deals with a reactive surface consisting of active 6-fold sites, direct CO activation (i.e., carbide mechanism) will have a lower barrier compared to the H-assisted path. However, when direct CO dissociation has a high barrier, H-assisted CO activation may be the preferred path. Comparison with CO dissociation on small Rh particles confirms this conclusion (see Figures 42 and 43).[82] On the Rh_6 cluster CO dissociation is a difficult process due to reconstruction of the cluster from strong adsorption of the C_{ads} and O_{ads} in the product state. Hence, hydrogenation of the adsorbed CO is the only initiation path. The H-assisted C−O bond cleavage via COH_{ads} has a reduced barrier of 185 kJ/mol. Interestingly, this competes with a barrier of CH_2O_{ads} formation of **113** kJ/mol formed from the HCO intermediate.[82]

Few studies are available on the activation of CH bonds with coadsorbed oxygen. A recent paper by Inderwildi et al.[83] considered the activation of CH adsorbed on the Rh(111) surface by coadsorbed atomic oxygen. As was previously discussed, the methylidyne species adsorbs in a 3-fold configuration on the Ru(0001) surface. They considered the energetics of oxygen activation when the CH and O are coadsorbed in pre-transition-state configurations. For the direct reaction of C−H to adsorbed C and H there is an activation barrier of 123 kJ/mol. The decomposition of CH_{ad} by reaction with coadsorbed O has a barrier of 141 kJ/mol and with coadsorbed OH 122 kJ/mol. In the latter case, OH

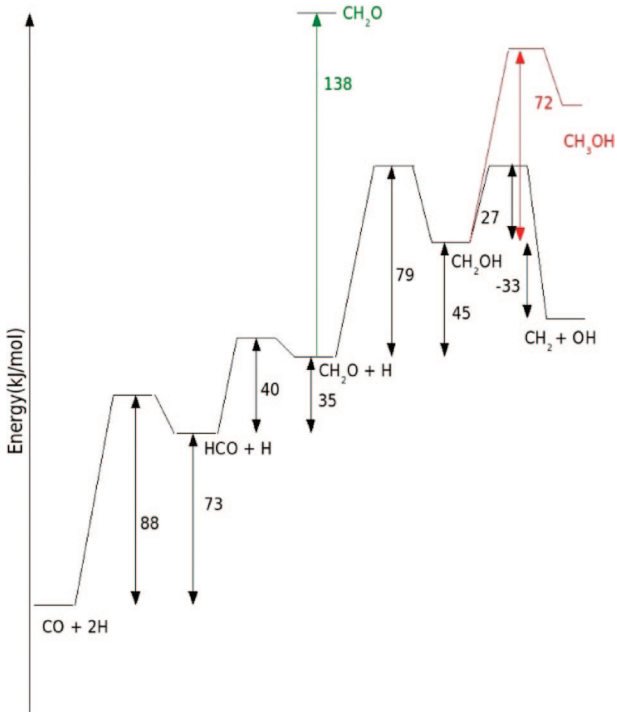

Figure 43. Formation of CH_x species via the HCO intermediate on the Rh_6 cluster.[82]

does not share metal atoms with the CH_{ads}. A technical issue with this data from the Inderwildi study is that all transition states are compared with respect to the coadsorbed state in which shared bonding between the reacting adsorbates and the surface metal atom is present. The overall barriers from the noninteracting reactant state would be higher. It also implies that relative comparisons have to be made with care. One concludes that C−H bond cleavage on Rh(111) is not promoted by coadsobed O or OH. An interesting issue also addressed in this study was formation of CO by recombination of surface CH_x species with coadsorbed atomic oxygen. The recombination of C_{ads} with O_{ads} to form CO_{ads} was found to have a barrier of 95 kJ/mol. Activation of C−H to form the adsorbed C_{ads}, however, was found to be significantly higher in energy (123 kJ/mol). An alternative path involves the reaction of CH_{ads} with oxygen to form the formyl intermediate and the subsequent C−H activation of the adsorbed formyl intermediate.

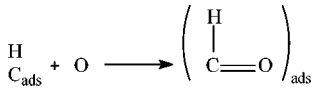

This $CH_{ads} + O_{ads}$ recombination reaction was found to be exothermic (−15 kJ/mol) with a barrier of 111 kJ/mol. The consecutive activation of the CH bond from the adsorbed formyl intermediate was only 29 kJ/mol. Formation of CO via the formyl intermediate therefore competes with the direct path via the C + O coadsorbed state.

4.4. Ammonia Activation

Activation of ammonia proceeds differently from methane mainly because the nitrogen atom of ammonia has a lone pair orbital available to bind to a surface metal atom. When ammonia adsorbs to a metal that has d atomic orbitals with a relatively large spatial extension and d-type valence orbitals that are nearly completely occupied by electrons, the molecule preferentially adsorbs in an atop configuration (see ref 33, p 235) in order to minimize the Pauli repulsive interactions. These repulsive interactions are expected to be larger in high coordinated sites. For this reason, on the transition metals of the fifth and sixth row of the periodic table ammonia prefers to adsorb on an atop site.[84]

Table 4. Energies of NH_2 and NH Adsorption (kJ/mol): Comparison of Atop and Bridge Adsorption[84]

NH_2	surface	atop	bridge
NH_2	111	−188	−230
NH_2	100	−207	−303
NH_2	211 (step edge)	−213[a]	−306
NH	111		−281
NH	100		−368
NH	211 (step edge)		−375

[a] Single-point transition-state geometry.

Adsorption of the NH_2 fragment is quite different than that of ammonia because NH_2 can also bind through the unoccupied nonbonding $2p_y$ orbital. This atomic orbital which is located on the N atom of the NH_2 fragment is perpendicular to the surface normal. The perpendicular orientation of the NH_2 $2p_y$ orbital remains asymmetric to the surface and interacts only with surface group orbitals that are asymmetric with respect to the surface normal. This configuration of the $2p_y$ orbital interacts with the out-of-phase combination of the two metal s atomic orbitals. This interaction helps the NH_2 to bind in a 2-fold configuration to the surface. As we will see, metals that have extended d atomic orbitals such as Pt and Rh can also stabilize NH_2 at an atop site. The d_{yz} metal atomic orbitals now have the right symmetry to interact with the nitrogen $2p_y$ orbital perpendicular to the surface normal. The large overlap with metal s atomic orbitals, however, provides a large driving force for NH_2 to adsorb at the 2-fold coordination site instead.[85−89] The reaction energy diagrams for ammonia activation over the Pt(111), Pt(100), and Pt(211) step surfaces are compared in Figure 40a. Surprisingly, the reaction energies for the transformation of $NH_{3,ads}$ to $NH_{2,ads}$ vary significantly; in contrast, the activation energies appear to be invariant. This implies that the BEP α value is near to 0. Investigation of the transition-state configurations in Figure 40b show them to be late with respect to NH bond activation.

This finding is in contradiction to the low value of α that seems to indicate an early transition state. In the transition state there is a two-step motion of atoms. A close examination of the structures of the reaction intermediates shown in Figure 40b indicate that in order to cleave the N−H bond it must be significantly extended in the transition state. The corresponding displacement of the nitrogen atoms is initially very small. While the transition states can be late with respect to H-atom displacement, it is still early with respect to that of N atom. The reaction energies of NH_3 dissociation relate strongly with the adsorption energy of NH_2 in 2-fold coordination. This energy is sensitive to the surface topology. The transition state of N−H bond cleavage in NH_3 is atop of the surface metal atom. Therefore, unexpectedly, this interaction is rather insensitive to surface structure.

The transition states for dissociating NH_3 and NH_2 result in formation of the NH_2 and NH fragments that adsorb in atop and bridge configurations, respectively, close to those of their initial states. A comparison of their energies is given in Table 4. The transition-state intermediates do not have configurations where the N atom is close to its stable reaction

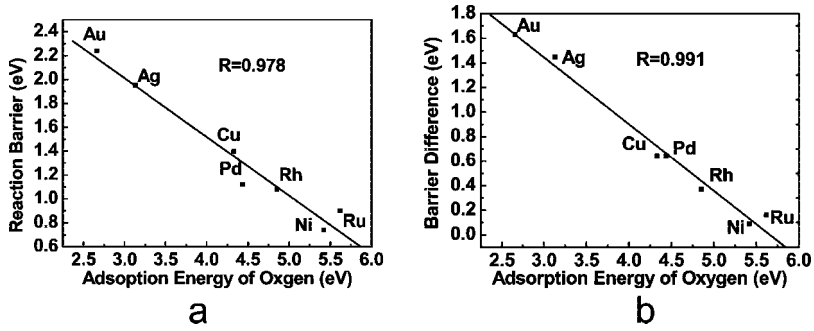

Figure 44. Relationship of reaction barrier differences for water dissociation on clean (a) and oxygen preadsorbed (b) metal surfaces and the adsorption energy of atomic oxygen. *R* is the correlation coefficient.[92]

product. For instance, while $NH_{2,ads}$, which is the product of the activation of $NH_{3,ads}$, prefers to adsorb at the 2-fold coordination site, it instead binds at the atop site in the transition state. The energies for the transition state then correlate with the energies for NH_2 bound to the atop site. Similarly, the transition state for NH_2 activation prefers the bridge site where as the NH product state that forms prefers the 3-fold hollow site. The energy of NH_2 adsorbed atop of a Pt atom is not very sensitive to the local environment of that Pt atom. In contrast, however, the energy of NH_2 adsorbed on a bridge site is very sensitive to surface topology. This difference in behavior is due to electronic effects. The low-energy $2p_y$ atomic orbital of atop adsorbed NH_2 can only interact with the asymmetric d_{yz} orbital of the surface metal atom with the same symmetry and not with the symmetric s metal atomic orbitals. NH_2 optimally interacts with the surface metal s atomic orbital combinations in 2-fold coordination sites. While the delocalized s electron density is very sensitive to surface metal atom coordination, this is much less the case for the more localized d valence electron density. It is interesting to note that the insensitivity of NH_3 activation with respect to the coordinative unsaturation of the surface topology is quite different from the strong dependence found earlier for methane activation. Activation of the NH bond of adsorbed NH behaves quite differently from activation of NH_3. As noted before by Crawford et al.,[52,65] the differences in the interaction between the coadsorbed H_{ads} and N_{ads} dissociation fragments now control the differences in activation barriers. As can be observed from a comparison of Figure 40, recombination of H_{ads} and N_{ads} proceeds through a pre-transition state where they have very different repulsive interactions. On the Pt(111) surface H_{ad} and N_{ad} share bonding with a surface metal atom, which results in a repulsive interaction. On the (100) surface the recombining atoms do not share bonding to the same surface metal atom. This is similar to the interaction of N and O on the (100) and (111) surfaces as we discussed previously in section 4.1.[56,57]

Electrocatalytic experiments also indicate unique features for the Pt(100) surface.[89] Whereas the Pt(111) surface shows extremely low activity for ammonia oxidation to N_2, the Pt(100) is quite active for N_2 production. On Pt(100), N_2 formation proceeds through the hydrazine intermediate. Surface NH recombination occurs through 2-fold coordination on the opposite sides of Pt(100) surface atom squares with a low barrier since no sharing of surface metal atoms occurs in the transition state between the reacting nitrogen atoms. The NH fragments are also destabilized because of their unfavorable interactions with four metal atoms in a square arrangement instead of a triangular 3-fold coordination site. The barrier for activation of the N−H bond of $NH_{2,ads}$ is reduced by more than 100 kJ/mol when dissociation occurs at surface sites; NH_2 is initially adsorbed at the hollow step site and hydrogen moving to the step edge (see Figure 40b). A similar reduction in the activation barrier at a step site is found for activation of adsorbed NH. These low barriers result from weakening of the N−H bond, which is due to the strong interaction of the H atom with the metal atom. This is similar to the agostic interaction in the organometallic complexes. Interestingly, this was also seen in the case of methane activation on Ru(1120) as discussed in section 4.2.1. The change in the chemical bonding during activation of the N−H bond can best be described by a push−pull mechanism. The overall barriers for NH_2 and NH activation compared to terrace activation are still higher than on the terraces because of the unfavorable adsorption energies of NH_2 and NH at the hollow positions of the step edges. On highly covered surfaces however the step-edge activation may result in large effective reductions in activation barriers.

Water dissociation on stepped Ni surfaces has been found to have an activation energy that is at least 50 kJ/mol less than on a Ni terrace surface.[90] In the transition state the oxygen atom as well as the H atom moves with respect to the adsorbed reactant state. In the transition state the oxygen atom moves to a 2-fold coordination site, where the p_x and p_y atomic orbitals can overlap with asymmetric Ni s atomic orbitals combinations. This interaction dominates because on Ni the d atomic orbitals are highly contracted and hence do not stabilize OH in the atop position. This is consistent with the slight preference of H_2O to dissociate on the Ni(111) surfaces at the hollow sites. In contrast, on Rh the activation energy of H_2O is independent of structure as also found for NH_3.[91] In the transition state there is no displacement of the oxygen atom of the water, and the situation is analogous to that of ammonia activation on Pt. Interaction with the more spatially extended metal d valence electrons on Rh and Pt stabilizes atop interactions.[33]

Activation of adsorbed water on different transition-metal (111) surfaces shows very similar trends as those found for ammonia activation.[92] On the oxygen-free metal surfaces a BEP relation with a value for $\alpha = 0.67$ is found (see Figure 44a). On all the metal surfaces studied the barrier to activate water is decreased in the presence of coadsorbed oxygen. The degree of reduction, however, depends on the adsorption strength of coadsorbed oxygen (see Figure 44b). The change in barrier height is largest when the interaction between the hydrogen atom and the metal surfaces as well as that of oxygen and metal surfaces is weaker. The OH bond then is relatively strong. When the water molecule and reactive oxygen atom are coadsorbed on the same sites, the changes in the H_2O bond interaction energy counteract. Then the activation energy for OH bond cleavage of H_2O_{ads} through

Table 5. Adsorption Energies of O and OH (eV): Interaction Energies at Different Sites Are Compared[85,87]

	Rh(111)			Pt(111)		
	bridge	fcc	hcp	bridge	fcc	hcp
O	−4.34	−4.87	−4.77	−3.33	−3.90	−3.55
OH	−2.85	−2.87		−2.14		
H	−2.73	−2.84	−2.81	−2.61	−2.61	−2.61

reaction with coadsorbed atomic oxygen becomes independent of metal with $E_{act} \approx 60$ kJ/mol.

Surprising are the large decreases in O−H transition-state distances found for reaction with coadsorbed oxygen compared to the free surface (see Table 7). On the oxygen-free surfaces the O−H bond distance in the transition state increases with the activation barrier. The short OH distances found for reaction with the coadsorbed oxygen are consistent with the small variation in activation energies found on the different surfaces. In essence, the transition state has changed from an intermediate one to late one on the clean surface to an early one on the oxygen precovered surface.

The two consecutive reactions that generate O_{ad} from H_2O are

$$H_2O \rightarrow H + OH \quad (17a)$$

$$OH + OH \rightarrow H_2O + O \quad (17b)$$

Instead, as mentioned, dissociation of H_2O can also be promoted by coadsorbed O as demonstrated in Figure 45. In Figure 44 BEP plots of these reactions are shown as a function of the O_{ads} adsorption energy. The low value of α found for H_2O dissociation indicates that for this reaction it is better to correlate with OH_{ads}. Applying scaling law relations the value of α is calculated as 0.8, in agreement with data cited earlier (see also refs 93 and 94). Since at the step-edge O and H_2O are adsorbed in different positions, coadsorption of O alters the activation energy of H_2O dissociation. Compared to the activation energy on the (111) surface for the same reaction, the activation energy decreases by 30 kJ/mol. Related is the issue of the dependence of the energies of OH activation or H and O recombination as a function of the O adsorption energy. This is practically important in the conversion of methane with steam or oxygen to produce H_2 or CO (see Table 8). As elucidated by Hickman and Schmidt,[95] the selectivity for H_2 formation is substantially higher for Rh than for Pt. This in line with the data shown in Table 8 that show a significantly high barrier for H and O recombination on Rh than on Pt because of the larger bond strength of O to the Rh surface.

Table 7. Transition-State OH Bond Distances (Å) on Clean and Oxygen Precovered Surfaces[92]

metal	clean surface	oxygen preadsorbed surface
Au	2.065	1.001
Ag	1.789	0.983
Cu	1.670	0.994
Pd	1.543	2.415 (dissociated)
Rn	1.543	0.991
Ni	1.881	1.465 (dissociated)
Ru	1.426	0.991

Similar to the assisting role of coadsorbed O_{ads} on the activation of H_2O, coadsorbed OH can assist H_2O dissociation also. The O_{ads} is generated from the two consecutive reactions shown by eqs 17a and 17b. These reactions lead to autocatalytic H_2O decomposition in adsorbed H_2O overlayers on a reactive metal catalyst. Experimental indications for autocatalytic decomposition of H_2O in H_2O overlayers adsorbed on Cu(110) surfaces have been reported on the basis of X-ray photoelectron sprectroscopy by Andersson et al.[96] In this study they report the enhanced adsorption strength of H_2O in the presence of coadsorbed OH. With respect to H_2O, OH_{ads} has stronger hydrogen bond acceptor properties than coadsorbed H_2O. This is essentially due to the increased ionicity of the OH bond compared to that of H_2O resulting from the transfer of electrons from the surface to the OH group.[97] It implies that upon H_2O dissociation to H_{ads} and OH_{ads} the produced OH_{ads} species becomes hydrogen bonded to another H_2O molecule, which also stabilizes the transition state.

4.4.1. Activation by Coadsorbed O or OH

In this section we will compare the activation path of ammonia by coadsorbed O or OH on Pt(111) and Rh(111) surfaces. Coadsorbed O and OH have very interesting differences in their ability to activate ammonia based on their different adsorption modes to the metal surface (see Table 5). The adsorption energy for OH on both Rh(111) and Pt(111) is found to be nearly one-half of the adsorption energy of O. The adsorption of oxygen on Rh is significantly stronger than on Pt. As we will see, the stronger interaction of adsorbed O with the Rh surface implies a weaker intermolecular OH bond for the corresponding adsorbed hydroxyl intermediate. This again is qualitatively understood based on the bond order conservation principle.[71] The larger

Table 6. Total Interaction Energies between the Fragments Resulting after an Elementary Step at the Transition State (eV)[87] [a]

reaction	$E_{tot\text{-}int}$ (eV)	$E_{vac\text{-}int}$ (eV)	$E_{metal\text{-}int}$ (eV)
NH_3(top) + O(fcc) → NH_2(bridge) + OH(top)	−0.18	−0.13	−0.05
NH_3(top) + O(hcp) → NH_2(bridge) + OH(top)	−0.21	−0.42	+0.20
NH_2(bridge) + O(fcc) → NH(fcc) + OH(bridge)	−0.32	−0.3	+0.07
NH_2(bridge) + O(fcc) → NH(hcp) + OH(top)	−0.78	−0.55	−0.23
NH_2(bridge) + O(hcp) → NH(hcp) + OH(top)	−0.78	−0.57	−0.21
NH(fcc) + O(fcc) → N(fcc) + OH(bridge)	−0.45	−0.42	−0.03
NH(hcp) + O(fcc) → N(hcp) + OH(bridge)	−0.79	−0.48	−0.31
NH(hcp) + O(hcp) → N(hcp) + OH(top)	−0.45	−0.67	+0.22
NH_3(top) + OH(top) → NH_2(bridge) + O(top)	−0.39	−0.19	−0.20
NH_2(bridge) + OH(top) → NH(fcc) + H_2O(top)	−0.88	−0.23	−0.64
NH_2(bridge) + OH(top) → NH(hcp) + H_2O(top)	−0.86	−0.20	−0.66
NH(fcc) + OH(top) → N(fcc) + H_2O(top)	−1.33	−1.00	−0.33
NH(fcc) + OH(bridge) → N(fcc) + H_2O(top)	−1.33	−1.00	−0.33
NH(hcp) + OH(top) → N(hcp) + H_2O(top)	−1.29	−1.10	−0.19
N(fcc) + N(hcp) → N_2(top)	+0.95	−0.67	+1.62

[a] The total interaction (second column) is split into a through space (third column) and a through metal (fourth column) part.

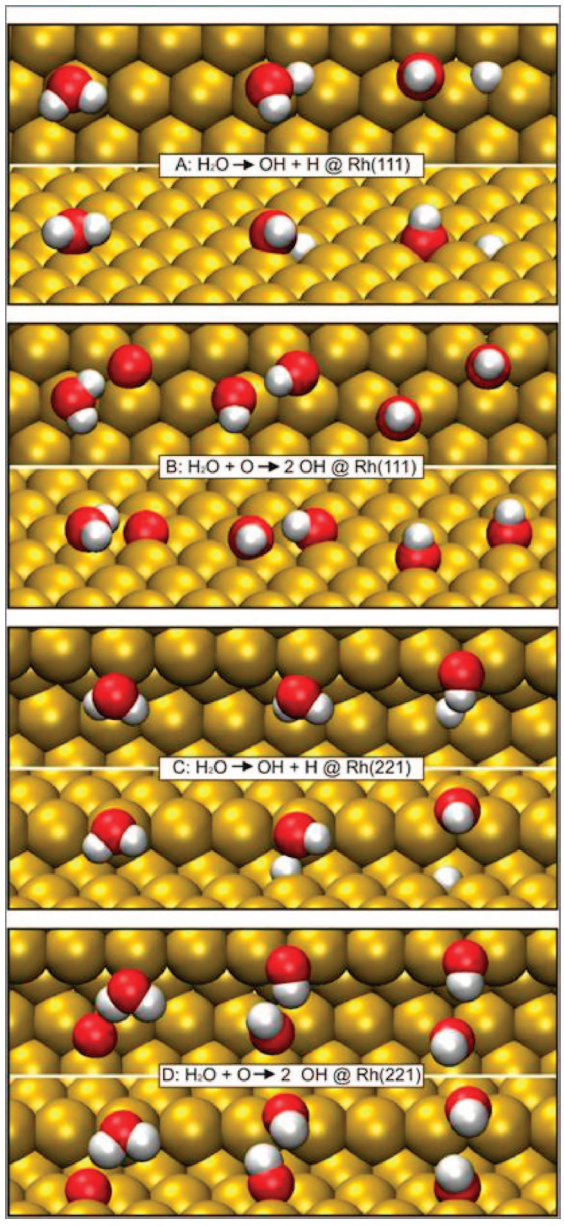

Figure 45. Decomposition of H_2O (A) direct and (B) in the presence of coadsorbed O on the Rh(111) surface and (C) direct and (D) in the presence of coadsorbed O on the Rh(221) surface.[91]

Table 8. Adsorption Energies of O (E_{ads}O), Activation Barriers To Form OH from O + H (E_{act}(H + O)) and H_2O and O_{ads} from OH + OH (E_{act}(OH + OH)), and Desorption Energy of H_2 (E_{des}(H_2)) on Rh and Pt Surfaces[95] [a]

	E_{ads}(O)	E_{act}(H + O)	E_{act}(OH + OH)	E_{des}(H_2)
Rh	−470	80	63	75
Pt	−390	10	51	75

[a] The energies are in kJ/mol.

involvement of the oxygen valence electrons with the Rh surface makes them less available for bonding with hydrogen. Analysis derived from Figure 46a indicates that although the presence of coadsorbed oxygen on Pt influences ammonia activation, it has a limited effect on the activation of NH_2 or NH.[85] On Rh(111) however the reaction with coadsorbed oxygen becomes inhibiting.[87]

A first observation that can be made from Figure 46a is that there is a significant reduction in the activation barrier of the N−H bond of adsorbed ammonia when it reacts with coadsorbed oxygen. The activation energy is reduced by 51 kJ/mol. Interestingly, the corresponding reaction energies decrease by only 32 kJ/mol, yielding an unrealistic value of $\alpha_{BEP} = 1.6$. This indicates that there is little relationship between the reaction paths for these two cases. Inspection of the isolated transition state shown in Figure 46b reveals that as the N−H bond stretches the oxygen moves toward the resulting hydrogen. The adsorbed oxygen moves from a 3-fold site in the reactant state to a nearest neighbor 2-fold site in the transition state. The nitrogen atom maintains its position atop a surface Pt atom. Because of the close proximity of the hydrogen from the activated N−H bond and the oxygen atom adsorbed in the bridge site, the stretching of the N−H bond in the transition state is 30% less than in the absence of coadsorbed atomic oxygen. The transition state takes on a much earlier character. In contrast, promotion of the N−H bond by coadsorbed oxygen is absent on the Rh(111) surface. The activation energies for the oxygen-promoted N−H bond vary between 111 and 96 kJ/mol on Rh and depend upon the specific site of the coadsorbed oxygen (fcc or hcp). This has to be compared with the activation energy of 113 kJ/mol for cleavage of the N−H bond over the metal in the absence of coadsorbed oxygen. The differences between Pt and Rh reflect the stronger interaction energy of oxygen with Rh as compared to Pt.

Among the different adsorbed NH_x species on the Pt(111) surface, NH_3 is the only one which is promoted by the coadsorption of oxygen. At the coverages examined here, ammonia and coadsorbed oxygen do not share a metal atom in the transition state. Adsorbed NH_2 and NH prefer bridge and 3-fold coordination sites, respectively. In order for them to react with coadsorbed oxygen, they must be in configurations where they share metal atoms with the coadsorbed oxygen in their respective transition states. The sharing of the metal atoms by these adspecies in the pre-transition state results in a repulsive interaction among the adspecies. This justifies the relatively large pre-transition-state energies for the $NH_{2,ads} + O_{ads}$ reactions ($\Delta E_{pre} = 22$ kJ/mol) as well as for the $NH_{ads} + O_{ads}$ reaction ($\Delta E_{pre} = 40$ kJ/mol). If one corrects for these repulsive energies the activation energy for the NH_2 reaction with oxygen is reduced by 30 kJ/mol and that of NH activation by 22 kJ/mol (see Figure 46).

The reactivity differences for the reaction of NH_x with coadsorbed OH intermediates, as compared to coadsorbed O, is quite striking. As discussed, the transition state for the reaction between the adsorbed NH_2 and O on the Pt(111) surface has to share bonding to the same surface metal atom. However, this is not the case for the reaction of $NH_{2,ads}$ with OH_{ads}. This is due to the fact that OH adsorbs atop on Pt. The barriers for reaction with OH_{ads} are much lower for reaction with $NH_{2,ads}$ and NH_{ads}. The decreased reactivity of adsorbed NH_3 with OH_{ads} results from the longer distance that the N−H bond must stretch in order to reach the transition state for reaction with OH_{ads} as compared to O_{ads}. On the Rh(111) surface, the same differences observed for Pt(111) are even more pronounced. The reactivity of the NH_2 and NH species with coadsorbed oxygen becomes very unfavorable. The pre-transition-state energies are very large due to the stronger repulsive interactions.

In contrast, activation of adsorbed NH_x species with coadsorbed OH has a significantly lower barrier on Rh(111) as well as on Pt(111). The calculated barriers are often not

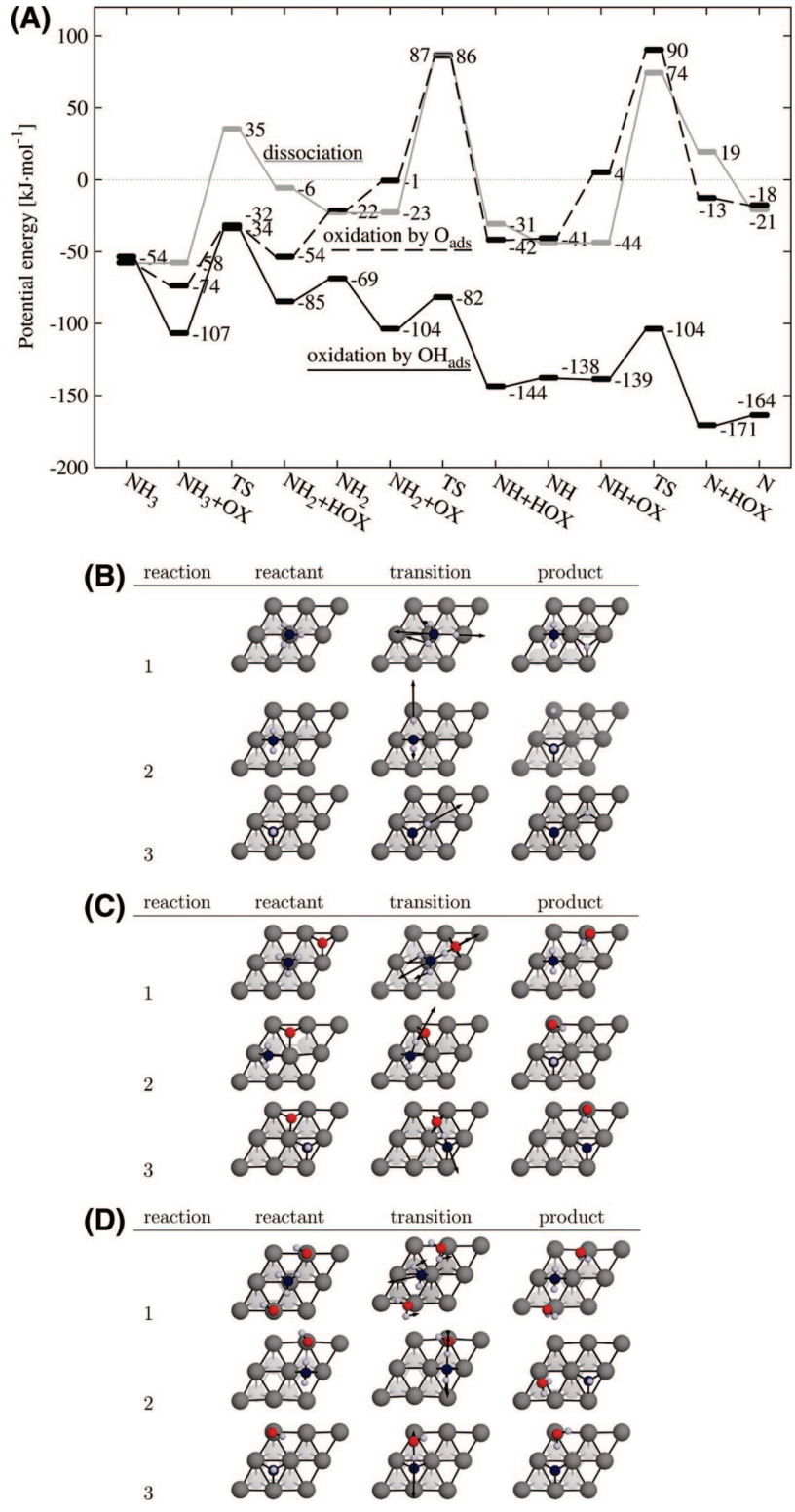

Figure 46. (A) Reaction energy diagram of the dehydrogenation reactions of NH_x on Pt(111). All total energies are with respect to $NH_{3(g)}$, $Pt(111)_{(s)}$, $3O_{ads}$, and $3H_{ads}$ and are zero-point energy corrected. OX or HOX on the abscissa mean oxidant or hydrogenated oxidant and can be OH, O, or an empty site or their hydrogenated forms. All NH_x + (H)OX coadsorbate states are with lateral interactions. In all "single" adsorbate states, we assume no lateral interactions.[85] (B) Dissociation of NH_x on Pt(111). The vertical projections of the unit cells show the reactant, transition, and product states. The arrows in the transition states are the vertical projections of the imaginary vibration. Hence, they point out the direction of the reaction path at the transition state. Black, white, and gray spheres indicate N, H, and Pt atoms, respectively. The second layer of the Pt surface has been shaded for clarity. (C) Oxidation of NH_x by O_{ads} on Pt(111). The vertical projections of the unit cells show the reactant, transition, and product states. The arrows in the transition states are the vertical projections of the imaginary vibration. Hence, they point out the direction of the reaction path at the transition state. Black, white, red, and gray spheres indicate N, H, O, and Pt atoms, respectively. The second layer of the Pt surface has been shaded for clarity. (D) Oxidation of NH_x by OH_{ads} on Pt(111). The vertical projections of the unit cells show the reactant, transition, and product states. The arrows in the transition states are the vertical projections of the imaginary vibration. Hence, they point out the direction of the reaction path at the transition state. Since we notice interactions between species of different unit cells in the NH_3 + OH reaction, we also show the mirror images of the OH species in this particular reaction. Black, white, red, and gray spheres indicate N, H, O, and Pt atoms, respectively. The second layer of the Pt surface has been shaded for clarity.

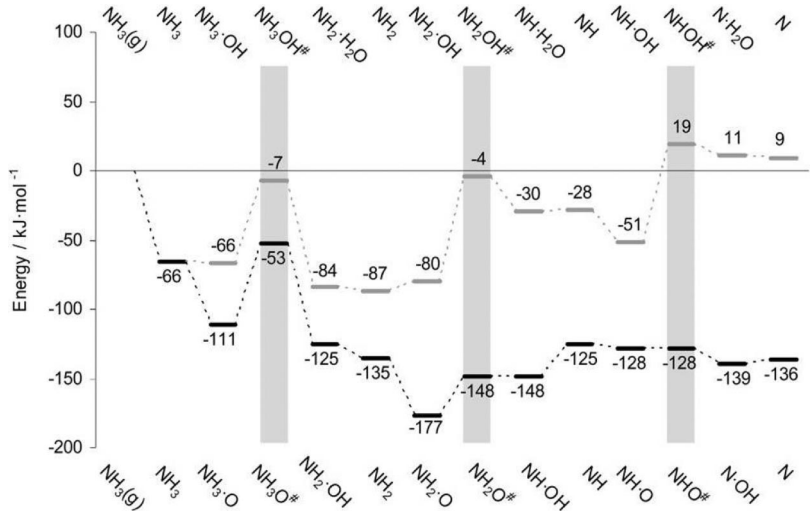

Figure 47. Reaction pathway for the oxidative dehydrogenation of ammonia over Pt(100) assisted by O (black line, bottom legend) and OH (gray line, top legend).[74] The energies are with respect to $NH_3(g) + 3O_{ads} + 3OH_{ads}$, ZPE corrected.

higher than 20 kJ/mol. The overall activation barriers can increase, as is the case for the NH_{ads} and OH_{ads} reaction, when there are significant repulsive pre-transition-state effects. The nature of the transition states varies significantly (see Table 6).[87] The values in Table 6 present the interaction energies of the reacting fragments according to Crawford and Hu's barrier decomposition analysis.[65] The interaction energies of $NH_2^{\ddagger}$ and $OH^{\ddagger}$ are calculated separately for their respective transition-state configurations. These energies are then compared with the energy of the transition-state complex, giving $E_{tot\text{-}int}$. These surface-bound interaction energies are compared with the interaction without metal surfaces $E_{vac\text{-}int}$ in order to evaluate the through-metal interaction. The interaction strength in the transition state is dominated by the direct $E_{vac\text{-}int}$, representative of hydrogen bonding for NH_3 and NH_2 dissociation and a more covalent interaction for the decomposition of NH_{ads}.

While the barrier for NH_2 activation by coadsorbed O is unfavorable on Pt(111), the barrier for this same reaction on the Pt(100) surface is lower (Figure 47).[74] Activation of NH_2 with oxygen can now occur through a transition state that does not require metal atom sharing, as illustrated in Figure 40c.

4.4.2. Activation on Stepped Surface: The Ostwald Process

The reaction energy diagrams and corresponding reaction intermediates shown in Figure 38 have been calculated for the reaction of adsorbed ammonia with coadsorbed oxygen on the stepped Pt(211) surface.[98] The data in Figure 48 are to be compared with those of Figure 40, which show the reaction barriers for ammonia at the same step edge but now in the absence of coadsorbed oxygen.

On the step edge, the unfavorable geometric arrangement of reactants in the transition state increases the activation energy of ammonia with coadsorbed oxygen even compared to the oxygen-free case. Also, two reaction situations for ammonia adsorbed at the bottom of a step are compared. In one case ammonia is adsorbed on a metal atom that is part of the (100) step. In the other situation ammonia is adsorbed to a surface Pt atom that is part of the (111) terrace. Compared to the interaction with terrace atoms there is a large repulsive interaction in the first situation resulting in an energy cost of 74 kJ/mol. One concludes that (100) step sites do not promote activation of the NH bond in NH_3 in the presence of coadsorbed oxygen. A very similar result is found for the overall barrier for the reaction of NH_2 with coadsorbed oxygen. Adsorption of NH_2 at the bottom of the step is very unstable. There is no difference in the overall activation barrier as compared with the presence of oxygen. Therefore, step sites also do not promote the overall reactivity of $NH_{2,ads}$ with coadsorbed oxygen.

In contrast to NH_3 and NH_2 activation, oxygen-assisted activation of NH on Pt is much more favorable than in the absence of oxygen. The position of NH adsorbed at the bottom of the step and oxygen at the top of the step results in an agostic type of interaction between the hydrogen and the oxygen, thus lowering the activation barrier to 32 kJ/mol. The transition state can now be described as an early transition state. Activation of the NH bond in the adsorbed state is chemically different from activation of NH_3. As noted before by Crawford and Hu,[65] now differences in the interactions between H_{ads} and N_{ads} determine the differences in activation barriers.

In the beginning of section 4.4 we observed for the Pt(111) surface that H_{ads} and N_{ads} recombination proceeds through a large pre-transition-state barrier. This is because of the sharing of bonds with the same surface metal atoms in the coadsorbed state. Novell-Leruth et al.[87] on the Pt(100) surface have shown that this barrier is substantially reduced because the pre-transition state is accessible in which the repulsive interaction is significantly reduced. This is attributed to the different geometric arrangement of the surface atoms and adsorbates (see Figure 40c). We also saw in section 4.4.1 that the coadsorbed state of NH_{ads} and O_{ads} on the Pt(111) surface is also highly repulsive, whereas on the Pt(100) surface activation of NH is promoted by reaction with coadsorbed O. This is again due to the nonsharing of the metal surface atoms by the reacting atoms in the transition state. For some reactions the same configurational low transition-state principle results in a strong preference for activation along a step-edge site. The reaction between adsorbed NH and the coadsorbed oxygen atom illustrates this. Figure 49a compares the reaction energies of NH with and without coadsorbed oxygen on a (111) surface and (211) surface. Figure 49b shows the structures of the corresponding reaction intermediates along the (211) step.

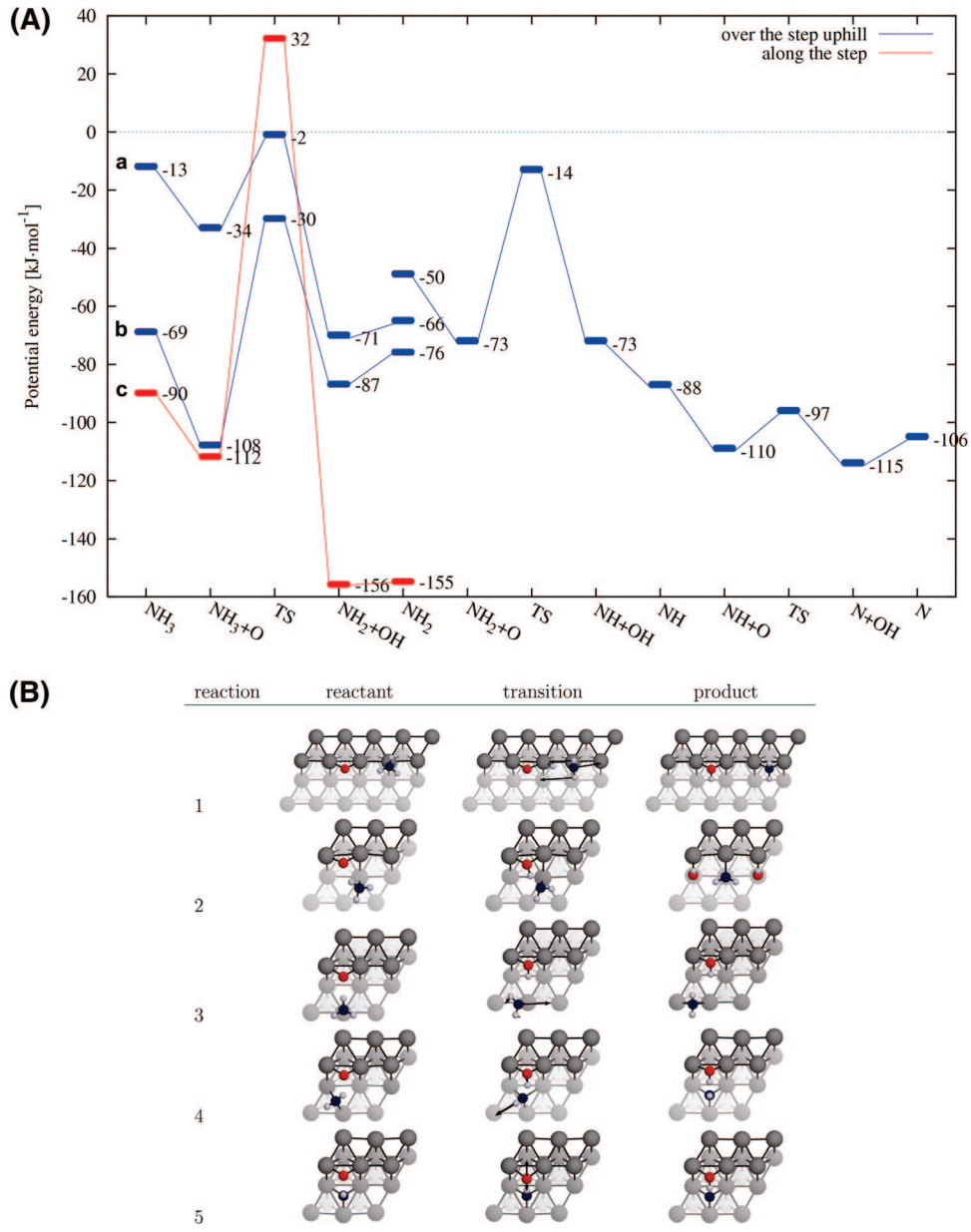

Figure 48. (A) Reaction energy diagram of the oxidation of NH_x by O_{ads} on Pt(211). All total energies are given with respect to $NH_{3(g)}$, $Pt(211)_{(s)}$, and $3O_{ads}$ and are not zero-point energy corrected. All NH_x + (H)O coadsorbate states are reported with lateral interactions. In all "single" adsorbate states, we assume no lateral interactions. (a) Reaction path of Figure 40b, 1. (b) Reaction path of Figure 40b, 3. (c) Reaction path of Figure 40b, 2.[98] (B) Oxidation of NH_x by O_{ads} on Pt(211). The vertical projections of the unit cells show the reactant, transition, and product states of the dehydrogenation reactions of $NH_{x,ads}$ by O_{ads}. The arrows in the transition states are the vertical projections of the imaginary vibration. Hence, they point out the direction of the reaction path at the transition state. Black, white, red, and gray spheres indicate N, H, O, and Pt atoms, respectively. The second layer of the Pt surface has been shaded for clarity.

Reaction over the step results in a significant reduction of the activation barrier. The barrier for NH activation by reaction with O_{ads} over the (211) step is only 36 kJ/mol. This is due to the fact that the N−H bond only has to stretch by 0.51 Å to reach the transition state. The pre-transition state again can be described as a state with agostic interactions. We have the remarkable result that activation or recombination at step-edge sites and (100)-type terraces have corresponding transition-state features (Figure 49). Notwithstanding this general result for low transition-state energies, there remain important differences between the two types of situations. The different elementary reaction energies are summarized in Figure 50. On the Pt(100) surface, NO and N_2 formation takes place with extremely low barriers. The high barriers on the stepped surface can be attributed to the unfavorable thermodynamics of the recombination reaction.

We will conclude with a short summary of the mechanistic steps for the ammonia oxidation reaction. At high temperatures (750−900°) mainly NO_x is produced, exploited in the Ostwald process for nitric acid production. At lower temperatures nitrogen can be selectively formed. N_2O formation occurs as a competitive reaction.[98] The lowest barrier path for the activation of NH_x proceeds via reaction with coadsorbed OH species. These hydroxyl intermediates can be readily formed by the reaction of water with coadsorbed oxygen. This agrees very well with experimental observations.[99] Surface science studies confirm the necessity of ammonia to be activated at least by coadsorbed O.[100,101] As we have seen, nitrogen formation can occur in a low-

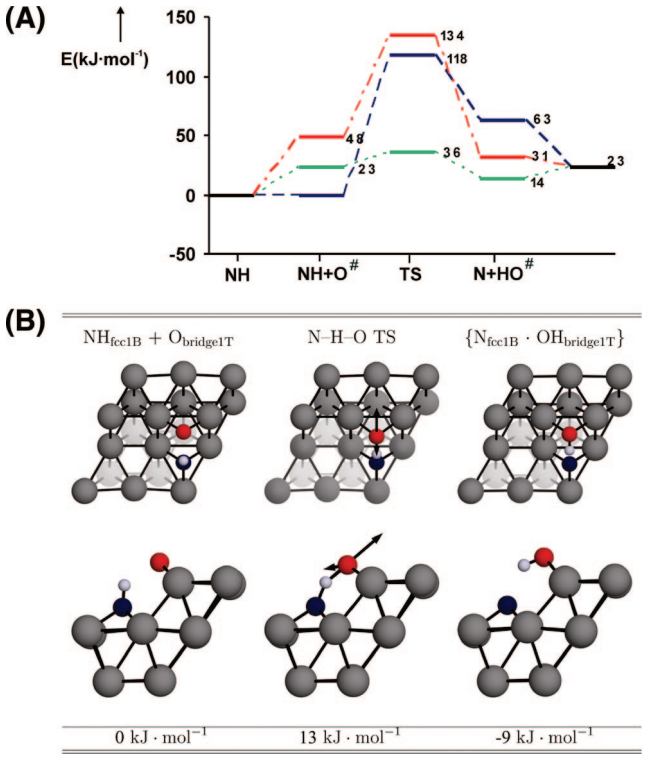

Figure 49. (A) Activation of NH_{ads} on Pt(111) without (---) and with coadsorbed O(-•-•-). A comparison is made with reaction of NH_{ads} with O_{ads} on Pt(211) (•••). (#) Reacton without oxygen activation and dissociation by metal surface.[87] (B) Structures and relative energies of NH_{ads} and O_{ads} along the (211)Pt step. Black, white, red, and gray spheres indicate N, H, O, and Pt atoms, respectively. The second layer of the Pt surface has been shaded for clarity.

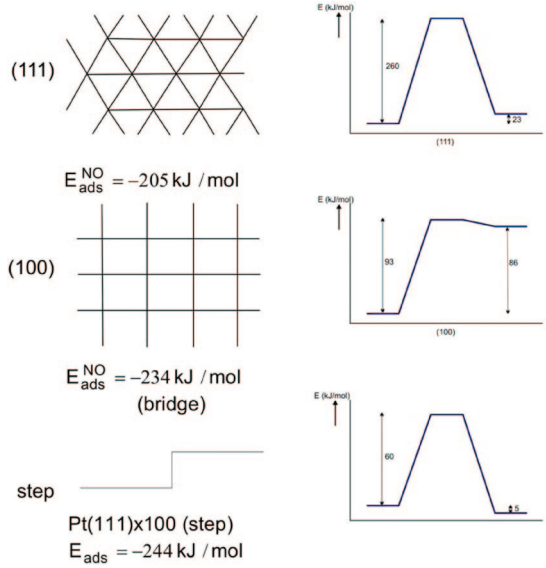

Figure 50. Schematic representation of NO dissociation on (top) Pt(111), (middle) Pt(100), and (bottom) stepped Pt surfaces.

temperature reaction by recombining N_{ads} species on the Pt(100) surface or analogous to the formation of NO by recombination of N and O adatoms on step edges. A different reaction path to produce nitrogen proceeds via the Fogel[102] reaction, where NH_3 reacts directly with NO and O_2. This is the dominating reaction path on Cu and Ag catalysts that have oxidized surfaces at reaction conditions.[103] This reaction has been studied computationally by Anstrom et al.[104] catalyzed by V_2O_5. At lower temperature, adsorbed NO can also recombine with N_{ads}[105] or at a high barrier with another NO molecule to give N_2O.[106]

The high desorption energy of NO as compared to that of N_2 suppresses overall NO formation at low temperatures.[107] The corresponding activation energies are compared in Figure 48. We have shown that NO recombination and NH_{ad} oxidation both require the presence of surface steps or a (100)-type surface. At low temperature the (100) surface is the preferred surface for high selectivity toward N_2. At low temperature there is a competition between N_2 versus N_2O formation. However, at high temperatures the relative rate of NO desorption increases compared to that of N_2 formation (Figure 49).

An early paper by Gland and Korchak[108] on ammonia oxidation on stepped Pt(111) single-crystal surfaces concluded that reaction predominantly occurs on the step sites. This agrees with the need for step edges for the rapid N_{ads} and O_{ads} recombination reaction. In the Ostwald process, the high selectivity toward NO at high temperatures depends on the rate of NO formation, low nitrogen adatom coverage, and use of high O_2. This is consistent with the results found from the calculations presented.

5. Microkinetic Derivation of the Volcano Curve: The Sabatier Effect

In the above sections we mostly focused on analysis of the transition state of the elementary reaction steps of important surface chemical reactions. The catalytic reaction is a combination of such elementary reaction steps that forms the catalytic reaction cycle. Trends in reactivity found for elementary reactions steps do not translate into trends for the overall catalytic reaction. To illustrate this, in the present section we provide an elementary analysis of the kinetic basis to the Sabatier effect. This leads to an explanation of the volcano curve relations that are formed when the overall rate of a catalytic reaction is studied as a function of a reactivity parameter as the adsorbate−surface interaction energy.

In microkinetics overall rate expressions are deduced from the rates of elementary rate constants within a molecular mechanistic scheme of the reaction. We will use the methanation reaction as an example to illustrate the derivation of the Sabatier volcano curve. We will use a simplified scheme that converges several of the reaction steps that we discussed in the previous sections in great detail into one single reaction step. The corresponding elementary reactions are

$$\begin{aligned} &CO_{gas} \rightarrow CO_{ads}; && k_{ads} \\ &CO_{gas} \leftarrow CO_{ads}; && k_{des} \\ &k_{ads}^{CO} = \frac{k_{ads}}{k_{des}} \end{aligned} \qquad (4.4a)$$

$$CO_{ads} \rightarrow C_{ads} + O_{ads}; \qquad k_{diss} \qquad (4.4b)$$

$$C_{ads} + 2H_2 \underset{r_H}{\rightarrow} CH_4\uparrow \qquad (4.4c)$$

where r_H, the rate of C_{ads} hydrogenation, depends implicitly on hydrogen pressure.

We will present expressions for reaction rates and steady-state concentrations using the simplifying assumption that C_{ads} hydrogenation to CH_4 occurs in one reaction step. We will also assume that O_{ads} removal is fast and that hydrogen adsorption is not influenced by the other adsorbates.

Then the activation energy for methane production from C_{ads} is the overall activation energy for the hydrogenation of C_{ads} to CH_4 and eq 4.5 gives the rate of methane production

$$R_{CH_4} = r_H \cdot \theta_c \tag{4.5}$$

where θ_C is the C_{ads} coverage. A closed expression for θ_C can be deduced

$$\theta_C = 1 + \frac{1}{2}\lambda - \frac{1}{2}\sqrt{\lambda^2 + 4\lambda} \tag{4.6a}$$

$$\approx \frac{1}{1+\lambda} \tag{4.6b}$$

with λ

$$\lambda = \frac{r_H}{k_{diss}} \frac{(K_{ads}^{CO} \cdot [CO] + 1)^2}{(K_{ads}^{CO}[CO])} \tag{4.7a}$$

$$= A\frac{r_H}{k_{diss}} \tag{4.7b}$$

One notes that the coverage of C_{ads} depends on two important parameters: The ratio ρ of the rate of hydrogenation of C_{ads} to give methane and the rate constant of CO dissociation

$$\rho = \frac{r_H}{k_{diss}} \tag{4.8}$$

and the equilibrium constant of CO adsorption, K_{ads}^{CO}. The coverage with C_{ads} increases with decreasing value of ρ. This implies a high rate of k_{diss} and slow rate of C_{ads} hydrogenation. The strong pressure dependence of CO is due to the need of neighboring vacant sites for CO dissociation.

Beyond a particular value of K_{ads}^{CO} the surface coverage with C_{ads} will decrease because CO dissociation becomes inhibited. In order to determine the dependency of the overall catalytic rate on the reacting parameter, one needs to know the relation between the rate constants and reaction energies. This determines the functional behavior of ρ. We will use the linear activation energy−reaction energy relationships, as deduced for the BEP relation, and write expressions for k_{diss}, r_H, and λ

$$k_{diss} = \nu_0 e^{-E_{diss}^0/kT} \cdot e^{-\alpha E'_{ads}/kT} \tag{4.9a}$$

$$= \nu'_0 e^{-\alpha' E_{ads}/kT} \tag{4.9b}$$

$$r_H = r'_H e^{xE_{ads}/kT} \tag{4.9c}$$

$$\lambda = A\frac{r'_H}{\nu'_0} e^{(x+\alpha')E_{ads}/kT} \tag{4.10}$$

The dissociation rate of CO_{ads} will increase with increasing exothermicity of the corresponding reaction energy. As a measure one can use the adsorption energy of the carbon atom. This is a simplifying assumption. The different trends in the reactivity of CO versus methane as a function of metal indicates that a better BEP relation then eq 4.9a is to relate it to the sum of C_{ads} and O_{ads} interaction energies. Whereas it is more accurate it complicates the expressions nonessentially, and in the following we will ignore this.

We will now study the consequences of these BEP choices to the dependence of the predicted rate of methane production on E_{ads}. Making the additional simplifying assumption that the adsorption energy parameters in eqs 4.9b and 4.9c are the same one finds for the rate of methane production expression

$$R_{CH_4} = C\frac{\lambda^{x/(x+\alpha')}}{1+\lambda} \tag{4.11a}$$

with

$$C = r'_H \left(\frac{r'_H}{\nu'_0} A\right)^{-[x/(x+\alpha')]} \tag{4.11b}$$

From chemisorption theory we know that adatom adsorption energies will decrease in a row of the group VIII metals when the position of the element moves to the right. The rate of hydrogenation of C_{ads} will decrease with increasing adsorption energy of C_{ads} and hence decrease in the same order with element position in the periodic system. In eq 4.11b the constant A depends on the equilibrium constant K_{eq}^{CO}. This will vary also with the adsorption energy of C or O but will be much less sensitive to these variations than the activation energies of CO dissociation and hydrogenation

The equilibrium constant variation affects the surface concentration of intermediates for dissociation reactions that need two or several empty surface sites. Volcano curve behavior can also be deduced by adjusting parameters such that there is no change in the rate-limiting steps of the reaction. Then the volcano curve simply arises from the decrease of neighboring surface sites at higher coverage Typically, the maximum of the volcano curve occurs at $\theta = 1/2$ when two empty neighboring sites are needed for the reaction.[6,7] Beyond the volcano curve maximum, the increase in the rate of CO dissociation with increased metal adsorbate interaction is counteracted by the decrease in the concentration of surface ensembles with two empty sites.

The Sabatier effect strictly refers to a change in the rate-limiting step at the volcano maximum. We will illustrate this here. We will assume K_{eq} to be a constant. The dependence of R_{CH_4} on λ is sketched in Figure 8. Equation 4.11a will have a maximum as long as

$$\frac{x}{x+\alpha'} < 1 \tag{4.12}$$

Within our model this condition is always satisfied. We now find the interesting result that the kinetic Sabatier volcano maximum is found when λ_{max} equals

$$\lambda_{max} = \frac{x}{\alpha'} \tag{4.13}$$

The controlling parameters that determine the kinetic volcano curve are the BEP constants of k_{diss} and r_H. It is exclusively determined by the corresponding value of ρ_{max}. It expresses the compromise of the opposing elementary rate events: CO dissociation versus product formation through hydrogenation of the surface. From eq 4.7a we can deduce the optimum value of E_{ads} of the Sabatier maximum rate. It depends through A on the CO partial pressure. For the methanation reaction, the volcanic maximum (eq 4.13) will give a relation between the elementary rate constants that will depend strongly on the CO partial pressure. The volcano curve is bound by the rate of dissociative adsorption of CO and hydrogenation of adsorbed carbon.

Interestingly, when the kinetic volcano curve maximum is at $\lambda = 1$, the surface coverage equals 0.5. This occurs when $\alpha = x$ and is independent of the actual value of the

BEP α parameter. The expression for the rate of methanation production R then becomes

$$R = \frac{r'_H \cdot x}{1 + A\frac{r'_H}{\upsilon'_0} \cdot x^2} \tag{4.14a}$$

with

$$x = e^{-\alpha'(E_{ads}/kT)} \tag{4.14b}$$

The maximum of 4.14a is found for

$$\lambda = \frac{r'_H}{\upsilon_0} e^{-[2\alpha'(E_{ads}/kT)]} = 1 \tag{4.15}$$

For related treatments, see ref 5. Whereas the above discussion limits itself to the conversion of CO to a single product, the treatment can be easily extended to a selectivity problem. This analysis can be easily generalized to reactions where the elementary dissociation step occurs. One such important reaction is the ammonia synthesis where low N_2 coverage is involved. Therefore, λ is now strictly inverse in partial pressure. One-half surface coverage with N_{ads} now determines the location of the volcano curve.

Interestingly, one can easily deduce an expression of the relative rate of coke formation versus that of methanation. The rate of initial coke formation depends on the combination probability of carbon atoms and hence is given by

$$R_{C-C} = r_{CC} \cdot \theta_C^2 \tag{4.16}$$

The relative rate of coke versus the rate of methane formation then follows from

$$\frac{R_{CC}}{R_{CH_4}} = \frac{r_{CC} \cdot \theta_C^2}{r_H \cdot \theta_C} \tag{4.16a}$$

$$= \frac{r_{CC}}{r_H} \cdot \theta_C \tag{4.16b}$$

The occurrence of a maximum depends on the BEP parameter α′ of the C−C bond formation rate. Volcano-type behavior for the selectivity is found as long as eq 4.17a is satisfied

$$2x + \alpha > \alpha'' > x \tag{4.17a}$$

Then

$$\lambda_{max}^{sel} = \frac{\alpha'' - x}{2x + \alpha - \alpha''} \tag{4.17b}$$

r_{CC} as well as r_H decrease when the carbon adsorption energy increases. Volcano-type behavior of the selectivity to coke formation is found when the activation energy of C−C bond formation decreases faster with increasing metal carbon bond energy than the rate of methane formation. Equation 4.17b indicates that the rate of the nonselective C−C bond-forming reaction is low when θ_C is high. Then the metal−carbon bond is so strong that methane formation dominates over carbon−carbon bond formation. The other extreme case of C−C bond formation rate occurs for very slow CO dissociation. Then θ_C is so small that the rate of C−C bond formation is minimized.

This analysis indicates the importance of a proper understanding of BEP relations for surface reactions. It enables a prediction of not only conversion rates but also selectivity trends.

6. Conclusions

For all surface reactions a low transition-state energy requires minimum reactive molecular bond stretching and also a minimization of through-metal repulsive interactions of adsorbed reaction fragments. According to the barrier decomposition model, the dissociated state with respect to the activation energy for recombination corresponds approximately to the sum of the adfragment displacement energies to form the coadsorbed pre-transition state and the weakening of the fragment surface bonds to form the transition-state intermediate in which the new bond is partially present. Very often the structures of the transition state and (sometimes transient) initial product state have close resemblance with respect to the geometry and electronic structure. The strong interaction with the surface necessary to activate molecular bonds implies a tight transition-state structure with immobilized character. It can be often described as late with respect to the dissociating bond.

However, this last notion has to be considered with care. To reach the product dissociated state several displacements of fragment atoms may occur, as we found for ammonia dissociation. These displacements are not always in phase. This implies that the reaction coordinate corresponding to N−H bond dissociation in NH_3 depends on two atomic displacements. One corresponds to the N−H bond stretching in the transition state. The other is the displacement of the N atom from the atop to a 2-fold site. The transition state only corresponds to the N−H stretching, and the N atom is still in the atop site. The displacement of the N atom from the atop site to the bridge site only takes place from the transition state to the final state. For example, the transition-state energies for ammonia activation over Pt or Rh and methane over Rh or Ru tend to correlate with the adsorption energies of NH_2 or CH_3, respectively, adsorbed to atop sites. However, the most stable sites for these fragments are the higher coordination sites.

With respect to the nondissociated molecular state the transition state is the result of molecular bond changes induced by the strong interactions with the metal surface. The transition-state activation energy is typically 10−20% of the bond cleavage energy. In the transition state the interaction energy with the surface is very large. The interaction energy between reacting fragments can also depend strongly on the presence of through-metal atom interactions in the transition state. If through-metal interactions are weak, for instance, in the case of dissociation of CO at a step edge, the interaction energy between coadsorbed dissociation fragments is only 10−20 kJ/mol. In contrast, on a surface terrace this interaction can increase to 50−100 kJ/mol, resulting into a high activation barrier. Even in this case the transition state is to be considered late with respect to the nondissociated molecule because of the strong attractive interaction with the metal surface necessary to activate the chemical bond. Whereas the dissociation reaction on clean metal surfaces generally occurs through transition states late, this concept cannot be as easily applied to the activation of X−H bonds with coadsorbed O or OH intermediates. Reaction with coadsorbed oxygen or hydroxyl species proceeds through a push−pull mechanism in which the oxygen surface species acts as a Lewis acid which accept electrons from the surface metal atoms which act as Lewis base.

Reaction with coadsorbed oxygen can become unfavorable by the very strong repulsive interactions of reacting adsorbed

oxygen with surface NH_x species. This occurs in the transition state for the reaction of coadsorbed NH_x with O on terrace sites when NH_x and O share binding to the same surface metal atoms. When one subtracts these repulsive interactions from the overall activation energy, the reaction with coadsorbed oxygen atoms appears to be more favorable than in the absence of oxygen. The pre-transition-state destabilization however tends to overrule these favorable effects. It will only become favorable on sites with low repulsive through-metal atom interaction. Hence, these reactions are highly structure sensitive.

Hydrogen-bonding interactions are especially important for reactions which involve surface OH species. The transition states are stabilized due to hydrogen bonding, which reduces the barriers. Reaction on terraces and step edges may behave dramatically different. Molecules with π-type chemical bonds have substantially lower activation energies when they dissociate over the step edge. Reaction occurs such that one atom finishes at the bottom of the step and the other at the step edge. The reactivity of terraces depends on the arrangement of the surface atoms. In the transition state if the reacting fragments do not share the metal atoms the barrier is significantly reduced.

The oxidative addition model in which dissociation of a molecular bond occurs by back-donation of electrons from the surface into unoccupied molecular orbitals is consistent with this lowered barrier for the forward as well as backward direction. The favorable overlap of the antibonding molecular orbital of the reacting molecule with the surface ensemble of atoms that forms the step edge, the small increase in bond length necessary to dissociate, as well as the absence of sharing of surface metal atoms by the dissociating fragments in the transition state are responsible for the lowered transition-state barrier. The sites along the step edges which have high coordinative unsaturation are responsible for low barrier dissociation. However, one should also note that during the reaction these sites should not reconstruct. For diatomic molecules at comparable surface sites BEP relationships are found with α values close to 1. This agrees with the late character of the dissociation transition state.

Activation of σ bonds such as C−H, N−H, or O−H tends to follow different rules. Bond dissociation typically occurs over a single metal atom. BEP-type relationships are also applicable when the surface coordination number changes. For CH_4 activation the forward reaction will have a decreased activation barrier when the surface metal atom coordination decreases. However, the activation energy of the reverse reaction will not be affected. As a consequence, the reverse reaction of the hydrogenation of surface alkyl species will be independent of the surface atom environment. This is the consequence of microscopic reversibility. For NH_3 and H_2O the dependence of the activation barrier for XH bond dissociation on surface atom unsaturation may be much less. The strong interaction with metal surface d electrons already creates a strong bond with the lone pair electrons of molecule before reaction.

The increased understanding of structure−reactivity relationships of surface chemical elementary reaction steps and the nature of the corresponding transition states as presented here has generated new insight that rationalizes the dependence of catalytic reactions on transition-metal particle size.[109]

Three different types of behavior can be distinguished.[110,111] They are illustrated in Figure 51. Many practical factors may play a role, such as catalyst deactivation by coke deposition, metal particle reconstruction, surface overlayer formation, etc. We consider the ideal case that the particle size dependence is only due to the reactivity of the metal particle in its unchanged state and coverage-dependent effects do not play a role. Analysis of transition states presented in this paper leads one to conclude that cases I and II are often inter related. In case I the turnover frequency (the conversion rate normalized per exposed surface metal atom) is independent of particle size, whereas in case II it increases with decreasing particle size. In case III the reactivity shows a maximum or strongly decreases beyond a minimum particle size.

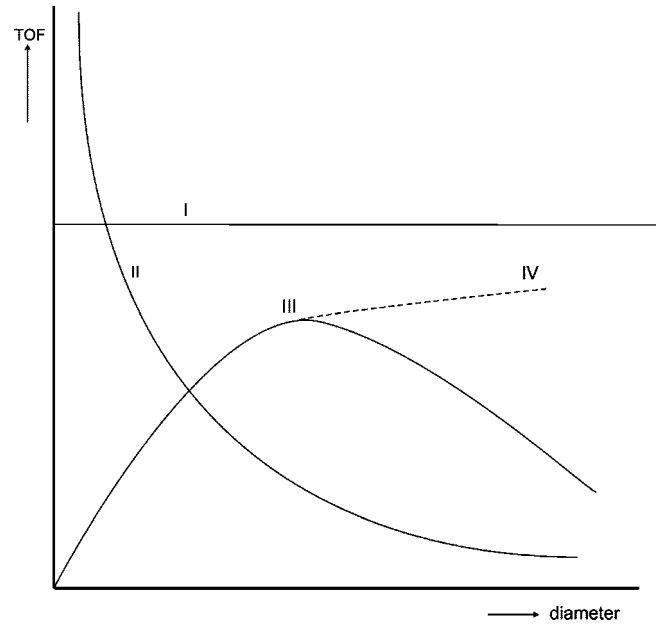

Figure 51. Particle size dependence of catalytic reactions.

A decrease in particle size increases the number of edge atoms over terrace atoms. The coordinative unsaturation of an edge atom is larger than that of a terrace atom, and hence, its reactivity is increased. The uniform increase in rate with decreasing particle size as in class II-type reactions relates to the increasing fraction of coordinative by unsaturated surface atoms. The prototype reactions that behave according to class I or II are catalytic reactions that involve activation of σ-type CH bonds in saturated molecules. The transition states of these reactions are usually located atop of a surface atom. The activation barrier for XH bond dissociation decreases with increasing exothermic reaction energy. Such dissociation reactions will show class II behavior. The TOF increases with decreasing particle size.

As discussed in section 3.2.2, in contrast to the high BEP α value of the forward reaction, the reverse reaction is invariant for reaction energy change (microscopic reversibility) and hence will show class I behavior. This behavior is typical for hydrogenation reactions. The reverse reaction of CH bond activation is hydrogenation of surface intermediate species.

A prototype reaction of class I behavior is the hydrogenation of olefins to form cyclohexene. The rate-liming step is hydrogenation of surface intermediate alkyl species (see ref 112, p 157). Hydrogenolysis reactions of hydrocarbons in which C−C bonds are broken are characteristic of class II behavior. Whereas the C−H bond is stronger than the C−C σ bond, carbon−carbon bond cleavage occurs after CH bond

dissociation. The α, β C−C bond cleavage reaction also preferentially occurs at step-edge sites, which is in agreement with computational predictions.[73] As indicated in section 4.2, the hydrogenolysis reaction requires multiple contacts of molecule-carbon atoms with the surface. This requires an ensemble of metal surface atoms to be active in the reactive center (see also ref 6, p 462) as deduced from alloying studies of a reactive metal such as Ni with a nonreactive metal such as Cu.[113] Such ensemble sizes are present on small metal particles at a much smaller size than the step-edge sites that disappear at a particle size around 3 nm. The selectivity change found by Somorjai et al.[114] for hexane activation with decreasing particle size strikingly illustrates the consequences of the complementary relationship of class I- and class II-type behavior. As a function of particle size change they find constant activation energy for hydrogenation of cycloalkene to produce cyclobenzene formation from cycloalkane, i.e., dehydrogenation, strongly increases with decreasing particle size.

Class III-type behavior concerns reactions that require a unique ensemble of surface atoms as formed by step edges. The prototype reactions are reactions as previously discussed the F−T reactions[75] or CO methanation. These reactions require low CO activation barriers as occur on step-edge sites. Such a step edge cannot be formed on a particle smaller than 3−4 nm. Below a particular particle size, reaction sites essential for low activation barriers of the CO dissocation reaction will not be present. Class III-type behavior will occur when the step-edge atoms also require high coordinative unsaturation; class IV-type behavior will occur when the reaction is less sensitive to the degree of coordinative unsaturation of the surface atoms. The generality of this concept is evident also from the particle size dependence of the ammonia synthesis reaction, involving N_2 dissociation reported for Ru[62] and even for O_2 activation by particles reported to be maximum for a smaller particle size on Au, stabilized on TiO_2.[67] The discovery of the structure sensitivity of the ammonia synthesis reaction has been elegantly described by Boudart et al.[112] Van Hardeveld and Hartog identified a unique configuration of surface atoms, similar to the surface step-edge site, as the reactive center on the Fe catalyst.[115] Somorjai identified these sites with surface ensembles on a coordinatively unsaturated (111) surface of the Fe bcc structures that are not present on the more stable (110) and (100) terraces of small Fe particles.[116]

We analyzed hydrogenation of $NH_{2,ads}$ intermediates on Pt surfaces in section 4.3. In contrast to methane activation, ammonia activation is independent of the reaction site, which leads to class I behavior. However, hydrogenation of NH_2 is strongly site dependent. Since NH_2 is most strongly adsorbed to the step edge, it will have the higher activation energy. For NH_2 hydrogenation (111) terrace sites are the most preferred sites when hydrogenation of this intermediate is rate limiting. Then the rate of reaction should decrease with particle size due to the decreasing fraction of terrace sites.[117] This corresponds to type IV behavior that now is complementary to type I behavior.

So far we discussed surface sensitivity as a function of the relative ratio of particle surface edge and kink sites and surface terrace atoms; the difference in reactivity between (111) and (100) surface of fcc-type lattices, as we discussed in section 4.2.2, provides a principle for particle shape effects. A cubic fcc particle would be exclusively terminated by (100) surfaces, whereas cuboctahedron-type particles may have a dominance of the more stable (111) surfaces. The Pt(100) surface provides sites for extremely low barriers of NO and N_2 recombination. On the (100) surface, the adsorption energy of N_2 is also low but that of NO is substantial. Notwithstanding the very similar activation energies for N_2 and NO formation, the strong interaction of NO with both surfaces implies that the selectivity of the reaction (toward N_2) will be high at low temperature. The NO once formed will not desorb and can only be removed as N_2O.

At low temperature reaction to form N_2 and N_2O preferentially occurs at the (100) surface, and hence, these reactions are shape sensitive. At higher temperatures, when NO readily desorbs, overall activation barriers for the product formation (Figure 49) on the different surfaces tend to become similar, and hence, surface sensitivity will become less. The high selectivity toward NO at higher temperatures relates to the rapid reaction of N_{ads} with coadsorbed O, whose coverage dominates and hence competitive N_2 formation has a slow rate. Recently, Shetty et al. investigated NO dissociation on corrugated Ru surface and 1.5 nm particle. Their results showed that although the barrier required for NO dissociation is extremely low (11 ± 7 kJ/mol), removal of O atoms is a difficult step.[118]

An interesting experimental system that shows related behavior is acetylene cyclotrimerization by Pd particles.[119] This reaction is surface sensitive and preferentially catalyzed by Pd (111) surfaces; on such surfaces three acetylene molecules are aligned in a suitable configuration. The rate of benzene formation increases on particles with increasing ratio of terrace sites.

The remarkable differences between the reactivity of adsorbed oxygen on Rh and Pt relates to the stronger Rh−O bond energy on Rh compared to that on Pt. This causes the selectivity of H_2O in methane reforming to be higher on Pt than on Rh.[95] The recombination of H_{ads} with O_{ads} to give OH_{ads}, which eventually recombines to form water, is the preferred path on Pt (weak metal−oxygen interaction). On the contrary, water formation from H_{ads} and OH_{ads} is the favorable path on Rh (strong metal oxygen interaction). One can see that formation of OH_{ads} is an important intermediate for water formation on Pt and Rh. Table 8 clearly shows that formation of OH on Pt has an about 70 kJ/mol lower barrier than on Rh. Therefore, the selectivity toward formation of water on Pt is higher compared to Rh.[95] Hydrogen-bonding effects that a play role in promoting H_2O formation as we discussed in section 5 are more general and very important in electrocatalysis.[97] Gong et al.[98] report a remarkable computational study of the enhancement of CO oxidation on Pt(111) by coadsorbed water. Whereas reaction of $CO_{ads} + O_{ads}$ on Pt(111) has a barrier of 80 kJ/mol, in the presence of H_2O_{ads} and OH_{ads} the barrier becomes 60 kJ/mol at 1/6 ML CO coverage and 33 kJ/mol at 1/3 ML coverage.

Formation of $(COOH)_{ads}$ intermediate by reaction of CO_{ads} with H_2O_{ads} is promoted by coadsorbed OH_{ads}. In a consecutive step the proton is transferred from $(COOH)_{ads}$ again to an adsorbed hydroxyl species. Formation of OH_{ads} from reaction of adsorbed oxygen with water was discussed in section 4.4. Interestingly, the activation energies for this reaction are independent of metal and are ~60 kJ/mol. The overall barrier for CO oxidation in the presence of water can therefore not be lower than this value.

In this concluding section we have summarized the most important concepts discussed in previous sections. These

concepts have been developed using BEP linear activation energy−free-energy relationship analysis as a leading approach. In this last section we have connected notions that relate to elementary reaction steps at metallic centers to the classical topic in heterogeneous catalysis of surface-sensitive and -insensitive reactions. We also have indicated the relevance of reactivity concepts relating to the reactivity of coadsorbed oxygen or hydroxyl to a wide class of problems in oxidation catalysis in the gas phase as well as liquid phase.

7. Acknowledgments

We gratefully are thankful for the fruitful discussions and help from many members of the Laboratory of Inorganic Chemistry and Catalysis. We especially want to thank I. M. Ciobica (Sasol Technology), W. K. Offermans, C. Popa, and A. P. J. Jansen. This work has been partially supported by the National Research School Combination Catalysis Controlled by Chemical Design (NRSC-C) and the Dutch Academy of Arts and Sciences (KNAW).

8. References

(1) Eyring, H.; Polanyi, M. *Z. Phys. Chem. B* **1931**, *12*, 279.
(2) Evans, M. G.; Polanyi, M. *Trans. Faraday Soc.* **1938**, *34*, 11.
(3) Kramer, G. J.; van Santen, R. A.; Emeis, C. A.; Nowak, A. K. *Nature.* **1993**, *363*, 529.
(4) (a) van Santen, R. A.; Neurock, M. *Catal. Rev. Sci. Eng.* **1995**, *37*, 557. (b) van Santen, R. A.; Niemantsverdriet, J. W. *Chemical Kinetics and Catalysis*; Plenum Press: New York, 1995.
(5) Hammer, B.; Nørskov, J. *Adv. Catal.* **2000**, *45*, 71.
(6) Masel, R. I. *Principles of adsorption and reaction on solid surfaces*; Wiley: New York, 1996.
(7) van Santen, R. A.; Neurock, M. *Molecular Heterogeneous Catalysis*; Wiley-VCH: Weinheim, Germany, 2006.
(8) Nilsson, A.; Pettersson, L. G. M. In *Chemical bonding at surfaces and interfaces*; Nilsson, A., Pettersson, L. G. M., Nørskov, J. Eds.; Elsevier: Amsterdam, The Netherlands, 2008; Chapters 2 and 4.
(9) Pallassanna, V.; Neurock, M. *J. Catal.* **2000**, *191*, 301.
(10) Michaelides, A.; Liu, Z.-P.; Zhang, C. J.; Alavi, A.; King, D. A.; Liu, P. *J. Am. Chem. Soc.* **2003**, *125*, 3704.
(11) Hammond, S. *J. Am. Chem. Soc.* **1955**, *77*, 334.
(12) Rice, O. K. *Statistical Mechanistic, Thermodynamics and Kinetics*; W. H. Freeman: San Francisco, 1967.
(13) Marcus, R. A. *Annu. Rev. Phys. Chem.* **1964**, *15*, 155.
(14) Hammett, L. P. *Physical Organic Chemistry*; McGraw-Hill: New York, 1970, p 356.
(15) Brønsted, J. N.; Pedersen, K. J. *Z. Phys. Chem.* **1924**, *108*, 185.
(16) Hinshelwood, C. N. *The Kinetics of Chemical Change*; Oxford University Press: Oxford, 1940.
(17) Hougen, O. A.; Watson, K. M. *Chemical Process Principles. Part three. Kinetics and Catalysis*; J. Wiley and Sons: New York, 1947.
(18) Stryer, L. *Biochemistry*; W.H. Freeman: San Francisco, 1995; Chapter 8.
(19) de Gauw, F. J. M. M.; van Grondelle, J.; van Santen, R. A. *J. Catal.* **2002**, *206*, 295.
(20) (a) Haag, W. O. *Stud. Surf. Sci. Catal.* **1994**, *84*, 1375. (b) Nabeshuber, F. F.; Brait, A.; Seshan, K.; Lercher, J. *J. Catal.* **1997**, *172*, 127.
(21) Sabatier, P. *La Catalyse en Chimie Organique*; Librairie Polytechnique: Paris, 1913.
(22) Thomas, J. M.; Thomas, W. J. *Heterogeneous Catalysis*; Wiley: New York, 1997.
(23) (a) Pocarero, T. A.; Chianelli, R. R. *J. Catal.* **1981**, *67*, 429. (b) Rayboud, P.; Kresse, G.; Hafner, J.; Toulhoat, H. *J. Phys.-Condens. Matter* **1997**, *9*, 11085. (c) Chianelli, R. R.; Berhault, G.; Rayboud, P.; Kasztelan, S.; Hafner, J.; Toulhoat, H. *Appl. Catal. A: Gen.* **2000**, *227*, 83.
(24) (a) Stoltze, P.; Nørskov, J. K. *Phys. Rev. Lett.* **1987**, *55*, 69. (b) Dahl, S.; Logadottir, A.; Jacobsen, C. J. H.; Nørskov, J. K. *Appl. Catal. A: Gen.* **2001**, *222*, 19. (c) Bligaard, T.; Nørskov, J. K.; Dahl, S.; Matthiesen, J.; Christensen, C. H.; Sehested, J. *J. Catal.* **2004**, *224*, 206.
(25) Bell, R. P. *The Proton in Chemistry*; Chapman and Hall: London, 1973.
(26) Horiuti, J.; Polanyi, M. *Acta Physicochim.* **1935**, *2*, 505.
(27) (a) Hoffman, R. *Solids and Surfaces*; Wiley VCH: Weinheim, Germany, 1988; (b) Woodward, R. B.; Hoffmann, R. *The Conservation of Orbital Symmetry*; Verlag Chemie: Weinheim, Germany, 1970.
(28) (a) Thorn, D. L.; Hoffmann, R. *J. Am. Chem. Soc.* **1978**, *100*, 2079. (b) Berke, H.; Hoffmann, R. *J. Am. Chem. Soc.* **1975**, *100*, 7224.
(29) Rozanska, X.; van Santen, R. A. In *Computer Modelling of Microporous Materials*; Catlow, C. R. A., van Santen, R. A., Smit, B., Eds.; Elsevier Academic Press: London, 2004; Chapter 6.
(30) Hammer, B.; Nørskov, J. K. *Nature* **1995**, *376*, 238.
(31) Sanchez Marcos, E.; Jansen, A. P. J.; van Santen, R. A. *Chem. Phys. Lett.* **1990**, *167*, 399.
(32) Lundquist, B. I.; Gornarsson, O.; Hjelunberg, H.; Nørskov, J. K. *Surf. Sci.* **1979**, *89*, 196.
(33) van Santen, R. A. *Theoretical Heterogeneous Catalysis*; World Scientific: Singapore, 1991.
(34) Mutterties, E. L.; Rhodin, T. N.; Band, E.; Brucker, C. F.; Pretzer, W. R. *Chem. Rev.* **1979**, *79*, 91.
(35) Mavrikakis, M.; Hammer, B.; Norskov, J. K. *Phys. Rev. Lett.* **1998**, *81*, 2819.
(36) van Helden, P. *Thesis*, University of Capetown (to be published).
(37) Diefenbach, A.; de Jong, G. Th.; Bickelhaupt, F. M. *J. Chem. Theory Comput.* **2005**, *1*, 286.
(38) Bunnik, B. S.; Kramer, G. J. *J. Catal.* **2006**, *242*, 309.
(39) (a) Triquero, L.; Petterson, L. G. M.; Minaev, B.; Agren, H. *J. Chem. Phys.* **1998**, *108*, 1193. (b) Föhlisch, A.; Nyberg, M.; Hasselstrom, J.; Karis, O.; Petterson, L. G. M.; Nilsson, A. *Phys. Rev. Lett.* **2000**, *85*, 3309.
(40) Pallassana, V.; Neurock, M.; Lusvardi, V. S.; Lerou, J. J.; Kragten, D. D.; van Santen, R. A. *J. Phys. Chem. B* **2002**, *106*, 1656.
(41) Popa, C.; van Bavel, A. P.; van Santen, R. A.; Flipse, C. F. J.; Jansen, A. P. J. *Surf. Sci.* **2008**, *602*, 2189.
(42) Föhlisch, A.; Nyberg, M.; Bennich, P. L.; Triquero, L.; Hasselstrom, J.; Karis, O.; Petterson, L. G. M.; Nilsson, A. *J. Chem. Phys.* **2000**, *112*, 1946.
(43) Ciobica, I. M.; van Santen, R. A. *J. Phys. Chem. B* **2003**, *107*, 3808.
(44) de Koster, A.; Jansen, A. P. J.; van Santen, R. A.; Geerlings, H. *Faraday Discuss. Chem. Soc.* **1989**, *87*, 221.
(45) Shetty, S. G.; Jansen, A. P. J.; van Santen, R. A. *J. Phys. Chem. C* **2008**, *112*, 17768.
(46) (a) Li, Y. S.; van Daelen, M. A.; Newsom, J. M.; van Santen, R. A. *Chem. Phys. Lett.* **1994**, *226*, 100. (b) Li, Y. S.; van Daelen, M. A.; Newsom, J. M.; van Santen, R. A. *J. Phys. Chem.* **1996**, *100*, 2279.
(47) Pidko, E. A.; Kazansksy, V. B.; Hensen, E. J. M.; van Santen, R. A. *J. Catal.* **2006**, *240*, 73.
(48) Barteau, M. A.; Madix, R. B. In *The Chemical Physics of Solid Surfaces and Heterogeneous Catalysis*; King, D. A., Woodruf, D. P., Eds.; Elsevier: New York, 1982; Vol. 4, p 95.
(49) Bickelhaupt, F. M. *J. Comput. Chem.* **1999**, *20*, 114.
(50) Bickelhaupt, F. M.; Baerends, E. J. *Rev. Comput. Chem.* **2000**, 1.
(51) Liu, Z.-P.; Hu, P. *J. Chem. Phys.* **2001**, *114*, 8244.
(52) Crawford, P.; Hu, P. *J. Phys. Chem. B* **2006**, *110*, 24929.
(53) Bunnik, B. S.; Kramer, G. J.; van Santen R. A. *Top. Catal.* **2009**, accepted for publication.
(54) Mayer, I. *Chem. Phys. Lett.* **1983**, *97*, 270.
(55) Popa, C.; van Santen, R. A.; Jansen, A. P. J. *J. Phys. Chem. C* **2007**, *111*, 9839.
(56) (a) Ge, Q.; Neurock, M. *J. Am. Chem. Soc.* **2004**, *126*, 1551. (b) Eichler, A.; Hafner, J. *Chem. Phys. Lett.* **2001**, *343*, 383.
(57) (a) Loffreda, D.; Simon, D.; Sautet, P. *J. Catal.* **2003**, *213*, 211. (b) Loffreda, D.; Simon, D.; Sautet, P. *J. Chem. Phys.* **1998**, *108*, 6447.
(58) Ge, Q.; Neurock, M. *J. Phys. Chem. B* **2006**, *110*, 15368.
(59) Ciobica, I. M.; van Santen, R. A.; van Berge, P. J.; van de Loosdrecht, J. *Surf. Sci.* **2008**, *602*, 17–27.
(60) (a) Liu, Z.-P.; Hu, P. *J. Am. Chem. Soc.* **2002**, *124*, 11568. (b) Gajdos, M.; Eichler, A.; Hafner, J. *J. Phys.: Condens. Matter* **2004**, *16*, 1141.
(61) Gajdoš, M.; Hafner, J.; Eichler, A. *J. Phys.: Condens. Matter* **2006**, *18*, 41.
(62) Honkala, K.; Hellman, A.; Remediakis, I. N.; Logadottir, A.; Carlsson, A.; Dahl, S.; Christensen, C. H.; Nørskov, J. K. *Science* **2005**, *307*, 555.
(63) Liu, Z.-P.; Hu, P. *J. Chem. Phys.* **2001**, *115*, 4977.
(64) van Santen, R. A.; Neurock, M. *Russ. J. Phys. Chem. B.* **2007**, *1*, 261.
(65) Crawford, P.; Hu, P. *J. Chem. Phys.* **2006**, *124*, 044705.
(66) Bezemer, G. L.; Bitter, J. H.; Kuipers, H. P. C. E.; Oosterbeek, H.; Hollewijn, J. E.; Xu, X.; Kapteijn, F.; van Dillen, A. J.; de Jong, K. P. *J. Am. Chem. Soc.* **2006**, *128*, 3956.
(67) Valden, M.; Lai, X.; Goodman, D. W. *Science* **1998**, *281*, 1647.
(68) Liu, Z.-P.; Hu, P. *J. Am. Chem. Soc.* **2003**, *125*, 1958.
(69) (a) Ciobica, I. M.; Frechard, F.; van Santen, R. A.; Kleijn, A. W.; Hafner, J. *J. Phys. Chem. B* **2000**, *104*, 3364. (b) Ciobica, I. M.; van Santen, R. A. *J. Phys. Chem. B* **2002**, *106*, 6200.

(70) (a) van Leeuwen, P. W. N. M. *Homogeneous Catalysis: Understanding the Art*; Kluwer Academic Publisher: Dordrecht, The Netherlands, 2004. (b) Brookhart, M.; Green, M. L. H. *J. Organomet. Chem.* **1983**, *250*, 395. (c) Versluis, L.; Ziegler, T.; Fan, L. *Inorg. Chem.* **1990**, *29*, 4530.
(71) Shustorovich, E. M. *Surf. Sci. Rep.* **1986**, *6*, 1.
(72) Abild-Pedersen, F.; Greeley, J.; Studt, F.; Rossmeisl, J.; Munter, T. R.; Moses, P. G.; Skúlason, E.; Bligaard, T.; Nørskov, J. K. *Phys. Rev. Lett.* **2007**, *99*, 16105.
(73) Watwe, R. M.; Cortright, R. D.; Nørskov, J. K.; Dumesic, J. *J. Phys. Chem. B* **2000**, *104*, 2299.
(74) Garin, F. *Top. Catal.* **2006**, *39*, 11.
(75) (a) Biloen, P.; Sachtler, W. M. H. *Adv. Catal.* **1981**, *30*, 165. (b) Anderson, R. P. *The Fischer−Tropsch Synthesis*; Academic Press: New York, 1984.
(76) Maitlis, P. M.; Long, H. C.; Quyoum, R.; Turner, M. L.; Wang, Z.-Q. *Chem. Commun.* **1996**, 1.
(77) Ciobica, I. M.; Kramer, G. J.; Ge, Q.; Neurock, M.; van Santen, R. A. *J. Catal.* **2002**, *212*, 136.
(78) (a) Cheng, J.; Gong, X.-Q.; Hu, P.; Lok, C. M.; Ellis, P.; French, S. *J. Catal.* **2008**, *254*, 285. (b) Cheng, J.; Hu, P.; Ellis, P.; French, S.; Kelly, G.; Lok, C. M. *J. Phys. Chem. C* **2008**, *112*, 6082. (c) Cheng, J.; Hu, P.; Ellis, P.; French, S.; Kelly, G.; Lok, C. M. *J. Catal.* **2008**, *257*, 221.
(79) van Santen, R. A.; Van Steen, E.; Ciobica, I. *Adv. Catal.*, submitted for publication.
(80) (a) Inderwildi, O. R.; Jenkins, S. J.; King, D. A. *J. Phys. Chem. C* **2008**, *112*, 1305. (b) Andersson, M. P.; Abild-Pedersen, F.; Remediakis, I. N.; Bligaard, T.; Jones, G.; Engbaek, J.; Lytken, O.; Horch, S.; Nielsen, J. H.; Sehested, J.; Rostrup-Nielsen, J. R.; Norskov, J. K.; Chorkendorf, I. *J. Catal.* **2008**, *255*, 6.
(81) Shetty, S.; Jansen, A. P. J.; van Santen, R. A. *J. Am. Chem. Soc.* **2009**, *131*, 12874.
(82) Shetty, S.; van Santen, R. A.; Stevens, P.; Raman, S. Unpublished results.
(83) Inderwildi, O. R.; Jenkins, S. J.; King, D. A. *J. Am. Chem. Soc.* **2007**, *129*, 1751.
(84) Fréchard, F.; van Santen, R. A.; Siokou, A.; Niemantsverdriet, J. W.; Hafner, J. *J. Chem. Phys.* **1999**, *111*, 8124.
(85) Offermans, W. K.; Jansen, A. P. J.; van Santen, R. A.; Novell-Leruth, G.; Ricart, J. M.; Pérez-Ramírez, J. *J. Phys. Chem. C* **2007**, *111*, 17551.
(86) Offermans, W. K.; Jansen, A. P. J.; van Santen, R. A. *Surf. Sci.* **2006**, *600*, 1714.
(87) Novell-Leruth, G.; Valcarell, A.; Pérez-Ramirez, J.; Ricart, J. M. *J. Phys. Chem C* **2007**, *111*, 860.
(88) Popa, C.; Jansen, A. P. J.; van Santen, R. A. *J. Phys. Chem. C* **2007**, *111*, 9839.
(89) Rosca, V.; Koper, M. T. M. *Phys. Chem. Chem. Phys.* **2006**, *8*, 2513.
(90) Bengaard, H. S.; Nørskov, J. K.; Sehested, J.; Clausen, B. S.; Nielsen, L. P.; Molenbroek, A. M.; Rostrop-Nielsen, J. R. *J. Catal.* **2002**, *209*, 365.
(91) Grootel, P.; Hensen, E.; van Santen, R. A. *Surf. Sci.* **2009**, *603*, 3275.
(92) Wang, G.-C.; Tao, S.-X.; Bu, X.-H. *J. Catal.* **2006**, *244*, 10.
(93) Michaelides, A.; Alavi, A.; King, D. A. *J. Am. Chem. Soc.* **2003**, *125*, 2746.
(94) Michaelides, A.; Hu, P. *J. Am. Chem. Soc.* **2001**, *123*, 4235.
(95) Hickman, D. A.; Schimdt, L. D. *Science* **1993**, *259*, 343.
(96) Andersson, A.; Ketteler, G.; Bluhm, H.; Yamamoto, S.; Ogasawara, V.; Petterson, L. G. M.; Salmeron, M.; Nilsson, A. *J. Am. Chem. Soc.* **2008**, *130*, 2793.
(97) (a) Karlsberg, G. S.; Wahnstrom, G. J. *J. Chem. Phys.* **2005**, *122*, 194705. (). (b) Karlberg, G. S.; Wahnstrom, G. *Phys. Rev. Lett.* **2004**, *92*, 136103. (c) Vassylev, P.; Koper, M. T. M.; Santen, R.A. v. *Chem. Phys. Lett.* **2002**, *359*, 337.
(98) Imbihl, R.; Scheibe, A.; Zeng, Y. F.; Günther, V. S.; Kraehnert, R.; Kondratenko, V. A.; Baerns, M.; Offermans, W. K.; Jansen, A. P. J.; van Santen, R. A. *Phys. Chem. Chem. Phys.* **2007**, *9*, 3522.
(99) van de Broek, A. C. M.; van Grondelle, J.; van Santen, R. A. *J. Catal.* **1999**, *185*, 297.
(100) Mieher, W. D.; Ho, W. *Surf. Sci.* **1995**, *322*, 151.
(101) Bradley, J. M.; Hopkinson, A.; King, D. A. *J. Phys. Chem.* **1984**, *88*, 3233.
(102) Fogel, Ya. M.; Nadykto, B. T.; Rybalko, V. F.; Shvachko, V. I.; Korobchanskaya, I. E. *Kinet. Catal.* **1964**, *5*, 431.
(103) (a) Gang, L.; Anderson, B. G.; van Grondelle, J.; van Santen, R. A. *J. Catal.* **2001**, *199*, 107. (b) Lu Gang, L.; Anderson, B. G.; van Grondelle, J.; van Santen, R. A. *J. Catal.* **1999**, *186*, 100.
(104) Anstrom, M.; Topsøe, N. Y.; Dumesic, J. A. *J. Catal.* **2003**, *213*, 115.
(105) Burch, R.; Daniells, S. T.; Hu, P. *J. Chem. Phys.* **2002**, *117*, 2902.
(106) Bogicevic, A.; Hass, K. C. *Surf. Sci.* **2002**, *506*, L237.
(107) Backus, E. H. G.; Eichler, A.; Grecea, M. L.; Kleyn, A. W.; Bonn, M. *J. Chem. Phys.* **2004**, *121*, 7946.
(108) Gland, J. L.; Korchak, V. N. *J. Catal.* **1978**, *53*, 9.
(109) van Santen, R. A. *Acc. Chem. Res.* **2009**, *42*, 57.
(110) Che, M.; Bennett, C. O. *Adv. Catal.* **1989**, *36*, 55. Henry, C. R.; Chapon, C.; Giorgio, S.; Goyhenex, C. In *Chemisorption and Reactivity on Supported Clusters and Thin Films*; Lambert, R. M., Pacchioni, G., Eds.; Kluwer Academic Publishers: Dordrecht, The Netherlands, 1997; pp 117−152.
(111) Boudart, M. *Adv. Catal. Relat. Subj.* **1969**, *20*, 153.
(112) Boudart, M.; Djéga-Mariadasson, G. *Kinetics of Heterogeneous Catalytic Reactions*; Princeton University Press: Princeton, 1984.
(113) Sinfelt, J. H.; Carter, H. L.; Yates, D. J. *J. Catal.* **1972**, *24*, 283.
(114) Somorjai, G. A.; Tao, F.; Park, J. Y. *Top. Catal.* **2008**, *47*, 1.
(115) van Hardevelt, R.; Hartog, F. *Surf. Sci.* **1969**, *15*, 169.
(116) Spencer, N. D.; Schoonmaker, R. C.; Somorjai, G. A. *Nature* **1981**, *294*, 643.
(117) (a) Feibelman, P. J. *Science* **2002**, *205*, 99. (b) Michaelides, A.; Alavi, A.; King, D. *J. Am. Chem. Soc.* **2003**, *125*, 2746.
(118) Shetty, S. G.; Jansen, A. P. J.; van Santen, R. A. *J. Phys. Chem. C* **2009**, *113*, 19749.
(119) Gong, X.-Q.; Hu, P.; Ravel, R. *J. Chem. Phys.* **2003**, *119*, 6324.

CR9001808